Submarine Landforms and Late Quaternary Ice Flow in Hinlopen Strait, Northern Svalbard Margin

By Christine Batchelor

Girton College

Scott Polar Research Institute,
University of Cambridge,
Lensfield Road,
Cambridge,
CB2 1ER

10th June 2010

Supervisor: Professor Julian Dowdeswell

This dissertation is submitted for the degree of Master of Philosophy

Declaration

This dissertation is the result of my own work and includes nothing which is the outcome of work done in collaboration except where specifically indicated in the text. My dissertation is not substantially the same as any I have submitted for a degree or any other qualification at any other university. This dissertation is no more than 20,000 words in length excluding the acknowledgements, declaration, list of references, tables, captions and appendices.

Acknowledgements

I would like to thank Professor Julian Dowdeswell for his guidance, helpful discussions and comments about this project. I would also like to thank Dr. Kelly Hogan for providing an introduction into post-acquisition data processing techniques and the MB-System™ software. Many thanks go to Dr. Suzanne MacLachlan for her assistance with sediment core preparations and the GEOTEK multi-sensor core scanner at BOSCORF, Southampton.

I would like to thank the staff and students at the Scott Polar Research Institute for an enjoyable year, and my family, friends, and Sami Husa for putting up with many conversations about 'troughs'. Finally, I would like to thank Phoebe Robinson, my swath-raging and white van-driving partner in crime, for helping me to get to grips with Linux and for keeping an eye on the kerb.

Contents

List of Figures

List of Tables

Abstract

The Hinlopen Trough is a 70km long cross-shelf trough on the Northern Svalbard margin. During the last glacial period, this trough is thought to have been occupied by an ice stream which flowed north across the continental slope (Ottesen et al., 2007). This project is concerned with examining the submarine landforms and acoustic stratigraphy of this palaeo-ice stream with a view to furthering our understanding of past ice-flow dynamics in this area. Establishing the direction and dynamics of ice flow around the margins of palaeo-ice sheets has recently become a topic of much geophysical and geological research; a comprehensive understanding of the geometry and dynamics of past ice sheets is crucial to predicting the behaviour of modern ice sheets in response to a changing climate.

The data that will be utilised in this project was collected during the geophysical cruise of the RRS *James Clark Ross* in 2006. This investigation will use a variety of geophysical and geological data sets to describe, map and interpret the geomorphology of the sea bed and to outline the distribution of the submarine landforms in Hinlopen Trough. Observations from this former ice stream will be considered in relation to their implications on the ice-flow dynamics of the last ice sheet present over Svalbard.

Chapter 1 - Introduction

1.1 Introduction and Aims

This project is an investigation of the morphology and distribution of submarine landforms in Hinlopen Strait, Northern Svalbard margin. Extensive data sets from EM120 multi-beam swath bathymetry, Topographic Parametric Sonar (TOPAS) sub-bottom acoustic profiling, and gravity cores allow the description and interpretation of the geomorphology of the sea floor. This investigation will aim to further our understanding of Late Quaternary ice-flow dynamics in this region and will contribute to a growing amount of data on the geomorphological imprint of palaeo-ice streams more generally (e.g. Stokes and Clark, 2002; Ottesen et al., 2005a).

Ice sheets in the Antarctic and Arctic have advanced and retreated across high-latitude continental margins a number of times during the Quaternary Period (Svendsen et al., 2004), often expanding to the continental shelf break (Fig. 1.1). Submarine glacial landforms are produced by ice-sheet advance and subsequent retreat across fjords and the continental shelf during glacial-interglacial cycles.

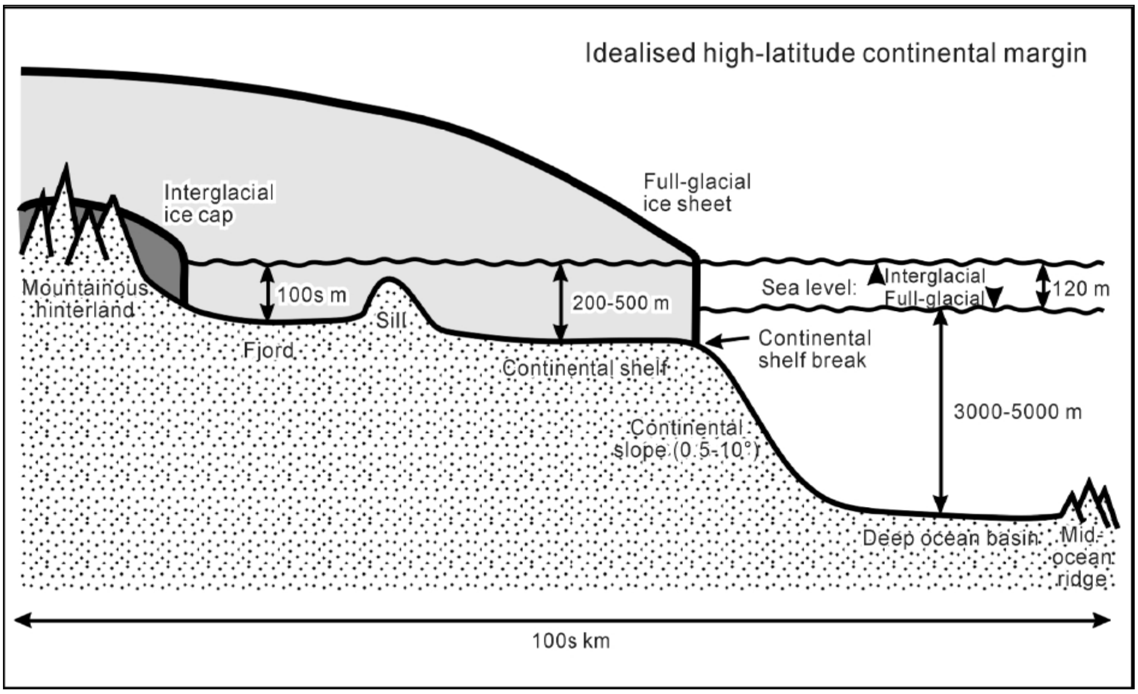

Figure 1.1 – An Idealised High-latitude Continental Margin (from Dowdeswell and Ó Cofaigh, 2002)

Whereas subaerial erosion and periglacial activity have created a fragmented glacial record in many terrestrial environments, submarine landforms preserved on the seafloor of deglaciated continental shelves often provide comprehensive records of past glacial activity.

A comprehensive understanding of the geometry and dynamics of past ice sheets is crucial for predicting the behaviour of modern ice masses in response to anthropogenic climate change. Using the geomorphological record from continental margins to establish the directions and dynamics of ice flow around the margins of palaeo-ice sheets has therefore become a topic of much geophysical and geological research (e.g. Ottesen et al., 2005a; Ó Cofaigh et al., 2005a; Evans et al., 2006; Dowdeswell et al., 2010a). Reconstructions of the former dynamics of ice streams – relatively narrow regions of fast-moving ice set within slower flowing ice – are of vital importance due to the high flow velocities exhibited by these features.

1.2 Location and Study Area

Svalbard is a group of islands located approximately 650 kilometres north of Norway in the north-west corner of the Barents Shelf at the southern margin of the Arctic Ocean (Fig. 1.2). The relatively shallow Barents Sea, in which water depths rarely exceed 400 metres (Harland et al, 1997), borders Svalbard to the south and the east and is separated from the Kara Sea by the Russian archipelago of Novaya Zemlya. A number of cross-shelf troughs and their associated trough-mouth fans exist on the northern and western continental margins of Svalbard (Vorren et al., 1998; Ottesen et al., 2005a). Hinlopen Strait (Hinlopenstredet in Norwegian) is a 110 km long, 5-10 km wide trough located between the islands of Spitsbergen and Nordaustlandet (Fig 1.2; Ottesen et al., 2007). This depression originates in the central region of Svalbard and continuous north across the continental shelf as a prominent cross-shelf trough, Hinlopen Trough (Fig. 1.3).

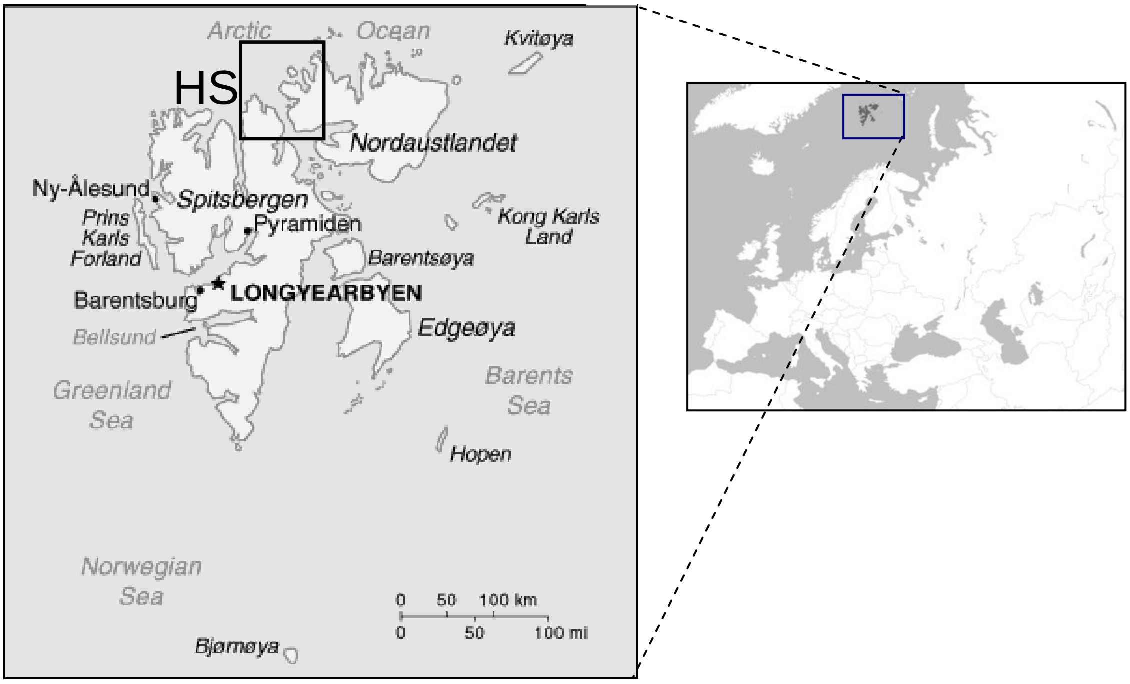

Figure 1.2 – The location of Svalbard and Hinlopen Trough and Strait (HS) (from www.intute.ac.uk/worldguide/countrymaps)

The identification of mega-scale glacial lineations (MSGLs) in Hinlopen Trough suggests that this bathymetric depression was the former location of an ice stream during the Late Weichselian glacial period about 20 kyr ago (Ottesen et al., 2007). Hinlopen Trough terminates at the shelf break, where the continental slope descends down to the Arctic Ocean Basin, with water depths rapidly plunging from around 500 m to more than 2000 m.

Bathymetric data from the shelf edge of Hinlopen Trough has revealed a massive slump headwall eroded back into the continental margin (Figure 1.3), northward from which repeated sliding has occurred (Cherkis et al., 1992, 1999). Slumping processes appear to have generated a massive submarine landslide into the Sophia Basin, which opens northwards to the Eurasian Basin and the Arctic Ocean. This mass movement event, termed the Hinlopen Slide, has been described as one of the largest landslides worldwide with around 1350 km^3 of sediment being evacuated from the continental margin (Vanneste et al., 2006).

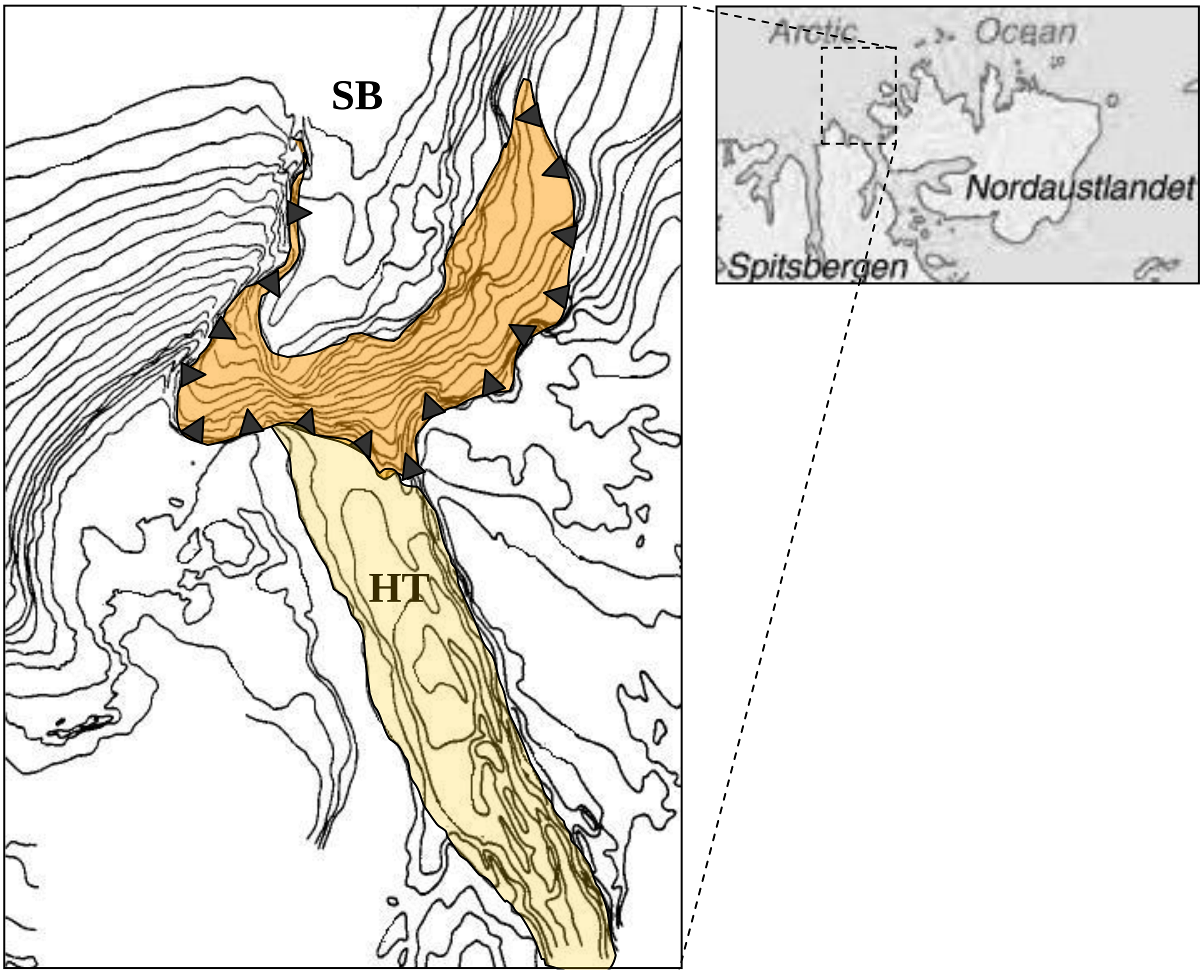

Figure 1.3 – Bathymetric data showing the location of Hinlopen Trough (HT), Sophia Basin (SB), and the Hinlopen Slide scar area (depicted by orange shading and triangles). Image adapted from Cherkis et al, 1992.

Whilst it has been proposed by some that the Hinlopen Slide comprised a series of slope failure events (Vanneste et al., 2006), other earth scientists maintain that it was a single catastrophic event, followed only by minor events during adjustment to a new morphological equilibrium (Winkelmann et al., 2008a). The initial slide event has been dated to Marine oxygen Isotope Stage 3 (MIS3), around 30 kyr ago (Winkelmann et al., 2008a).

Large sediment slides are relatively common on previously glaciated high-latitude margins, and are typically caused by high rates of sediment deposition and the overloading of steep slopes (e.g. Vorren et al., 1998). It has been suggested that the bathymetry of the slumps from the Hinlopen Slide do not support slide triggering by sediment unloading alone (Cherkis et al., 1992). Additional causes of failure proposed for this submarine landslide have included seismic activity (Cherkis et al., 1992; Vanneste et al., 2006) and gas hydrate decollement mechanisms (Winkelmann et al., 2008a).

1.3 Tectonic and Glacial Development of Svalbard's Northern Margin

1.3.1 Pre-Quaternary Evolution of Svalbard's Northern Margin

Svalbard has undergone a complex geological history which is largely a product of the plate tectonic evolution of the Greenland Sea and the Arctic Ocean (Sundvor and Eldholm, 1979). The oldest geological formation on the archipelago is the Basement formation, which includes rocks of Precambrian, Cambrian and Ordovician age (4500 to 440 million years ago). These rocks can be identified along the west coast of Spitsbergen, between Wijdefjorden and Hinlopen Strait on the northern margin, and also in the most northerly region of Nordaustlandet (Fig. 1.4).

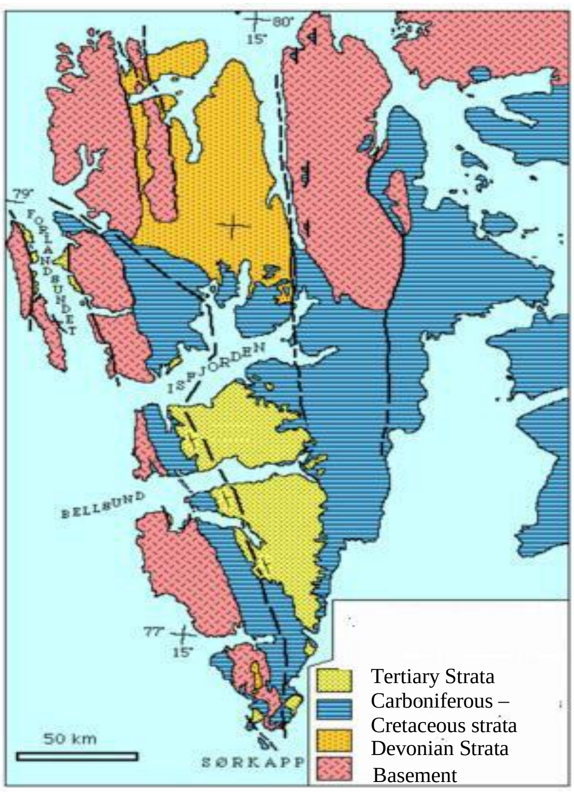

Figure 1.4 – Map depicting the geology of Svalbard (from Hjelle, 1993)

The continental margins of Svalbard and Greenland collided during the early Tertiary Period around 60 million years ago, causing a sheared-rifted margin on the west coast of Svalbard and the formation of a basin to the east (Hjelle, 1993). The separation of the Lomonosov Ridge from the northern Svalbard margin also took place during the Tertiary, causing the opening of the Eurasian Basin, followed by slow yet continuous spreading of the sea floor (Vanneste et al., 2006). The Barents Sea region has experienced uplift since Early Tertiary rifting and the opening of both the Norwegian-Greenland Sea and the Eurasian Basin. It is now widely accepted that the Svalbard Platform then attained a subaerial position, after which substantial erosion was initiated on the islands (Dimakis et al., 1998; Vanneste et al, 2006).

The dramatic scale of Svalbard's Cenozoic erosion is evident through analysis of the large amounts of sediment deposited as trough-mouth fans on the edges of the island's northern and western margins (Vorren et al., 1998). The existence of these huge fans can be best explained by assuming that erosion took place through glacial processes and that the rates of erosion were extremely high (Dimakis et al., 1998; Elverhøi et al., 1998; Dowdeswell and Siegert, 1999). It has therefore been argued that the majority of the pre-glacial Barents Sea area would have needed to have been subaerial in order to allow for the initial growth of ice during cold periods (Dimakis et al., 1998; Siegert et al., 2001). The operation of intense glacial erosion subsequently produced isostatic uplift during interglacial periods, and facilitated the continued maintenance of raised and glaciated land surfaces during the Quaternary (Dimakis et al., 1998).

1.3.2 Quaternary Development of Svalbard's Northern Margin

Although much of Svalbard's current shape and size was attainted by the end of the Tertiary Period, the present fjord, valley and mountainous morphology of the archipelago is largely a product of erosion from the successive glaciations which inundated these islands throughout the Quaternary Period (Svendsen et al., 2004).

The Quaternary, which dates from approximately 2.6 million years ago until the present, has been characterised by a distinctive pattern of alternating glacial and interglacial cycles. These large-scale climatic fluctuations are forced by variations in the Earth's orbital parameters of eccentricity, precession, and axial tilt, which operate on timescales of 100 kyr, 23 kyr, and 41 kyr, respectively. The ice cover of Svalbard has fluctuated in approximate unison with these orbitally-forced climatic changes. Many of the large Quaternary ice sheets that developed over Svalbard and the Barents Sea reached the continental shelf break to the west and north of the archipelago, where they deposited large amounts of sediment.

1.3 3. The Last Glacial-Interglacial Cycle

The last glacial-interglacial cycle encompassed the period of time from the end of the Eemian Interglacial (MIS 5e) through the Weichselian glacial period and the present Holocene interglacial. The Weichselian glacial period is understood to have started at approximately 117 kyr and covers MIS 5d to 2 (Svendsen et al., 2004). A wide variety of evidence has demonstrated that a Svalbard-Barents Sea ice sheet existed over the Svalbard archipelago during at least three separate occasions during the Weichselian. The Early Weichselian glaciation lasted from approximately 100 kyr to 80 kyr; the Middle Weichselian glaciation is considered to be synonymous with MIS 4; and the Late Weichselian glaciation reached its maximum at MIS 2 around 20 kyr ago (Fig 1.5). These glaciations were separated by long periods of time during which conditions were generally colder than today, but adjacent seas were at least seasonally free of ice and the glaciers on Svalbard were not significantly larger than their Holocene limits (Salvigsen et al., 1995; Ingólfsson et al., 1995).

Evidence for three large-scale fluctuations of the Svalbard-Barents Sea Ice Sheet during the Weichselian period includes terrestrial morphological and lithostratigraphic evidence (Mangerud and Svendsen, 1992; Ingólfsson et al., 1995), raised shorelines and emergence curves (Forman et al., 1995; 2004), the occurrence of ice-rafted debris (IRD), glacier-derived diamict, certain stable isotopes or diagnostic foraminifera within marine sediment cores (Hebbeln et al., 1994; Siegert et al., 2001; Knies et al, 2001; Spielhagen et al., 2004), analyses of sea floor morphology (Polyak et al., 1997; Ottesen et al., 2005; 2007), and predictions from numerical ice-sheet models (Siegert et al., 2001; Svendsen et al., 2004).

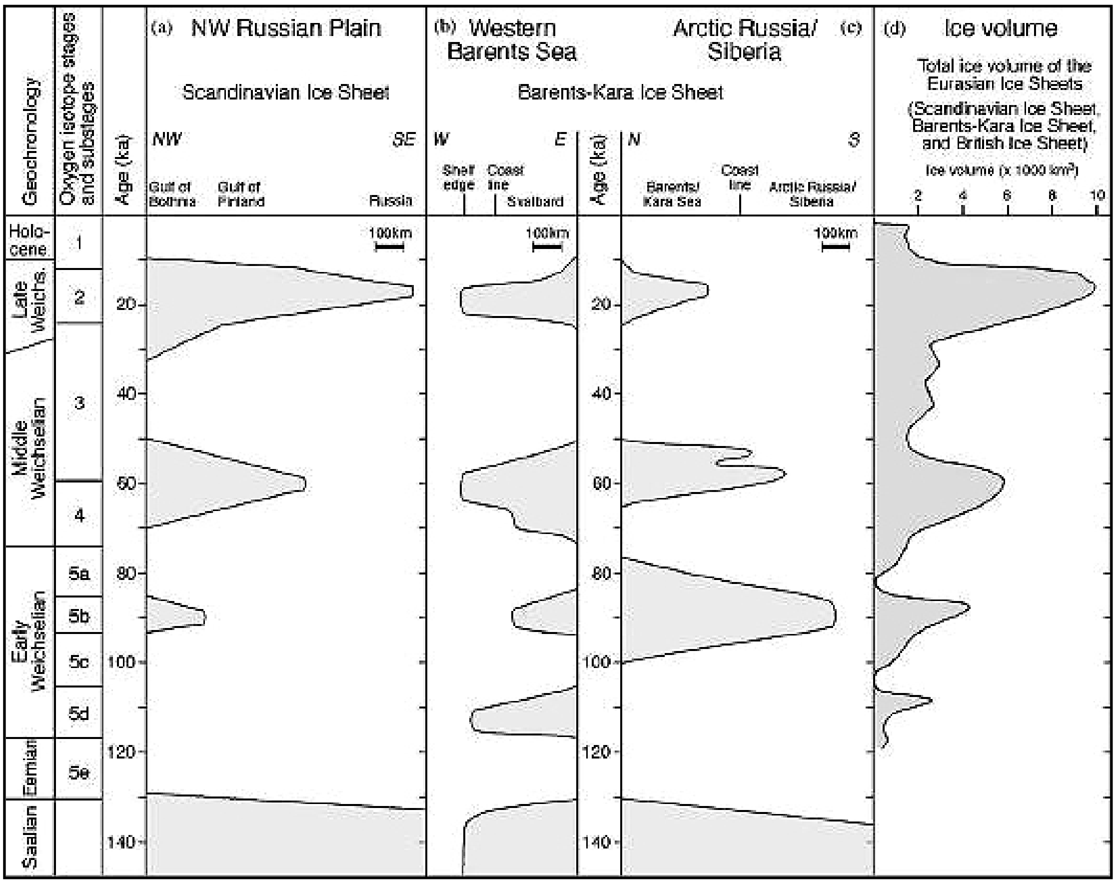

Figure 1.5 – Time-distance diagrams showing the growth and decay of the Eurasian ice sheets a) the Scandinavian Ice Sheets in Finland and Russia, b) the Barents-Kara Ice Sheets on Svalbard in the western Barents Sea, c) the fluctuations of the Barents-Kara Ice Sheets in northern Russia/ Siberia, d) curve showing the volumes of the Eurasian ice sheets as modelled by Siegert et al., 2001. Diagram taken from Svendsen et al., 2004

The southerly extent of the Svalbard-Barents Sea ice sheet is inferred to have become progressively reduced during each glaciation throughout the Weichselian (Fig. 1.5C). Whereas the Scandinavian Ice Sheet attained its maximum size during the Last Glacial Maximum (LGM) about 20 kyr (Fig. 1.5A), the Svalbard-Barents Sea ice sheet reached its maximum easterly extent in the Early Weichselian, and was even larger during the Saalian (Svendsen et al., 2002, 2004). The existence of an extensive Early Weichselian ice sheet over Svalbard has, however, recently become a topic of much debate. Winkelmann et al.'s (2008b) investigation of terrigenous input events in the ocean sedimentary record failed to identify evidence of an Early Weichselian glaciation and concluded that a major glacier advance to the northern shelf break was not likely to have occurred during this period.

The extent of Svalbard's ice cover during the LGM has also proved to be a highly contested subject of debate (Salvigsen et al., 1995; Landvik et al., 1998; Siegert et al., 2001; Svendsen et al., 2002; 2004; Spielhagen et al., 2004). Theories of the maximum extent of Late Weichselian ice cover in this area have ranged from a massive grounded ice sheet complex covering much of Eurasia (Grosswald, 1970 in Siegert et al., 2001), to a localised ice dome over Svalbard (Boulton, 1979; Velichko et al., 1997). Although it is now accepted that a major Svalbard-Barents Sea ice sheet existed during the LGM, this ice mass is not considered to be as extensive as the huge pan-Arctic ice sheet described in several papers by Grosswald and others, and is not thought to have expanded onto mainland Russian and Siberia, or to have reached the Arctic island of Severnaya Zemlya during this time period (Figure 1.6).

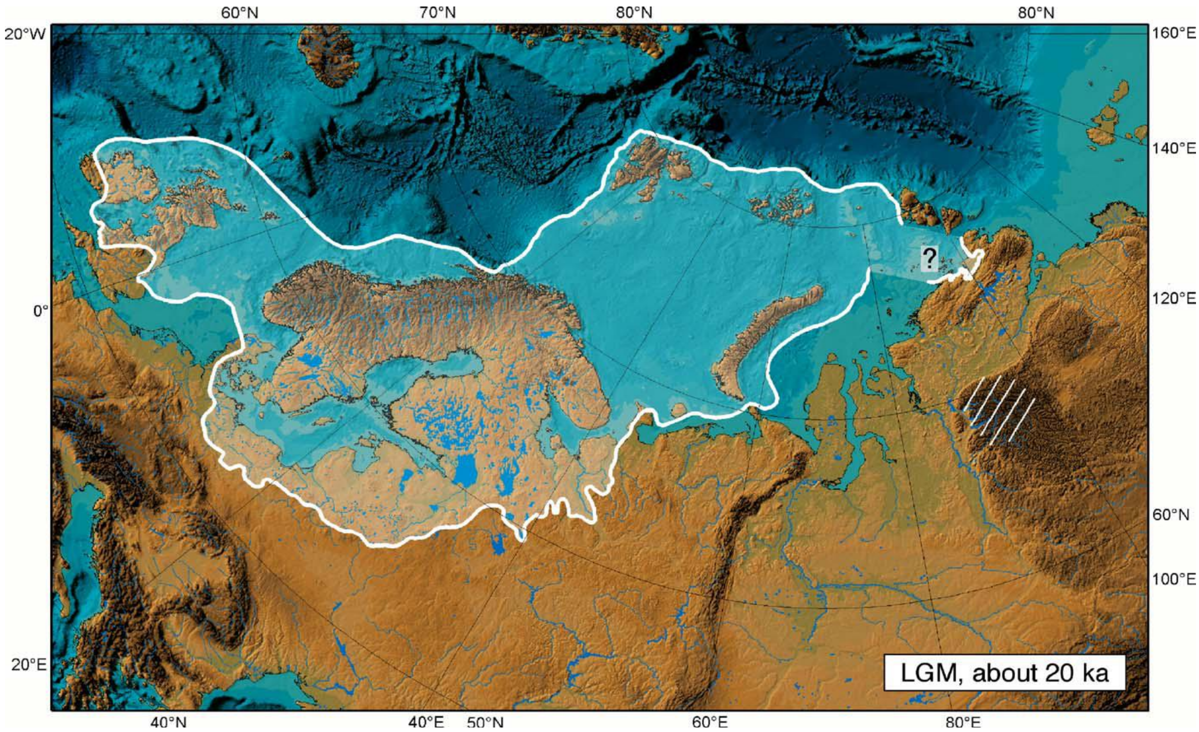

Figure 1.6 - A reconstruction of the Eurasian Ice Sheet during the Late Weichselian glacial maximum around 20 kyr (from Svendsen et al., 2004)

Radiocarbon dates indicating high sedimentation rates of diamictic debris off the shelf edge west of Svalbard suggest that ice reached the continental shelf edges during the Late Weichselian (Svendsen et al., 1992; 1996; Elverhøi et al., 1995; Landvik et al., 1998; 2005; Dowdeswell and Elverhøi, 2002). Unequivocal evidence for an extensive and grounded ice sheet to the shelf edge during this period includes the distribution of submarine landforms such as terminal moraines, flutes, and mega-scale glacial lineations (MSGLs) (Polyak et al., 1997; Ottesen et al., 2005a, 2007; Ottesen and Dowdeswell, 2009). A large grounding-zone wedge identified off the northwest coast of Svalbard has been interpreted to mark the maximum extent of this ice sheet, revealing that ice did not reach the adjacent Yermak Plateau during this period (Ottesen et al., 2007; Ottesen and Dowdeswell, 2009; Dowdeswell et al., In Press A). Models of ice-sheet extent during this period, which produce a Late Weichselian ice sheet terminating at the western and northern shelf edges, are in general agreement with the observational record (Lambeck, 1995; 1996; Siegert et al. 2001).

Bathymetric mapping of submarine landforms and trough-mouth fans has revealed that the Late Weichselian ice sheet displayed dynamic flow patterns and was partitioned into ice streams surrounded by slower-flowing inter-ice stream areas (Vorren and Laberg, 1997; Dowdeswell and Siegert, 1999; Ottesen et al., 2005a; Ottesen and Dowdeswell, 2009). On its northern margin, the majority of ice flowed northwards through Woodfjorden, Wijdefjorden, and Hinlopen Strait (Fig. 1.7) (Ottesen et al., 2007). Geophysical data has confirmed that grounded ice reached the shelf break to the north of these three locations during the LGM (Ottesen et al., 2007; Winkelmann et al., 2008a). Ice streams form in bathymetric troughs because the thicker ice found in these locations leads to elevated basal pressures and temperatures, therefore increasing ice movement by the flow mechanisms of till deformation and basal sliding in the presence of water at the bed. The configuration of glacial lineations on the northern continental margin demonstrates that ice flowed northwards out of Wijdefjorden and was confluent with an ice stream in Hinlopen Trough (Fig. 1.7) (Ottesen et al, 2007). It has been proposed that a major ice dome was located either at the eastern corner of Spitsbergen or around the southern entrance to Hinlopen Strait (Dowdeswell et al., 2010a).

The deglaciation of the Late Weichselian ice sheet on Svalbard has been identified in a number of marine sediment cores through increased levels of IRD and light oxygen isotope values (Elverhøi et al., 1995; Svendsen et al., 1996; Dowdeswell and Elverhoi, 2002). The retreat of this ice sheet off the west coast of Svalbard has been demonstrated to have been stepwise in nature and to have involved two separate decay events (Elverhøi et al. 1995).

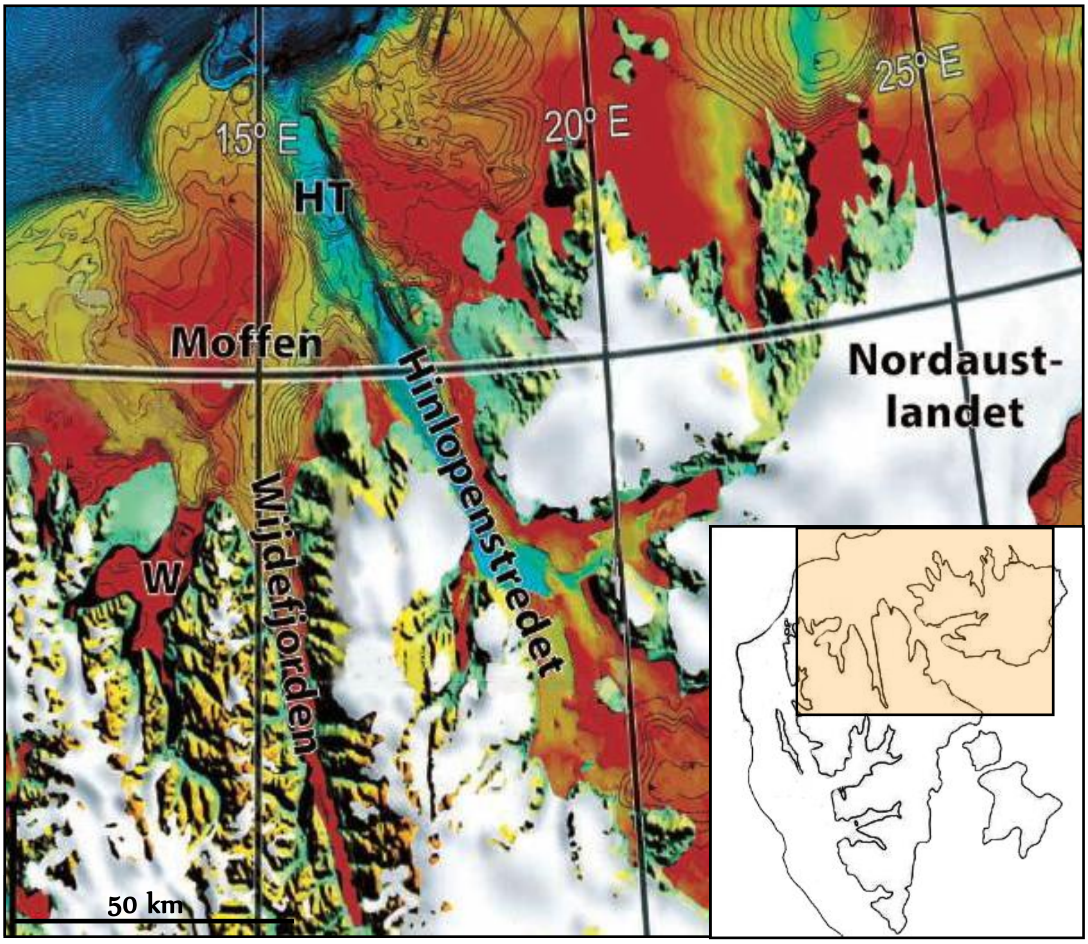

Figure 1.7 – Map showing the regional bathymetry of the northern fjord and shelf area around Svalbard; 20 m depth contours. W = Woodfjorden; HT = Hinlopen Trough. Image adapted from Ottesen et al., 2007

Two periods of enhanced sediment accumulation have been identified within deglacial sediments in Hinlopen Strait (Koç et al., 2002), suggesting a similar two-step warming and disintegration of the ice sheet in this location. Whereas previous investigations concluded that the Barents Sea ice sheet started to withdraw from its northern margin at around 15 kyr BP (Elverhoi et al., 1995; Landvik et al., 1998; Knies et al., 2001; Kleiber et al., 2000), a more recent study by Koç et al. (2002) suggests that this retreat took place between 13.9 and 13.7 kyr BP. This conclusion implies that the retreat of ice at the northern Svalbard margin was roughly synchronous with the disintegration of the western ice margin. The preservation of undisturbed streamlined sea-floor lineations, and a lack of grounding-zone deposits or superimposed moraine ridges, suggests rapid ice retreat through Hinlopen Trough (Ottesen et al., 2007).

The Younger Dryas in Svalbard is recorded as only a minor ice readvance initiated close to 12.4 kyr (Elverhøi et al., 1995). Whilst the Younger Dryas in Britain and Scandinavia was marked by extensive glacier growth, the ice cover of Svalbard during this period was actually less extensive than during the Little Ice Age - a brief cold climate event during the Holocene (Mangerud and Landvik, 2007). Explanations for the restricted growth of glaciers during the Younger Dryas in Svalbard allude to the role of easterly winds in producing a precipitation shadow and starvation of precipitation over much of the archipelago (Mangerud and Landvik, 2007).

1.4 Modern Oceanography

Svalbard's present oceanographic conditions were established close to 10.5 ka BP (Duplessy et al., 2001) and are dominated by two main sources of surface ocean water; the Western Spitsbergen Current and the East Spitsbergen Current (Harland et al, 1997). One of the defining features of contemporary global oceanography is the existence of large-scale thermohaline circulation, which facilitates the transfer of heat to the North Atlantic Ocean via the Gulf Stream and the North Atlantic Current (Duplessy et al., 2001). The North Atlantic Current transfers warm, saline water into the Nordic Seas, where it submerges in Fram Strait and forms a strong boundary current called the West Spitsbergen Current (Figure 1.8). This current is the most northwards remnant of the Gulf Stream and delivers relatively warm water northwards along the west coast of Spitsbergen and along the northern continental slope of Svalbard (Harland et al., 1997; Duplessy et al., 2001). The North Atlantic Current moderates Svalbard's temperatures, keeping the climate relatively warm in comparison with other regions of similar latitude.

The continental slope north of Hinlopen Strait is affected by the Northern Svalbard and Yermak Branches of the Western Spitsbergen Current (Vanneste et al., 2006). The temperate Northern Svalbard Branch has been observed to flow along this shelf between 100 and 800 m water depth, possessing core temperatures of between 3 and 4.5°C (Koç et al., 2002; Vanneste et al., 2006).

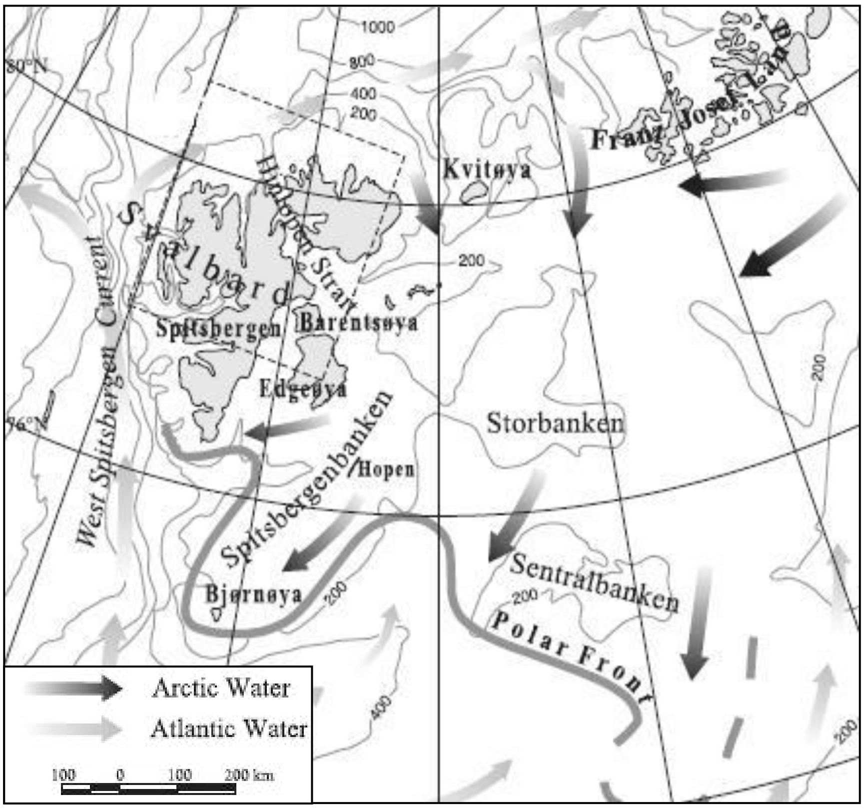

Figure 1.8 – Regional map depicting the present oceanic circulation around Svalbard (adapted from Koç et al, 2002)

The East Spitsbergen Current, which transfers cold water in a southerly direction east of Spitsbergen, eventually meets with the Western Spitsbergen Current off Edgeøya (Fig. 1.8), resulting in the deflection of cold water northwards, between the warmer current and the coast (Harland et al., 1997).

1.5 Thesis Structure

Chapter 2 will describe the rationale, acquisition methods, and processing techniques for each of the three data sets used in this project: swath bathymetry, sub-bottom acoustic stratigraphy and sediment cores. Chapter 3 will display the results from the multi-beam swath bathymetry in order to illustrate the distribution of submarine landforms in Hinlopen Strait. Chapter 4 will focus upon the acoustic stratigraphy of Hinlopen Strait, and Chapter 5 will concentrate on developing a lithostratigraphy from the four gravity cores. Chapter 6 represents a synthesis of information from all three data sets. The findings will be interpreted in the context of Late Quaternary ice-flow dynamics on Svalbard's northern margin and the geomorphological imprint of palaeo-ice streams. Chapter 7 will present a summary of the conclusions drawn from this project and will suggest ways in which this investigation could be extended.

Chapter 2 - Methodology

2.1 Introduction

The geophysical and geological data utilised in this thesis were collected during the JR142 geophysical cruise of the R.R.S *James Clark Ross* in August 2006. Swath-bathymetric and TOPAS (Topographic PArametric Sonar) 3.5 kHz sub-bottom profiler data provide regional analyses of the sea-floor morphology and the underlying shallow acoustic stratigraphy of Hinlopen Trough. Geological data consist of four gravity cores obtained from the sea floor, complementing the more extensive geophysical data sets and providing geological point samples of the sediment within the trough.

2.2 Multi-Beam Swath-Bathymetry Data

2.2.1 EM120 system

Swath bathymetry systems operate using the same theoretical principles as many acoustic or seismic methods; an acoustic signal (a ‘ping’) is transmitted towards the sea floor from a source instrument on a vessel and is reflected by acoustic boundaries in the underlying terrain (Hogan, 2008). The two-way travel time of this signal can then be converted into a measurement of depth, using information on the sound-velocity profile of the water column.

While traditional single-beam echo sounders only return bathymetry along the track line of a ship, multi-beam swath bathymetry systems transmit a large number of energy beams during each ping, allowing broader widths of the sea floor to be imaged at a greater resolution (Hogan, 2008). Each ping of acoustic energy is emitted by a piezoelectric transducer array and comprises a number of beams orientated at known angles in a plane perpendicular to the ship’s motion (Fig. 2.1).

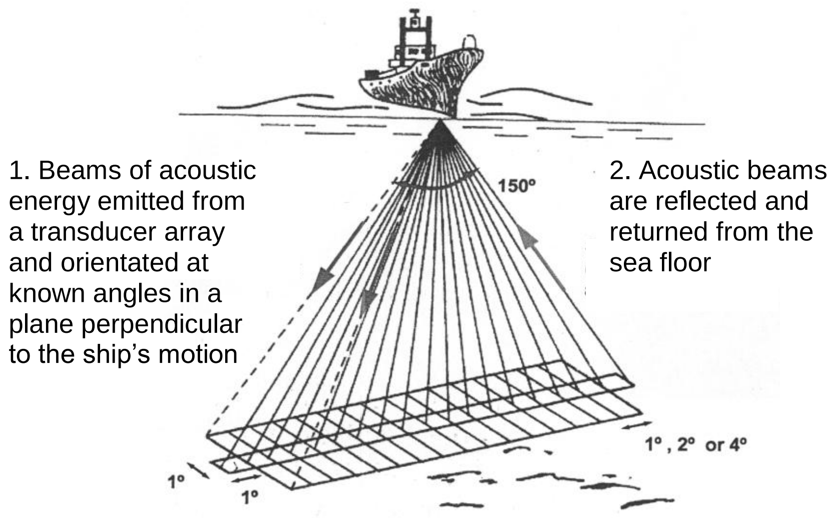

Figure 2.1 – Schematic diagram of a multi-beam echo-sounding system (Modified from Renard and Allenou, 1979 in Hogan, 2008)

The range and bearing of the returning acoustic signals are recorded and converted into depth measurements using the known configuration of the transducer array, the position of the ship, and the speed of the acoustic signal through the water column. Sequential depth profiles are compiled as the vessel advances and are combined to form a bathymetric map of the sea floor.

A hull-mounted Kongsberg Simrad EM120 multi-beam echo sounder was used to acquire bathymetry data during the JR142 geophysical cruise. This system emits 191 acoustic beams during every swath ping and operates with a frequency of 12 kHz and a starboard angle of 75° (Hogan, 2008). The EM120 system was run in its 'automatic ping mode', which selects 1 of 5 preset ping modes determined by the depth of the water. Although wider swaths of the sea floor can be imaged at greater water depths, the accuracy and resolution of the EM120 system decreases with water depth due to the increased angles of the acoustic beams.

The speed of sound through the water column was calculated by constructing a number of location-specific sound velocity profiles (SVPs). These profiles illustrate the changing speed of the acoustic pulses with water salinity, temperature and depth, and were measured by expendable bathythermograph (XBT) instruments. Raw data collected during the JR142 cruise were digitally archived and stored on DVD. These data were then transported to the Scott Polar Research Institute, University of

Cambridge, where files were transferred onto a Linux platform for processing and archiving (Hogan, 2008)

2.2.2 Swath Data Processing

It is possible for a number of external factors, such as the presence of sea ice, high winds or large waves, to disrupt the steady motion of the ship and affect the quality the reflected acoustic signal (Hogan, 2008). Swath-bathymetric data are also greatly affected by the speed of the acoustic signal through the water column, a variable which is constrained through the application of suitable location-specific SVPs. Processing of the raw bathymetry data was completed on a Linux platform and performed using the open-source software MB-System^{TM}. Data processing aimed to eliminate acquisition-system based artefacts and consisted of three principle stages; the assessment of data quality and identification of any navigation errors, the application of suitable SVPs to the data set, and the editing of erroneous data points recorded by the acoustic beams (Hogan, 2008; online MB-System^{TM} 'Cookbook').

The EM120 system performed well during data acquisition and collected high-quality data from a wide area of the sea floor of Hinlopen Trough (Fig. 2.2). A small number of thin data gaps are apparent in the imagery and record short periods of time during which the system stopped logging (Fig. 2.2A). Pings which recorded unrealistic latitudes and longitudes were interpreted as navigation errors and were also removed from the data set.

XBT measurements were made regularly throughout the JR124 geophysical cruise and were also performed ‘on demand’ upon recognition of significant changes in water depth or in the quality of the reflected acoustic signal (Table 2.1). Poor SVPs serve to disproportionately affect the accuracy of outer beam depths, producing data ‘stripes’ along the edges of each swath track (Fig. 2.3). Appropriate SVPs were applied to the data files during post-acquisition data processing using the ‘mbvelocitytool’ function in MB-System^{TM}. Although the effect of data stripes was minimised by this process, striped artefacts are still evident along the edges of some swath tracks (Fig. 2.3B).

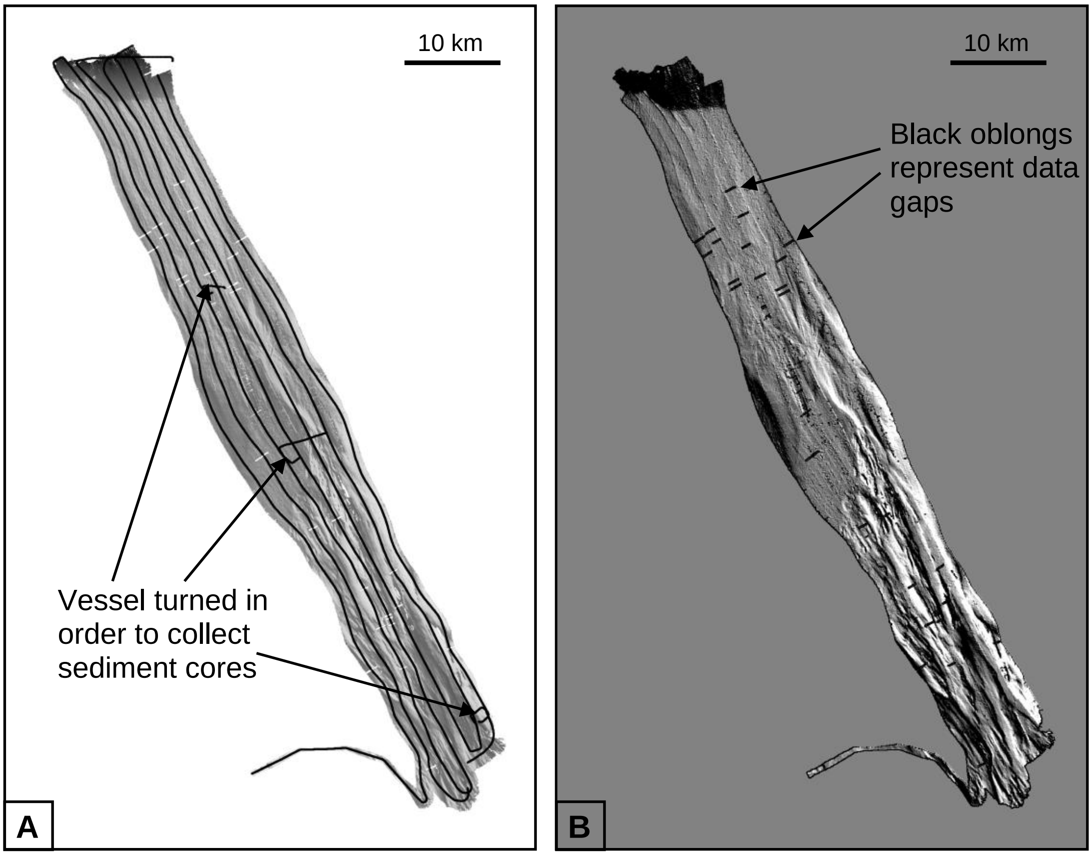

Figure 2.2 A) – Shaded relief map of the swath bathymetry of Hinlopen Trough, overlain by the track lines taken by the R.R.S *James Clark Ross* during the JR142 geophysical cruise. B) – Shaded relief map of the swath bathymetry of Hinlopen Trough, showing the extent of the surveyed area and the location of data gaps

Erroneous data points affected the swath bathymetry data in a number of locations and were caused principally by rotation of the EM120 system during turns of the vessel. These artefacts can be identified as rosette-shaped speckles of data on unprocessed maps of the bathymetry (Fig. 2.3A). Erroneous data points were removed through a combination of automatic and manual editing using the ‘mbclean’ tool in the MB-System^{TM} software.

The completion of the application of these post-acquisition processing techniques was followed by recalculation of the bathymetry and the creation of ‘cleaned’ and processed swath files (Hogan, 2008; Fig. 2.3B). The MB-System^{TM} ‘mbgrid’ tool was then used to grid the processed bathymetry data at regular intervals and these grids were viewed and analysed using Generic Mapping Tools (GMT), ArcView and Erdas Imagine software. All the data from Hinlopen Trough were gridded with cell sizes of between 25 and 55 m, with the most landward region of the trough permitting the highest resolution.

Preset ping mode	Filename (.asvp)	Filename (.RDF)	Latitude (Degrees)	Longitude (Degrees)	Water Depth (m)	Salinity (p.s.u)
T7	20060728_191108	T7_00040	78°08.92'N	010°39.57'E	254	33.45
T7	20060813_192406	T7_00053	80°8.52881'N	17°15.74117'E	497	34.15
T5	20060809_103618.17726	T5_00050	81°12.2291'N	15°72.0479'E	1650	32.65
T7	20060807_033647	T7_00049	81°33.5306'N	21°674926'E	490	33.66

Table 2.1 - Table of XBT information used to calculate SVPs in Hinlopen Trough. The preset ping mode column describes whether T7 shallow water (<760 m) or T5 deep water (<1830 m) settings were used by the EM120 system

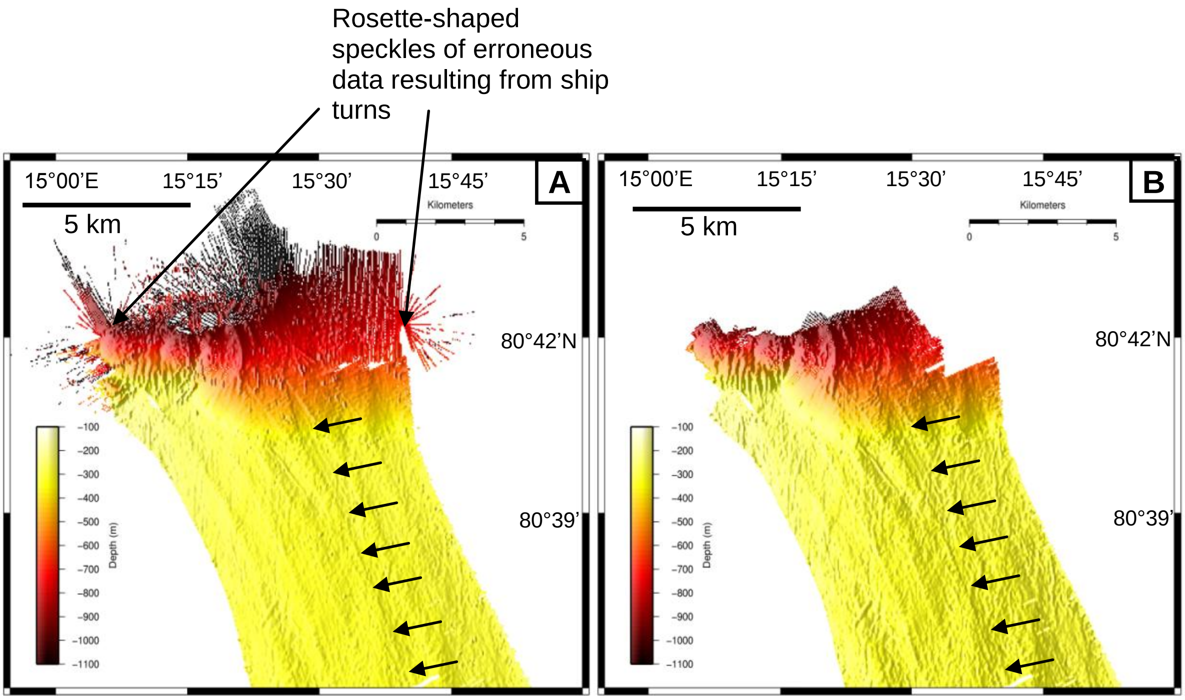

Figure 2.3 A) – Colour swath bathymetry image constructed from raw unprocessed bathymetry data at the northern extent of the surveyed area in Hinlopen Trough. 'Striped' artefacts resulting from unsuitable SVPs are arrowed.
B) – Colour swath bathymetric image constructed from processed bathymetry data at the northern extent of the surveyed area in Hinlopen Trough. Although some artefacts remain (arrowed), an obvious reduction in erroneous data points is apparent

2.2.3 Swath Data Interpretation

Although the majority of swath bathymetry data was analysed through qualitative assessments, some degree of quantification was possible through topographic analysis of submarine landforms within Geographical Information System (GIS) software applications. The complexities associated with qualitative assessments of sea floor morphology can be reduced through application of a glacier inversion model. This technique has been previously employed in a number of terrestrial and glacimarine investigations (e.g. Stokes and Clark, 1999; Ottesen and Dowdeswell, 2006; Ottesen et al., 2008; Hogan, 2008) and provides a structural framework for the classification and interpretation of glacigenic landforms.

This thesis utilised a simplified form of the glacial landsystem model to aid interpretations of past ice behaviour within Hinlopen Trough (Table 2.2). Individual landforms were classified into landform suites; that is, distinct groups of features formed during the same glacial event. The law of superimposition then enabled cross-cutting relationships to reveal the relative ages of these groups of landforms. Genetically-linked suites of landforms combine to form glacial landsystems (Benn and Evans, 1998; Ottesen and Dowdeswell, 2006; Ottesen et al., 2008; Hogan, 2008).

Process	Description
1. Identification	Identify submarine landforms, e.g. drumlin
2. Group into landform suites	Group landforms into suites of common origin and age, e.g. a suite of drumlins
3. Relative chronology	Examine cross-cutting relationships
4. Group into glacial landsystems	Group genetically linked landform suites into glacial landsystems, e.g. formed in the subglacial environment
5. Absolute chronology	Constrain absolute ages with dated samples from sediment cores, e.g. formed during the Late Weichselian glaciation
6. Correlation	Compare and correlate with other data sets in the region

Table 2.2 – A simplified glacial landsystem model (adapted from Hogan, 2008)

2.2.4 Swath Bathymetry and Submarine Landforms

High-resolution maps produced from swath bathymetry data have facilitated the identification and interpretation of a wide range of submarine landforms in the glacimarine record (e.g. Dowdeswell et al., 2002, 2004, 2010a, In Press A; Ottesen and Dowdeswell, 2006; Ottesen et al., 2005a, 2007, 2008; Shipp et al., 1999; Canals et al., 2000; Wellner et al., 2001; Evans et al., 2006; Hogan, 2008). A summary of these landforms is presented in Table 2.3.

Geomorphological data allow the maximum extent and flow directions of past ice sheets to be determined and can facilitate the identification of fast-flowing ice streams (Stokes and Clark, 1999; Dowdeswell and Ó Cofaigh, 2002; Dowdeswell et al., 2006; Ottesen et al., 2005a, 2007). Mapping the distribution of submarine landforms can also provide information about the form of the subglacial hydrological system and about the style of retreat of an ice mass (e.g. Dowdeswell et al., 2008). MSGLs are considered to represent the end point of a spectrum of elongate subglacial landforms (Schoof and Clark, 2008). This spectrum also contains less elongate sedimentary ridges, termed glacial lineations or flutes, and sedimentary drumlins. The mechanisms by which these features are formed remain enigmatic and several theories for their genesis have been proposed (e.g. Clark, 1993; Ó Cofaigh et al., 2005a; Schoof and Clark, 2008). Common hypotheses include origins through deformation of sediment by attenuation from a point source or from groove-ploughing of sediment by ice keels at the base of an ice mass (Ó Cofaigh et al., 2005a). A close association between MSGLs and areas of deformable sediment within cross-shelf troughs has been established. These features are, therefore, commonly regarded as diagnostic indicators of fast ice flow within former ice streams (Clark, 1993; Stokes and Clark, 1999, 2002; Canals et al., 2000; Ó Cofaigh et al., 2002, 2005a, b; Ottesen et al., 2005a; King et al., 2009; Dowdeswell et al., 2008, 2010a).

Glacial Landsystem	Landform	Description	Examples of Identification
Subglacial	Glacial lineations, mega-scale glacial lineations (MSGLs)/ flutes	Streamlined sedimentary ridges with high elongation ratios (>10:1), found in association with fast-flowing ice streams and the presence of deformation till. Precise mechanism of formation is enigmatic	Stokes and Clark, 1999; Canals et al., 2000; Ó Cofaigh et al., 2002, 2005a, b; Ottesen et al., 2005a, 2008; Dowdeswell et al., 2008, In Press A; Hogan et al., 2008
	Drumlins	Elongate ridges with higher and wider blunt faces and tapered lee sides. Precise mechanism of formation is enigmatic	Shipp et al., 1999; Wellner et al., 2001; Ó Cofaigh et al., 2005a; Dowdeswell et al, In Press A
	Crag-and-tails	Bedrock knobs with sedimentary tails, formed by fast ice flow over bedrock obstacles	Wellner et al., 2001; Ottesen et al., 2005a
	Hill-hole pairs	Glacitectonic landforms consisting of topographic depressions and adjacent down-flow sedimentary hills. Formed when freezing basal ice removes and subsequently deposits material from the sea floor	Ottesen et al., 2005a, 2007; Hogan, 2008; Dowdeswell et al., 2010a
	Crevasse-fill ridges	Rhombohedral ridges, formed by soft sediment injection into crevasses prior to glacier stagnation	Ottesen and Dowdeswell, 2006; Ottesen et al., 2008
	Meltwater channels and cavities	Erosional features formed by the presence of meltwater at the glacier bed	Ó Cofaigh et al., 2002, 2005a, b; Lowe and Anderson, 2003
	Eskers	Elongate sinuous ridges of sediment, formed by the in-filling of ice-walled channels	Ottesen and Dowdeswell, 2006; Ottesen et al., 2008
Ice-proximal	Terminal moraines	Ridges of diamictic sediments, representing the maximum extent of an ice mass	Ottesen et al., 2002, 2005a, 2007
	Lateral moraines	Ridges of diamictic sediment, representing the maximum lateral extent of an ice mass	Ottesen et al., 2005a, 2007
	Small transverse retreat ridges	Small recessional moraines, formed as annual push moraines during slow retreat of an ice mass	Ottesen and Dowdeswell, 2006; Ottesen et al., 2005a, 2007, 2008
	Grounding-zone wedges	Wedges of glacigenic sediment, representing major ice-front still-stands during retreat	Ó Cofaigh et al., 2005a; Ottesen et al., 2007
Ice-marginal	Iceberg ploughmarks	Irregular linear to curvilinear features formed by the grounding of iceberg keels on the sea floor	Barnes and Lien, 1988; Dowdeswell et al., 1993, In Press A; Polyak et al., 2001; Syvitski et al., 2001

Table 2.3 – Table of landforms previously identified in the glacimarine morphological record

2.3 TOPAS (TOpographic PArametric Sonar) Profiler Data

2.3.1 TOPAS PS 018 System

Sub-bottom acoustic profiling is a shallow seismic reflection technique which permits characterisation of the upper layers of sediment beneath the sea floor. It relies upon the generation and detection of acoustic waves; energy is reflected from acoustic boundaries within the sediment and is returned to the vessel where it is detected, processed electronically, and displayed as a measurement against time (Davis et al., 1997; Hogan, 2008). The resulting seismic profiles do not represent geological cross-sections of the strata; energy is reflected from boundaries in acoustic impedance within the sediment, not from geological boundaries. The strength of the reflected signal reveals the extent of the contrast in impedance between overlying and underlying material (Davis et al., 1997). The large proportions of coarse or bedded material within glacial successions can result in the scattering of a considerable amount of acoustic energy, thus limiting further penetration of the signal. Data artefacts, such as multiple horizons or the scattering of acoustic energy, are also frequently imaged from areas of rough topography or coarse material.

A Kongsberg TOPAS PS 018 sub-bottom profiler system was used to collect shallow seismic data during the JR142 geophysical cruise. This system operates at a frequency of 3.5 kHz, permitting high-resolution characterisation of the upper few tens of metres within unconsolidated sediments, but little deep penetration into any sedimentary substrates or bedrock. The resolution of the TOPAS PS 018 system is influenced by water depth and can produce horizontal and vertical resolutions of less than 5° by 5° and less than 30 cm, respectively (Hogan, 2008).

2.3.2 TOPAS Data Visualisation and Interpretation

Visualisation of the TOPAS data was performed using the tool swath_profile_utility.exe, which was developed by Toby Bentham at the Scott Polar Research Institute. This tool allowed acoustic profiles to be viewed alongside their corresponding ship tracks and enabled the straightforward correlation of TOPAS data with swath bathymetry and geological data. All TOPAS data obtained from Hinlopen Trough were then examined in the Kongsberg post-processing software TOPAS Mk II V1.0 and greyscale images were produced of the acoustic profiles.

The interpretation of shallow seismic profiler data in this thesis followed the framework developed by Damuth (1975, 1978, 1980) and used for comparable shallow geophysical datasets in many formerly glaciated regions (e.g. Elverhøi et al., 1998; Taylor et al., 2000; Kleiber et al., 2000; Hogan, 2008). This method involved the identification of discrete stratigraphic units called acoustic facies, together with a number of acoustic reflectors representing the boundaries between acoustic units. Acoustic facies and reflectors were defined based upon a number of criteria, including the internal structure of each unit, the configuration and continuity of any internal reflectors, the fill style, and the external morphology of each unit (Damuth, 1975, 1978, 1980; Davis et al., 1997; Hogan, 2008).

2.4 Geological Data

2.4.1 Core Lithostratigraphy and Gravity Cores

Core lithostratigraphy can be used to identify the products of certain glacimarine processes within the sedimentary record and can allow spatial and temporal patterns of sedimentation to be inferred. The interpretation of geological data also permits correlation between the acoustic stratigraphy and the lithostratigraphy of an area.

Sediment descriptions allow glacimarine deposits to be divided into facies - individual units possessing distinctive properties that allow differentiation from overlying and underlying sediments (Benn and Evans, 1998). Sedimentary facies can be combined to form facies associations – genetically related units of sediment emplaced in an unbroken vertical succession (Benn and Evans, 1998). Cycles of ice-sheet growth and decay can, therefore, produce characteristic 3-D patterns of sedimentary facies, formed by the changing proximity of the ice front to the core site (Dowdeswell and Scourse, 1990).

Four sediment cores, between 80 and 266 cm in length, were recovered from the sea floor of Hinlopen Trough during the JR142 geophysical cruise (Fig. 2.4 and Table 2.4).

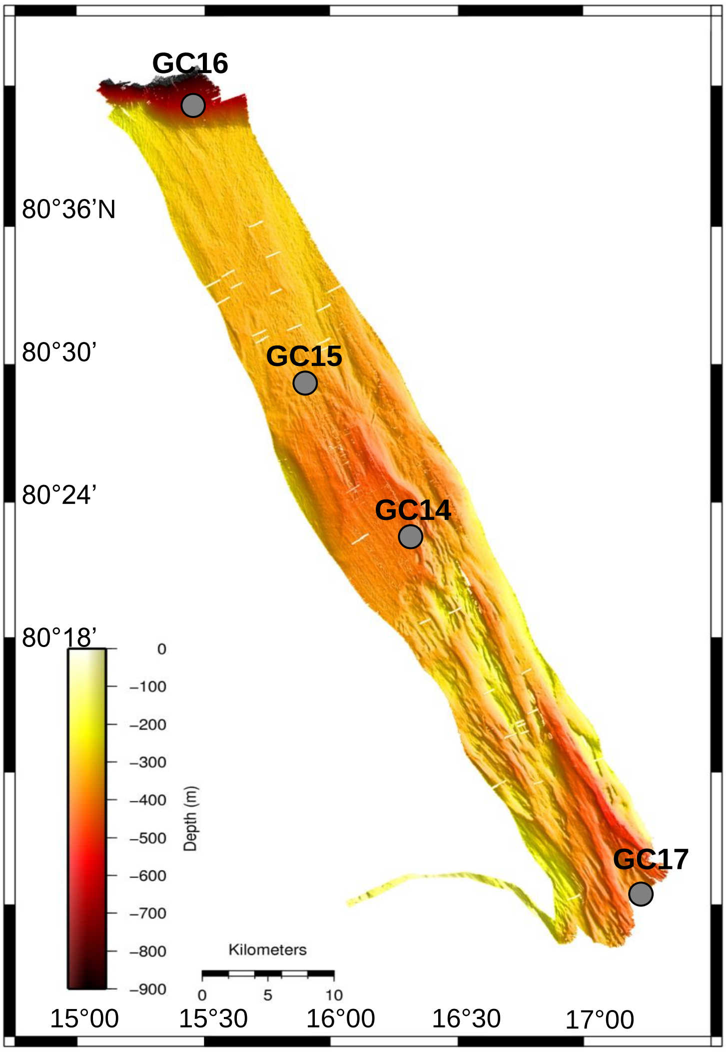

Figure 2.4 – Locations of the four sediment cores recovered from Hinlopen Trough

Core Number	Latitude (Degrees decimal)	Longitude (Degrees decimal)	Water Depth (m)	Core Recovery (cm)
GC14	80 23.460	16 26.450	352	266
GC15	80 30.740	15 54.040	345	210
GC16	80 42.000	15 36.500	728	80
GC17	80 08.680	17 10.870	462	219

Table 2.4 – Details of the four sediment cores recovered from Hinlopen Trough

2.4.2 Core Preparation and Interpretation

The cores were split, cleaned, described and photographed at the British Ocean Sediment Core Research Facility (BOSCORF) laboratory in Southampton. One intact bivalve was identified from these cores, but was not considered large enough to permit radiocarbon dating. Sediments were described according to a number of macro-sedimentological criteria, including clast fabric, sediment colour, the nature of unit contacts, and the presence of macrostructures.

Core logging followed a modified version of Eyles et al.'s (1983) sediment classification scheme. This system reduces the complexities of sediment description by allocating standardised lithofacies codes to units of sediment (Table 2.5). The Eyles et al. classification scheme is based upon a four-part code whereby different letters indicate the basic subdivisions of sediment into diamicts, gravels, sands and fines. Additional letters are then used to signify the internal structure of each facies. X-radiographs of the cores were produced at the East Midlands Airport, and were used to support visual observations of clast content and internal structures.

A number of quantitative measurements were also obtained from the geological data. Sediment samples were taken from the cores and analysed using a Malvern Mastersizer Particle Size Analyser at the Geography Department, University of Cambridge. This technique uses laser diffraction to measure the grain size of particles with diameters between 0.02 and 2000 µm.

Lithofacies	Description
Diamict	
Dm	Massive, matrix-supported diamict. Diamicts are defined as poorly-sorted sediments containing a range of particle sizes
Dc	Massive, clast-supported diamict
Fine-grained mud	
Fm	Massive fine-grained mud
Fmd	Massive fine-grained mud with clasts
Fm(d)	Massive fine-grained mud with rare clasts
Fs	Stratified fine-grained mud. Stratification is defined as banding of layers with widths of more than 1 cm, whereas lamination is defined as banding of layers between 0.1 and 0.9 mm in width (Eyles et al., 1983, in Ó Cofaigh and Dowdeswell, 2001)
F(s)	Weakly-stratified fine-grained mud

Table 2.5 - Table describing the different lithofacies identified within the four cores recovered from Hinlopen Trough. (Adapted from Eyles et al., 1983)

Magnetic susceptibility and colour information were obtained at intervals of 1 cm from the sediment cores using a non-destructive ITRAX micro-X-ray fluorescence core scanner at BOSCORF, Southampton. Magnetic susceptibility measurements record the ability of sediment to become magnetised and generally serve to parallel records of the coarse material content (Nørgaard-Pedersen et al, 2009).

Whereas visual descriptions record a subjective measure of sediment colour, laser spectrophotometry methods digitally record and assign uniform values to sediment colour. The ITRAX scanner presents these colour values in both the Munsell and the Commission Internationale de l'Eclairage (CIE) L* a* b* classification systems (Nederbragt et al., 2006). Lightness (L*) values are measured on a scale from black (0) to pure white (100) and typically mimic variations in greyscale reflectance (nm) (Nederbragt et al., 2006). These variables provide reasonable proxies for the organic carbon, carbonate and clay content of cored sediments (Bond et al., 1992; Cortijo et al., 1995; Cowan et al., 1999; Møller et al., 2001). The colour hue of the sediment is represented by the a* and b* measurements. Values for a* range from pure red (-60) to pure green (60), whilst b* values range from pure blue (-60) and pure yellow (60) (Nederbragt et al., 2006). Variations in these parameters often reflect the changing mineralogical, diatomaceous or organic composition of sediment (Nederbragt et al., 2006).

The ITRAX core scanner performed well during the majority of data acquisition. Infrequent data gaps occurred as a result of the uneven and clast-rich nature of the sediment, which prohibited contact between the scanner and the core surface. The limitations of sediment cores include under-sampling of geological data, which may prevent correlation of geological data with all identified acoustic facies, and the poor aerial coverage inherent within this point-source method of data collection. The use of contemporary models of glacimarine sedimentation to infer the nature of former processes and patterns of sedimentation rests upon the assumption that analogous links can be established between ancient and modern glacimarine systems (Dowdeswell and Scourse, 1990; Hogan, 2008). Despite the successful application of this approach in a number of glacimarine investigations, it should be noted that the record can become complicated when a variety of processes result in the creation of similar sedimentary signals or when multiple processes act contemporaneously.

Chapter 3 – Submarine Landforms

3.1 Regional Bathymetry

The bathymetric depression of Hinlopen Trough is depicted in its regional context on Svalbard's northern margin in Fig. 3.1. The first-order morphology of this area is consistent with the large-scale topography of Svalbard's continental margins; cross-shelf troughs branch out from the interior of the archipelago, dissecting the broad and relatively shallow continental shelf before terminating at the shelf edge (Ottesen et al., 2007).

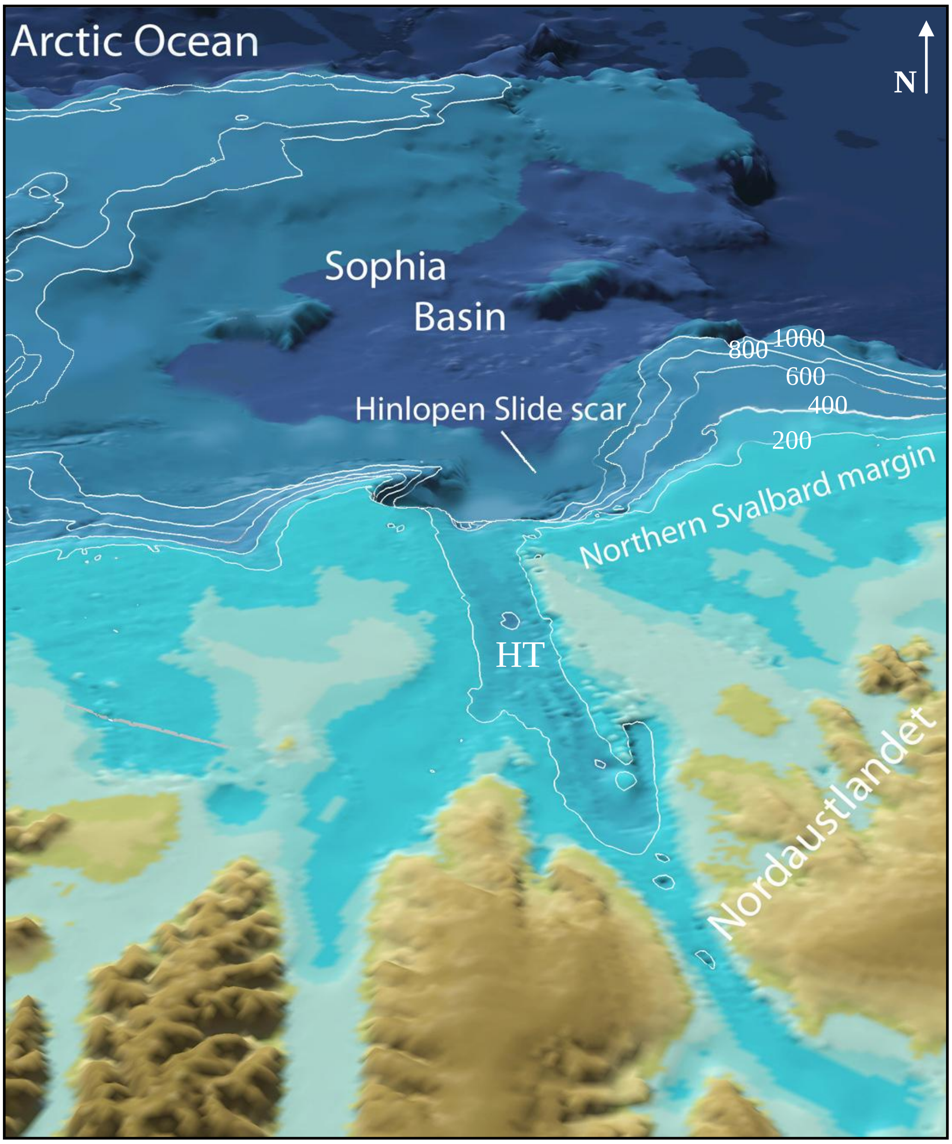

Figure 3.1 – The regional bathymetry of Hinlopen Trough (HT). Adapted from Dowdeswell et al., In Press A

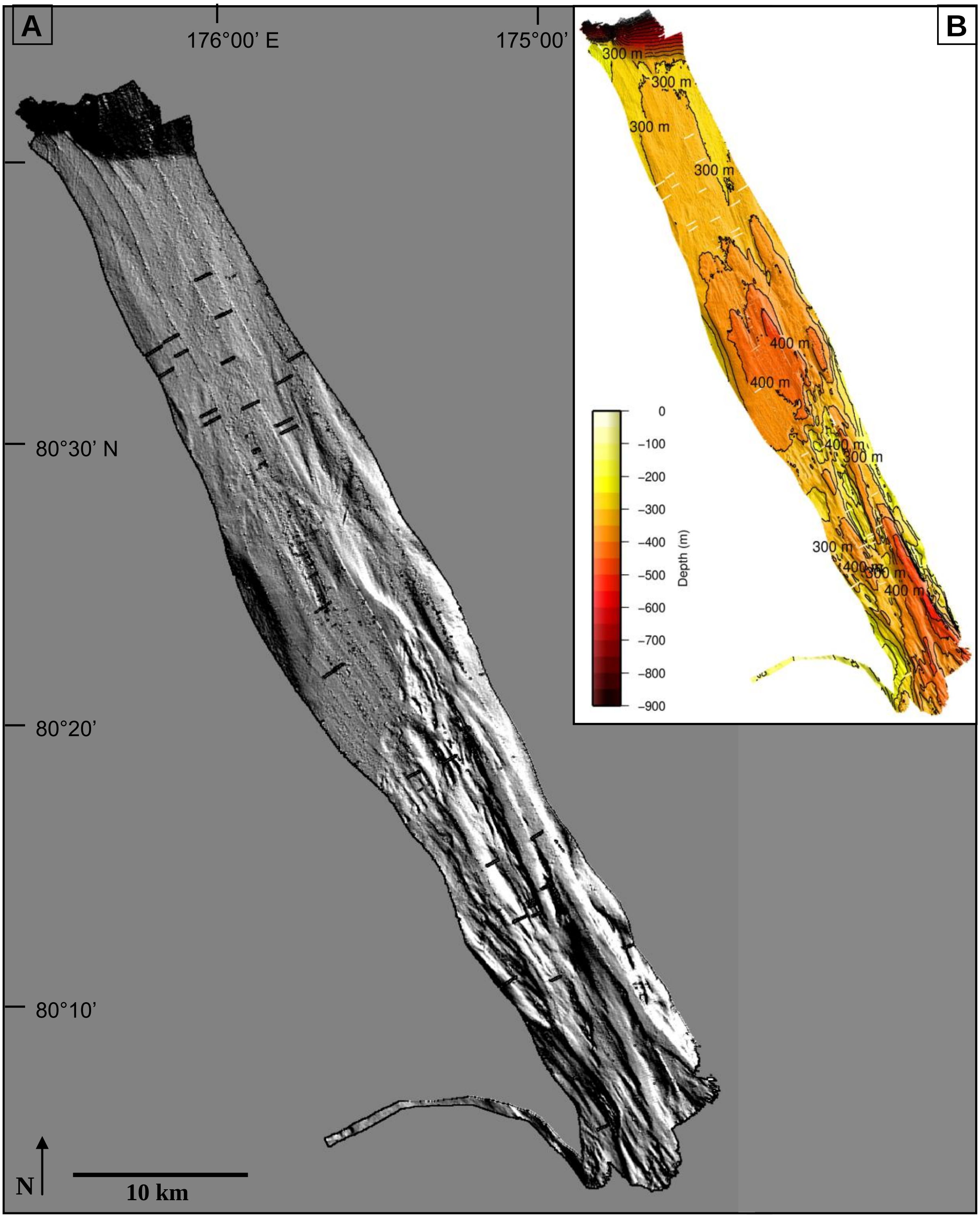

Figure 3.2 A) – Swath bathymetric greyscale shaded relief image of Hinlopen Trough. Black oblongs illustrate data gaps (Illumination from the west, data gridded at 50 m) B) – Contoured colour swath bathymetric image of the surveyed area

Hinlopen Trough traverses the continental shelf in a north-north-westerly direction, before terminating at the shelf edge in the form of a slump headwall eroded back into the margin (Vanneste et al., 2006; Winkelmann et al., 2008a). The majority of the 70 km long trough exhibits water depths between 200 and 400 m (Figs. 3.1 and 3.2).

Swath bathymetric images reveal the presence of a number of submarine landforms superimposed upon the large-scale morphology of Hinlopen Trough (Figs. 3.2 and 3.3). Along-trough differences in the types of imaged landforms and in the composition of the sea floor are apparent, suggesting three main morphological zones. First, the inner-shelf of the trough is characterised by a rugged and uneven terrain, depicted in Figure 3.3E by the contrasting bright and shadowed areas of the sea floor. The swath bathymetric images and sub-bottom acoustic profiles suggest that the sea floor in the inner-trough region is at least partially composed of exposed bedrock.

The transition from bedrock to a sedimentary substrate represents a boundary between the inner- and middle-shelf areas of the trough, and is marked by a distinctive change in the nature of the sea floor (Fig. 3.3D). The middle-shelf area of Hinlopen Trough, a second major zone, is characterised by a deep basin containing several NNW-SSE trending linear features and is bordered on one side by a prominent topographical high (Fig. 3.3C). This basin possesses a gently undulating sea floor surface and is most likely composed of unlithified sediment.

Thirdly, the sea floor in the outer-shelf area is relatively flat and is composed of a sedimentary substrate. The surface of the sea floor appears to be disturbed by a large number of iceberg keel ploughmarks (Figure 3.3B).

3.2 Submarine Landforms in Hinlopen Trough

High resolution bathymetric mapping has revealed an extensive pattern of submarine landforms on the sea floor of Hinlopen Trough (Fig. 3.2). These features include sedimentary elongate streamlined landforms, bedrock streamlined landforms, and iceberg keel ploughmarks.

3.2.1 Description of Sedimentary Elongate Streamlined Landforms

The sedimentary elongate streamlined landforms identified within Hinlopen Trough can be divided into crude parallel-sided sedimentary features and drumlinised features. Both types of landform are located on the middle-shelf area of the trough (Fig. 3.4).

Crude parallel-sided landforms. A flowset of low-relief parallel-sided landforms is located at the western margin of the middle-trough area, orientated in a N - S direction (Figs. 3.4). Vertical profile data (Fig. 3.5) reveal that these features are characterised by heights of 7 to 12 m and widths of up to 300 m. These landforms vary in length from 1.8 to 3 km, with elongation ratios of up to 20:1. Sub-bottom acoustic profiling reveals that these features are formed in an acoustically semi-transparent unit, overlying an acoustically impenetrable reflector.

Drumlinised landforms. Crudely drumlinised landforms are present in two locations on the middle-shelf. They occur immediately down-flow from the deepest part of the middle-shelf, and are also evident on the eastern side of the trough, formed within, as well as just down-flow from, a prominent bathymetric ridge (Figs 3.3 - 3.6). These landforms demonstrate elongation ratios of around 15:1 and display a characteristic drumlinised form, with blunt stoss sides and tapered down-flow lee ends. They are orientated in a NNW-SSE direction and are formed in an acoustically semi-transparent unit, overlying an acoustically impenetrable reflector (Fig. 3.4). Vertical profile data (profile B – B’ in Fig. 3.5 and profile A – A’ in Fig. 3.6) demonstrates that these features have heights of up to 20 m, widths between 200 and 1000 m, and lengths ranging from 2.3 to 7.5 km.

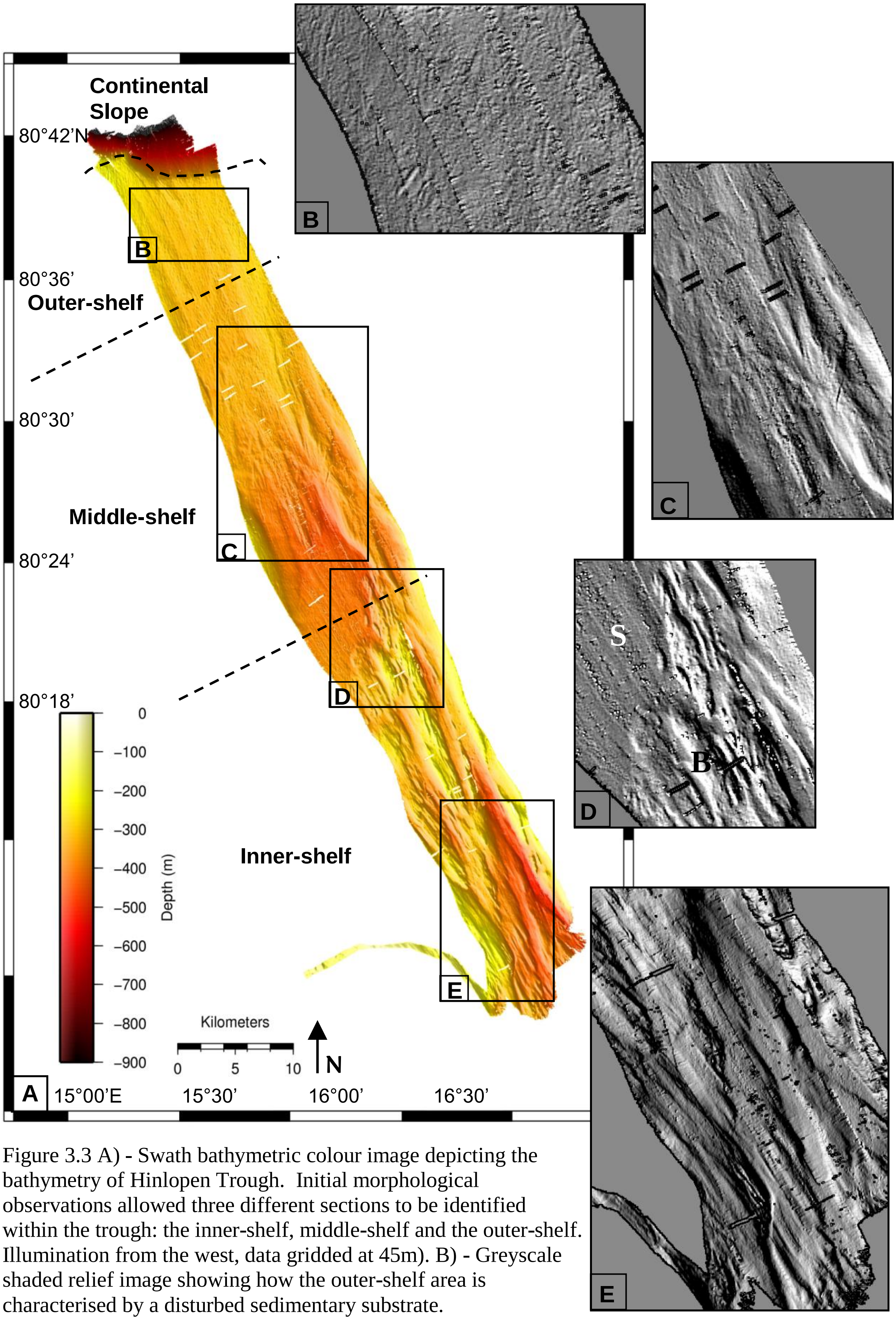

Figure 3.3 A) - Swath bathymetric colour image depicting the bathymetry of Hinlopen Trough. Initial morphological observations allowed three different sections to be identified within the trough: the inner-shelf, middle-shelf and the outer-shelf. Illumination from the west, data gridded at 45m). B) - Greyscale shaded relief image showing how the outer-shelf area is characterised by a disturbed sedimentary substrate.
C) - Greyscale shaded relief image showing how the middle-shelf region is dominated by linear bedforms down-flow from a topographical depression. D) - Greyscale shaded relief image depicting the middle- to inner-shelf transition from a sedimentary (S) to crystalline bedrock (B) substrate.
E) - Greyscale shaded relief image showing how the inner-shelf area is characterised by rugged streamlined topography and a crystalline bedrock substrate

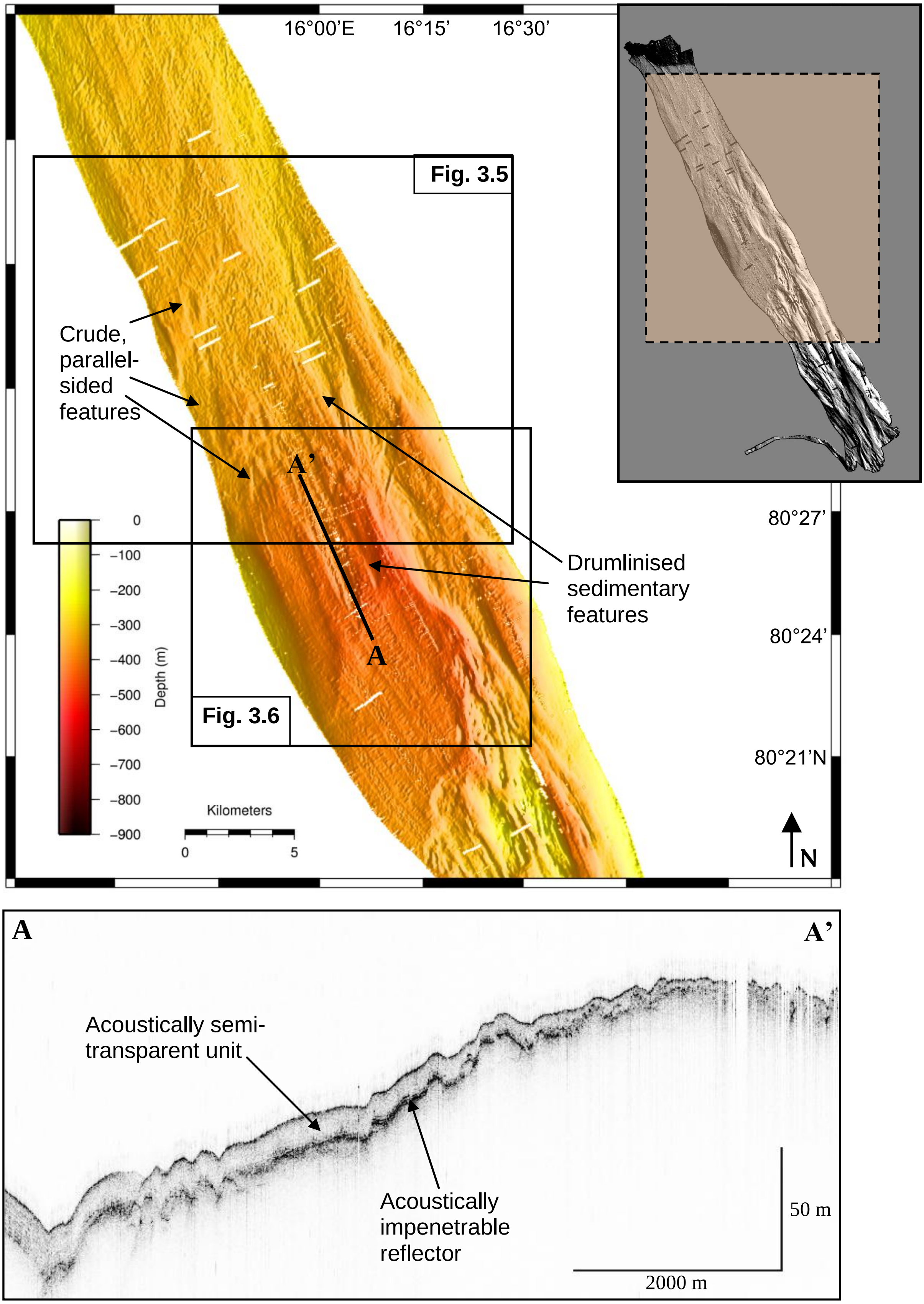

Fig. 3.4 – Colour swath bathymetric image of the middle-shelf area showing the locations of the elongate and drumlinised sedimentary bedforms. Profile A – A' demonstrates how these features are formed in an acoustically semi-transparent unit, overlying an acoustically impenetrable reflector

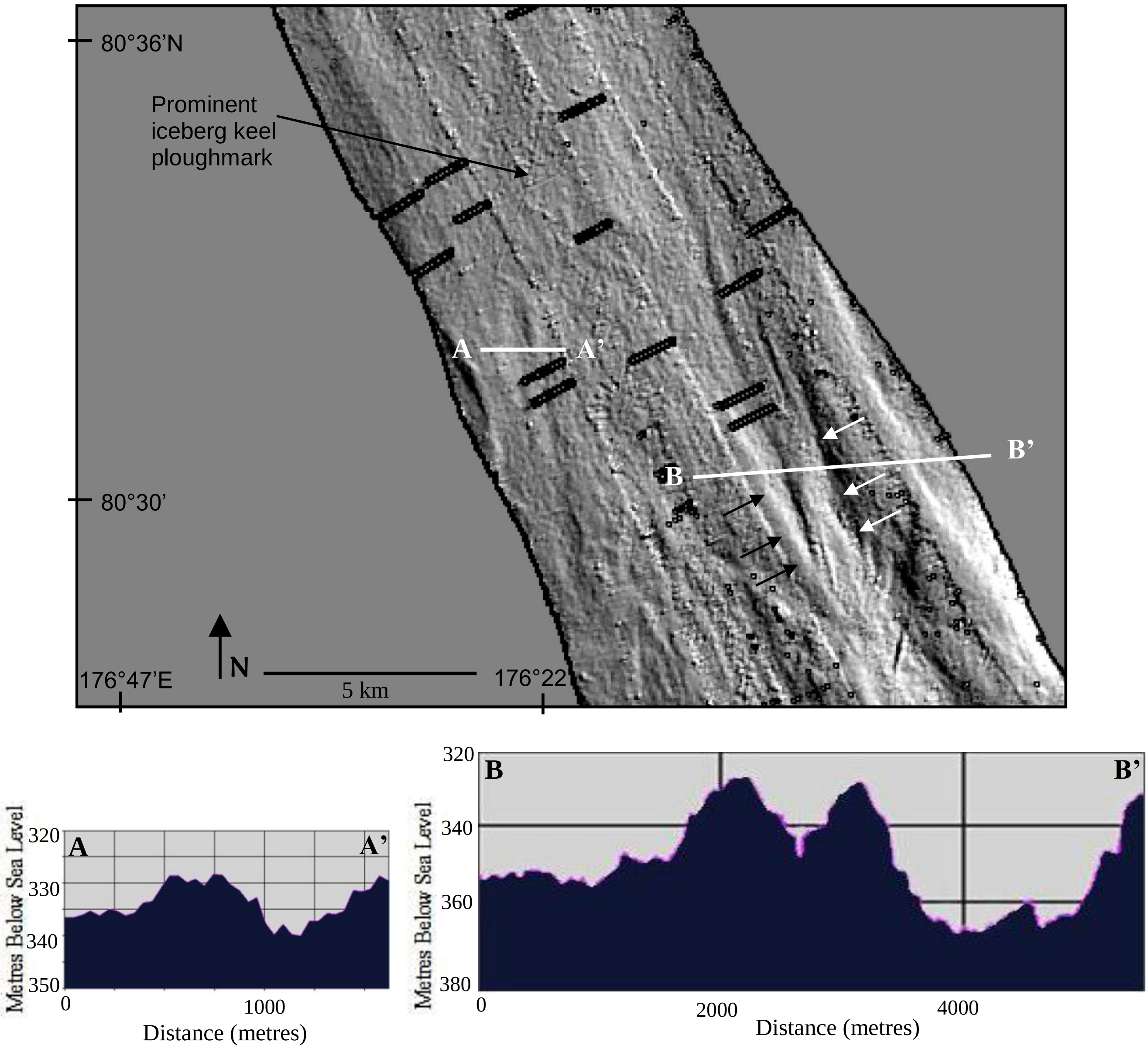

Figure 3.5 – Swath bathymetric greyscale shaded relief image of the crude elongate sedimentary bedforms and drumlinised bedforms (arrowed) identified in the middle-shelf area of Hinlopen Trough. (Illumination from the west, data gridded at 50m). Vertical profile data across the streamlined bedforms is also given for profiles A –A' and B- B'.

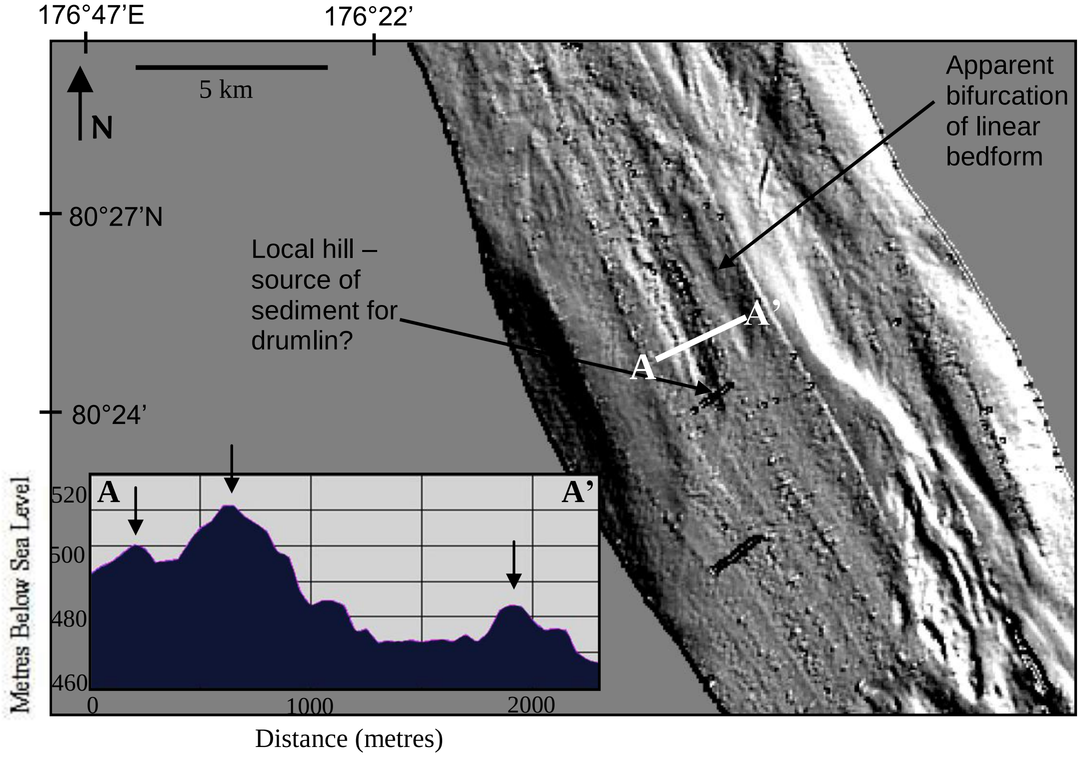

Figure 3.6 – Swath bathymetric greyscale shaded relief image of some of the drumlinised sedimentary bedforms identified in the middle-shelf area of Hinlopen Trough (Illumination from the west, data gridded at 55m). Vertical profile data across the streamlined bedforms (arrowed) is also given for profile A –A'.

3.2.2 Interpretation of Sedimentary Elongate Streamlined Landforms

Crude parallel-sided landforms. The location of the crude parallel-sided landforms just down-flow from the deepest area of the middle-shelf, their formation in a sedimentary rather than a bedrock substrate, and their high elongation ratios suggest that these features are glacial lineations formed at the former ice-sheet bed. In other Arctic and Antarctic locations, the onset of glacial lineations typically occurs close to the outer-shelf, beyond the transition from crystalline bedrock to a softer sedimentary substrate, due to the availability of deformable sediment (Wellner et al., 2001; Ottesen et al., 2005a). Elongate landforms also characteristically form in the deepest areas of the shelf, where thicker ice can lead to the presence of water at the bed and increased ice movement by till deformation and basal sliding (Ó Cofaigh et al, 2005a). High elongation ratios of up to 20:1 imply that these landforms record the former presence of fast ice-stream flow (Clark, 1993; Stokes and Clark, 2002; Dowdeswell et al., 2010a).

The N-S trending lineations in Hinlopen Trough are an order of magnitude smaller than the MSGLs described from the formally-glaciated continental margins of Antarctica and from other areas of the Arctic (e.g. Shipp et al., 1999; Canals et al., 2000; Ó Cofaigh et al., 2002; 2005a; Jakobsson et al., 2005; Evans et al., 2006; Dowdeswell et al., 2010a). Whilst the lineations in Hinlopen Trough do not exceed 3 km in length, these other MSGLs are described to have lengths of several tens of kilometres (Wellner et al., 2001; Ottesen et al., 2005a; Dowdeswell et al., 2010a; In Press A). MSGLs have also been described from Svalbard's continental margins, reaching lengths of over 10 km in the cross-shelf troughs of Bellsund, Isfjorden, and Kongsfjorden (Ottesen et al., 2007).

The imaged glacial lineations are, instead, similar in size and morphology to crudely-formed parallel-sided features identified by Hogan (2008) on Svalbard's eastern margin. These lineations, which exhibit heights of 2 to 8 m and lengths of up to 7 km, were interpreted as megaflutes – elongate sedimentary landforms possessing greater lengths than flutes, but smaller dimensions than MSGLs (Hogan, 2008). The landforms observed in Hinlopen Trough are, therefore, interpreted as megaflutes and are understood to have been produced within deforming sediments at the base of a former ice stream (Dowdeswell et al., 2004; Schoof and Clark, 2008). Evidence for this method of formation is provided from analogous data from the beds of deglaciated continental shelves (e.g. Elverhøi et al., 1995; Shipp et al., 1999; Canals et al., 2000; Ó Cofaigh et al., 2002; 2005a; Dowdeswell and Elverhøi, 2002; Dowdeswell et al., 2010a) and also from investigations of the beds of active modern ice streams (King et al., 2009).

Drumlinised landforms. The location of the drumlinised sedimentary landforms just down-flow from the deepest area of the middle-shelf and their relatively high elongation ratios of around 15:1 support a subglacial origin associated with the operation of streaming ice flow and a deformable substrate. The bifurcation observed in these sedimentary bedforms provides additional evidence of their formation by deformation of a soft substrate, and is most likely related to a change in either bed topography or in ice dynamics (Hogan, 2008).

The characteristic shape of these landforms, with blunt stoss sides and tapered down-flow tails, facilitates their interpretation as sedimentary drumlins (e.g. Shipp et al., 1999; Clark et al., 2009; Dowdeswell et al, In Press A). The categorisation of these features conflicts with that of Ottesen et al. (2007), who interpreted these elongate features as MSGLs. Whilst their large elongation ratios may support such an analysis, the drumlinised shape of these features precludes this interpretation. Drumlins typically possess lower elongation ratios (between 3:1 and 6:1) than glacial lineations (Hogan, 2008; Dowdeswell et al., 2010a). The relatively large elongation ratios (around 15:1) exhibited by the drumlins in Hinlopen Trough, combined with their extensive lengths of over 7 km, suggests that these landforms represent highly attenuated drumlins (Ó Cofaigh et al., 2005a).

Drumlins are frequently identified in transitional regions between crystalline and sedimentary substrates (Wellner et al., 2001; Ó Cofaigh et al., 2002), and their presence is often interpreted to indicate a former zone of ice acceleration (Shipp et al., 1999). The identification of attenuated sedimentary drumlins in the middle-shelf area of Hinlopen Trough implies, therefore, the former initiation of fast-flowing ice in this location. Whereas the glacial lineations only provide simple orientation information, the streamlined shape of the drumlins in Hinlopen Trough indicates an absolute direction of flow and confirms that ice flowed through the trough from the south towards the shelf break in the north.

Both the parallel-sided and drumlinised sedimentary landforms in Hinlopen Trough are interpreted to have formed in association with the last ice advance across Svalbard’s northern continental margin from an ice centre on the archipelago during the Late Weichselian glaciation (e.g. Svendsen et al., 2004; Ottesen et al., 2007; Dowdeswell et al., 2010a). This interpretation is supported by the fresh appearance of the bedforms on swath bathymetric images and the relatively thin layer of Holocene sediment cover apparent on the acoustic profiler data (Fig. 3.4).

3.2.3 Description of Bedrock Streamlined Landforms

A number of crude lineations and drumlinised landforms have been imagined within the inner-shelf area of Hinlopen Trough (Fig. 3.7). These landforms are located in the inferred bedrock region of the trough and are associated with an acoustically impenetrable surface reflector, often conformably overlain in bathymetric depressions by a thin acoustically semi-transparent unit (Profile B – B' Fig. 3.7).

Drumlinised Bedrock Landforms. A well-defined flowset of drumlinised landforms is present at the most land-ward end of the inner-shelf (Fig. 3.7C). These landforms possess a NW orientation and are characterised by lengths between 1.5 and 2.5 km. Vertical profile data (Fig. 3.7) demonstrate that these features have heights of up to 40 m and widths of around 500 m, producing elongation ratios of between 3:1 and 5:1.

Linear Bedrock Landforms. The morphology of the inner-shelf area of Hinlopen Trough is dominated by the presence of many crudely-formed linear ridges and grooves (Fig. 3.7A). The orientation of these linear bedrock features exhibits variation both across and along the trough. Bedforms at the most landward end of the surveyed area possess a greater degree of across-trough variation in orientation (arrowed in Fig. 3.7A). Features located close to the mid-point of the trough's width are orientated in a NW direction, while the bedforms close to the left margin of the trough exhibit a progressively larger degree of orientation to the west. Landform orientation is shown to become more uniform down-trough, with the majority of these streamlined features exhibiting NW orientations.

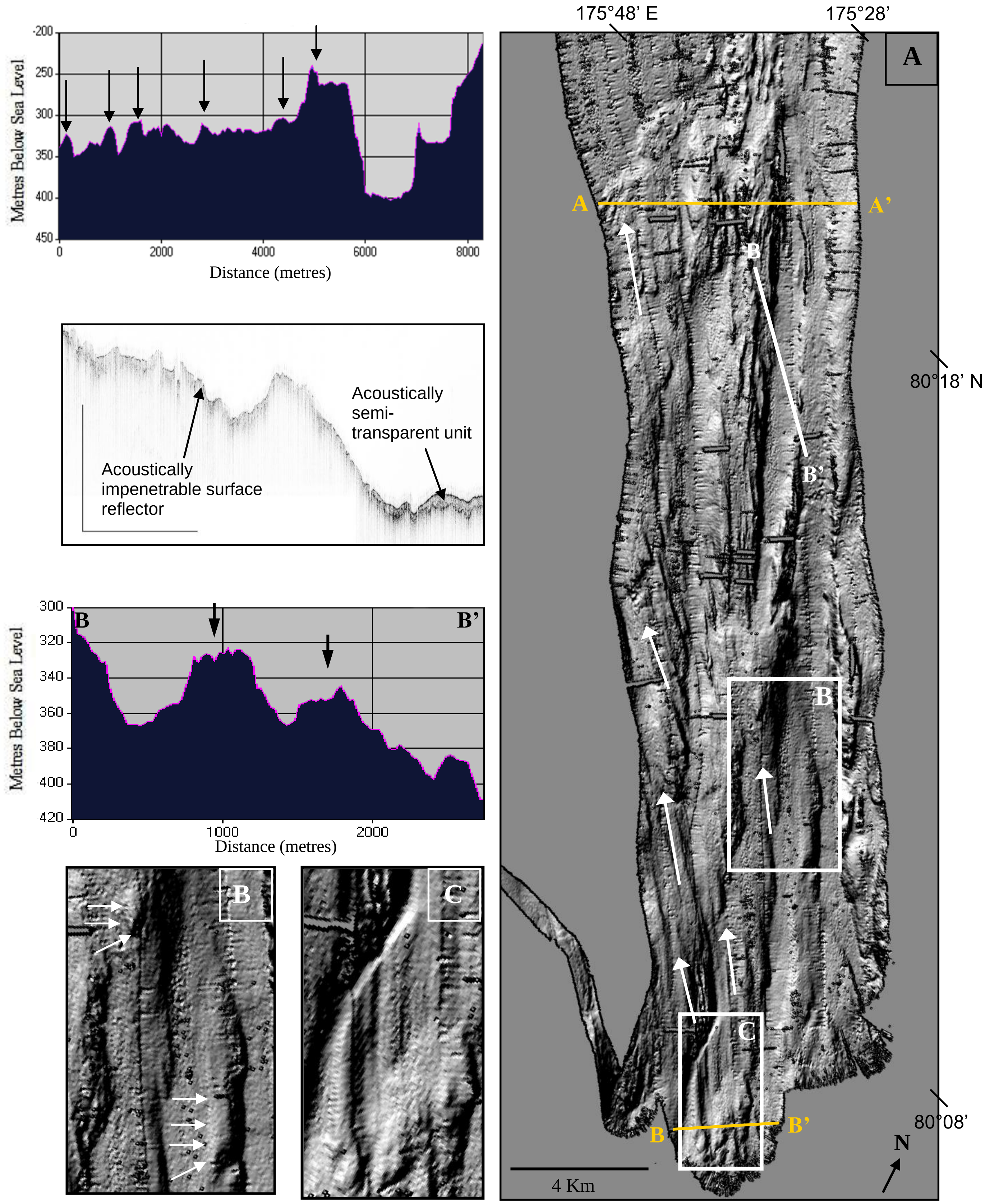

Figure 3.7 A) - Swath bathymetric greyscale shaded relief image of the ice-sculpted inner-shelf area in Hinlopen Trough (Illumination from the west, data gridded at 28 m). The direction of inferred former ice flow is indicated by the white arrows. Vertical profile data for profile A – A' shows the rugged nature of the terrain in this section, enhanced by the presence of many small streamlined ridges (arrowed in profile A – A'). Profile B – B' displays acoustic profiler data, showing the nature of the seafloor in this area. Vertical profile data for profile C-C' illustrates the dimensions of the identified bedrock drumlin features (arrowed). B)- Shaded relief image of bedrock knobs (arrowed). C) - Shaded relief image of bedrock drumlins.

3.2.4 Interpretation of Bedrock Streamlined Landforms

Drumlinised bedrock landforms. The characteristic shape of the drumlinised landforms, combined with their low elongation ratios and formation in a bedrock substrate, indicates that these features are bedrock drumlins. Although rarely identified on Svalbard's continental margins (Ottesen et al., 2007; Hogan, 2008), drumlins formed within bedrock areas of cross-shelf troughs have been identified from many areas of the Antarctic continental shelf (e.g. Shipp et al., 1999; Wellner et al., 2001; Lowe and Anderson, 2003; Ó Cofaigh et al., 2005a; b; Evans et al., 2006), often representing one extreme of a down-trough landform progression from bedrock drumlins, to sedimentary drumlins, to glacial lineations (Ó Cofaigh et al., 2002). The presence of bedrock drumlins in Hinlopen Trough indicates that ice advanced across the inner-shelf area, but was unable to produce the glacial lineations indicative of fast flow due to an absence of an easily-eroded or deformable substrate.

Linear bedrock landforms. The ridges and grooves that are superimposed upon the rugged bathymetry of the inner-shelf are interpreted as ice-sculpted bedrock, formed from the erosional action of ice over the pre-existing topography. The orientation of these linear landforms (Fig. 3.7A) varies across the survey area and suggests that ice flow followed the structural grain of the rock as it eroded into the underlying bedrock. These chaotic former ice directions contrast to the more uniform orientations of the glacial lineations formed in the sedimentary substrate, where the direction of flow was orientated almost directly offshore (Wellner et al., 2001). This region of sculpted bedrock terrain may also include other intermediate-scale erosional landforms, such as roché moutonnés and meltwater channels, which are difficult to identify at the resolution of our swath bathymetric images (Hogan, 2008).

3.2.5 Description of Large- and Small-Scale Linear to Curvilinear Landforms

The outer-shelf area of Hinlopen Trough is heavily scoured by a multitude of large- to small-scale linear to curvilinear landforms. The sea floor close to the continental shelf edge is the most densely scoured location within the trough (Fig. 3.8). The majority of the ploughmarks are orientated in a NW-SE or NE - SW direction and possess berms either side of the main depression of up to 6 m in height (Fig. 3.9B).

Two different types of ploughmark have been identified from swath bathymetric images (Figs. 3.8 and 3.9). Type 1 ploughmarks typically exhibit depths of 5 to 12 m, sea floor widths of less than 40 m, and lengths of 930 to 3500 m. Type 2 ploughmarks display similar lengths to Type 1 features, but possess characteristic deeper and wider flat-bottomed depressions of up to 20 m in depth and 200 m wide. Both types of ploughmark exist in contemporary water depths shallower than 400 m, but occur most frequent in water depths between 200 and 300 m.

A prominent Type 2 ploughmark is shown to crosscut the top of a large topographic ridge in the middle-shelf area of the trough (Fig. 3.10). This feature is the widest and deepest ploughmark identified within Hinlopen Trough, possessing depths of around 20 m and a basal width of more than 200 m.

3.2.6 Interpretation of Large- and Small-Scale Linear to Curvilinear Landforms

The linear to curvilinear landforms observed in the outer- and middle-shelf areas of Hinlopen Trough are interpreted to have formed from the ploughing action of the keels of icebergs as they grounded on the sea floor. Iceberg scour marks are common features in the glacimarine morphological record and can provide information on the former dimensions and travel paths of icebergs (e.g. Barnes and Lien, 1988; Dowdeswell et al., 1993; In Press A; Polyak et al., 1997, 2001; Syvitski et al., 2001; Jakobsson et al., 2005; Jokat et al., 2005; Kuijpers et al., 2007).

The keels of contemporary icebergs around northern Svalbard rarely exceed 100 m in depth (Dowdeswell and Forsberg, 1992; Solheim, in Davis et al., 1997; Polyak et al., 2001). Assuming a maximum glacial sea level lowering of 120 m, the ploughmarks identified in Hinlopen Trough would have made contact with the sea floor at between 80 and 300 m. These depths far exceed the dimensions of contemporary icebergs in this area and suggest that the ploughmarks represent relic features produced during the deglaciation of Hinlopen Trough at the end of the Late Weichselian. The fresh appearance of the iceberg scours, combined with their superimposition on top of the elongate bedforms and the limited sediment infilling of their depressions, also constrains their time of formation to the end of the last glacial period. The high density of scouring towards the shelf break suggests that iceberg calving acted as the dominant process of mass loss during deglaciation.

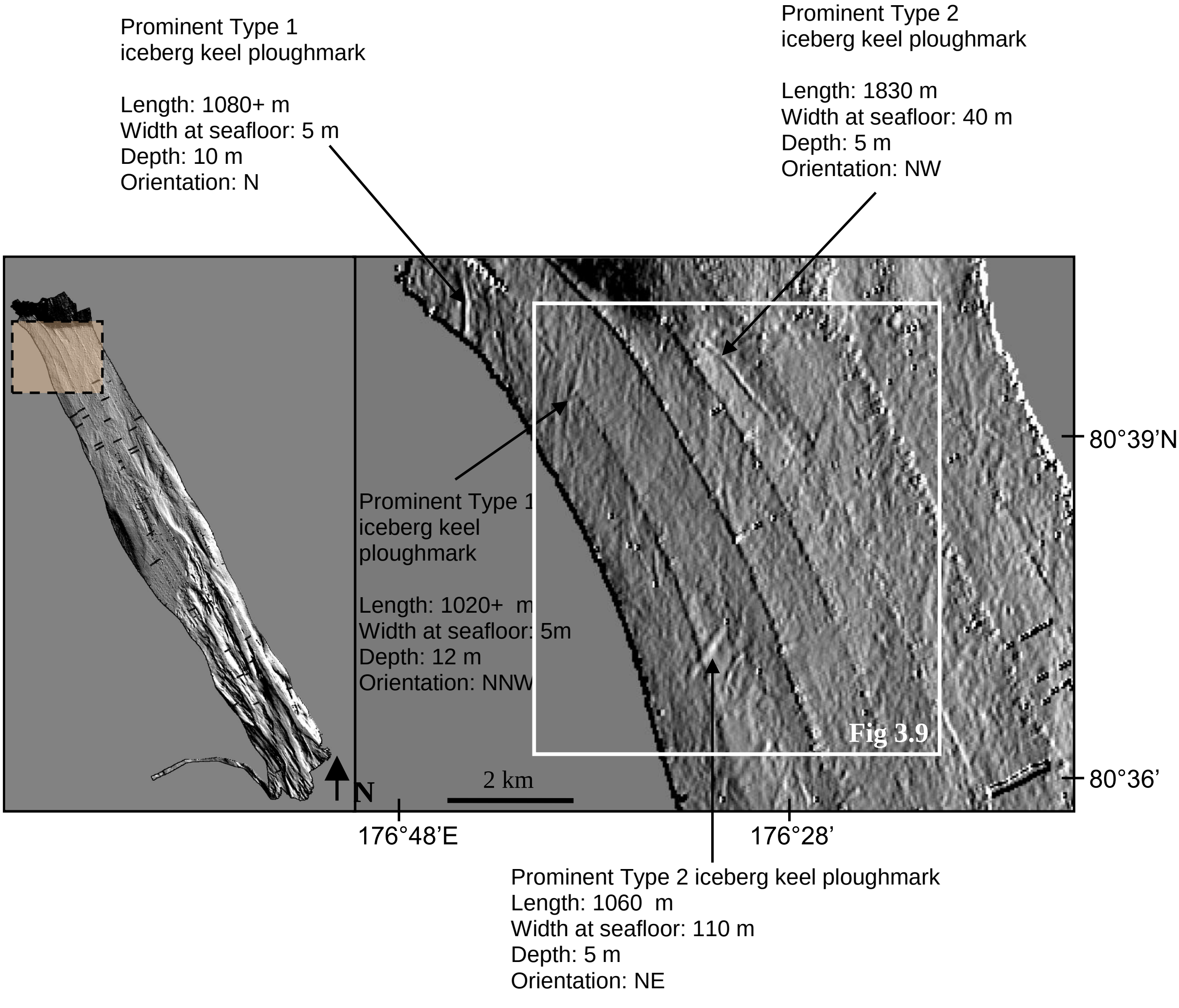

Figure 3.8 – Swath bathymetric shaded relief image depicting the location of the most densely-scoured region of the outer shelf (Illumination from the west, data gridded at 30 m). Annotations describe the dimensions of four prominent iceberg keel ploughmarks

The dominant NE-SW orientation of the scours suggests that the icebergs were derived mainly from the ice streams within Hinlopen Trough and Wijdefjorden Trough before travelling across the shelf break in a north-easterly direction, possibly influenced by the course of the West Spitsbergen Current (Cherkis et al., 1992). The wider Type 2 ploughmarks probably represent grounding events from larger tabular icebergs (Hogan, 2008).

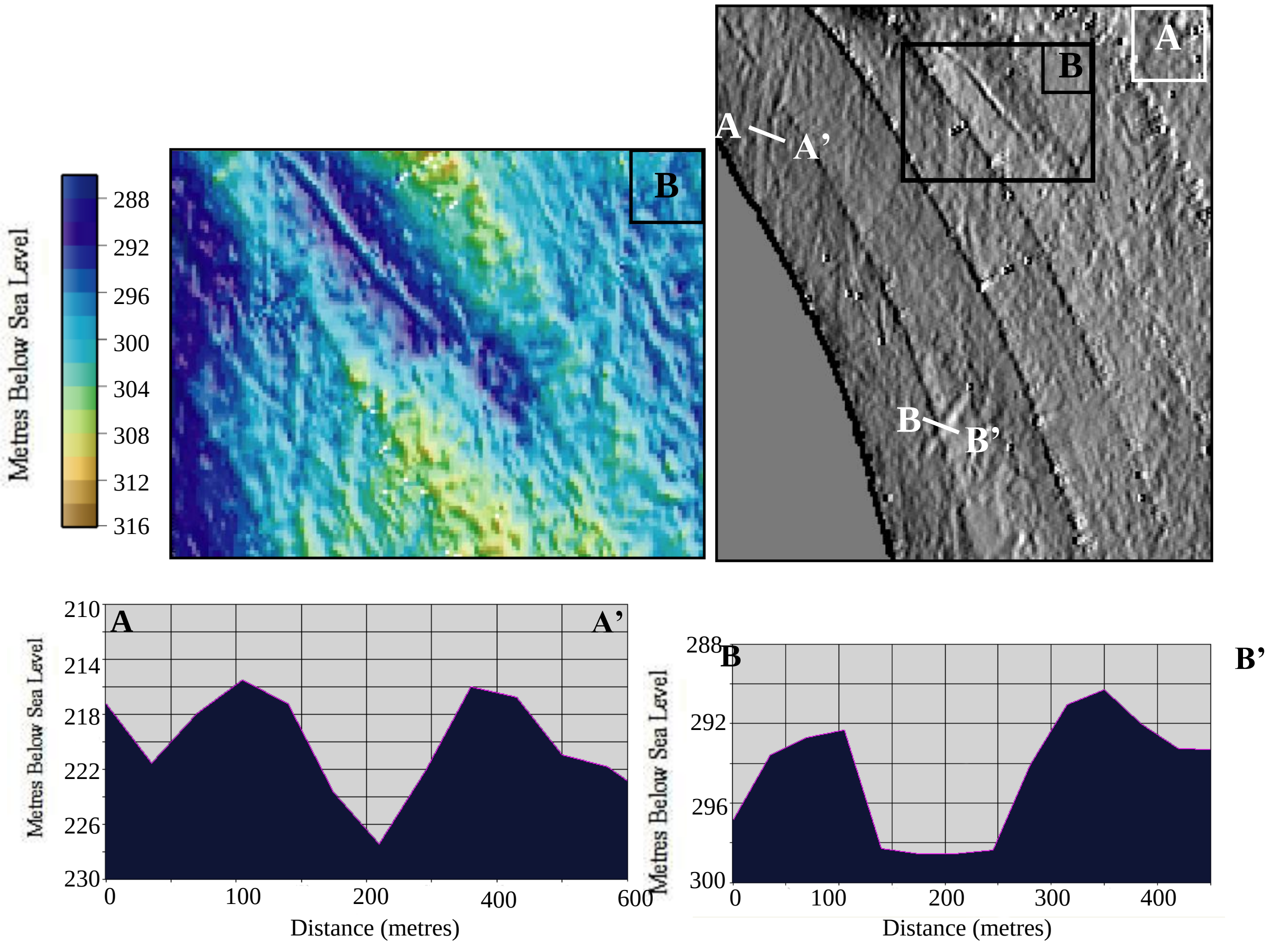

Figure 3.9 A) - Swath bathymetric greyscale shaded relief image of a heavily scoured area of the outer-shelf (see Fig. 3.7) (Illumination from the west, data gridded at 30m). Vertical profile data for profiles A – A' and B – B' show the depth, width, and berm height of two prominent iceberg keel ploughmarks. Profile A – A' describes the characteristic shape of a ploughmark from a Type 1 iceberg with a narrow keel, coming to a point at the seafloor. The wide base of the scour depicted in profile B – B' suggests that this Type 2 ploughmark may have been formed by grounding of a larger tabular iceberg. B) - Colour swath bathymetric image of a large iceberg ploughmark close to the shelf edge (Illumination from the west, data gridded at 25 m). The berms either side of the scour are shown to rise over 4 m higher than the surrounding topography.

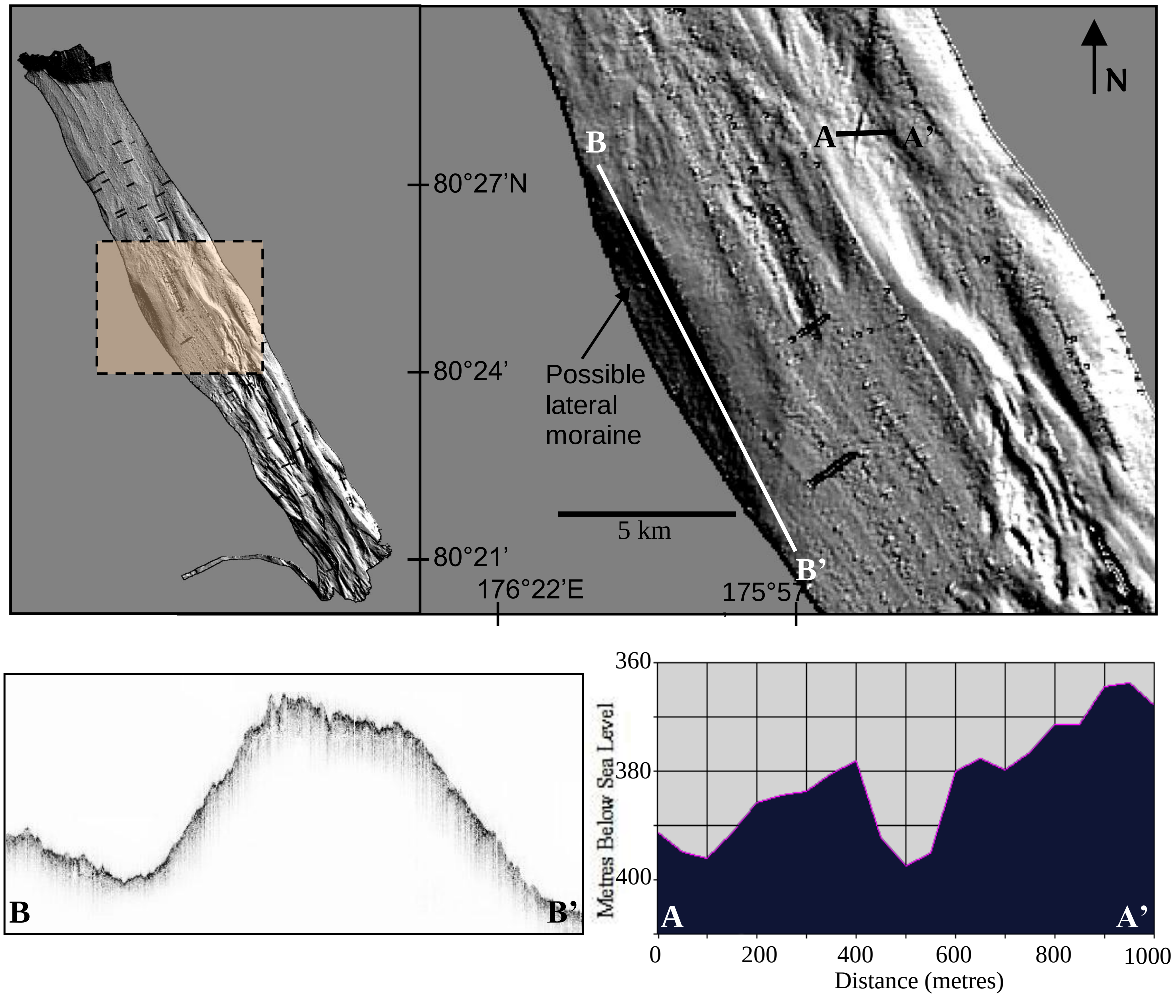

Figure 3.10 – Swath bathymetric greyscale shaded relief image showing the location of the large iceberg plough mark superimposed upon a prominent ridge in the middle-shelf area. Profile A – A’ illustrates the vertical profile data for this feature. Profile B – B’ illustrates the acoustic profile of a prominent ridge located on the western margin of the trough – this feature is shown to display only a small amount of acoustic penetration

3.2.7 Other Morphological Elements

A number of submarine landforms which are characteristic of former subglacial and ice-contact deposition are not found in Hinlopen Trough.

Featureless Areas of the Sea Floor. Large areas of the sea floor in Hinlopen Trough appear flat and apparently featureless at the resolution of the swath bathymetric images. Apparently featureless sections of sea floor are interpreted as the product of hemipelagic sedimentation of fine particles throughout the Holocene (Dowdeswell et al., In Press A). These areas possess depths greater than that of any iceberg keels, allowing them to remain undisturbed in contrast to the shallower sections of the trough. This interpretation is further supported by the acoustically stratified and conformable nature of the stratigraphy in these areas (Fig. 3.4). Some flat and featureless areas of the sea floor in the inner-shelf are also characterised by layers of acoustically transparent units interpreted as the products of sediment gravity flows (e.g. Damuth, 1978; Dowdeswell et al., 1997; In Press A; Canals et al., 2000; Taylor et al., 2000; Kleiber et al., 2000; Hjelstuen et al., 2009).

Ridges Parallel to the Inferred Flow Direction. The location of a steep ridge situated at the eastern margin of Hinlopen Trough and orientated parallel to the inferred ice flow direction is shown in Figure 3.10. The limited extent of the survey area prohibits any conclusive interpretation of this feature; it is not clear whether it represents a lateral shear moraine produced at an ice stream margin or merely the existence of the shallower adjacent region of the shelf. However, this landform's proximity to the elongate features within the trough, combined with the small amount of acoustic penetration observed from the acoustic profiles (Fig. 3.10), suggests that a lateral moraine origin for this feature remains a viable hypothesis (Ottesen et al., 2005a).

Lateral moraines are not always present in the geomorphological record of past ice streams and have not been conclusively identified from the margins of former ice streams in Antarctica (Ottesen et al., 2005a; Shipp et al., 1999; Canals et al., 2000). They have, however, been identified from terrestrial settings in the Canadian Arctic (Stokes and Clark, 2002), and from numerous locations along the Norwegian and Svalbard continental margins (Ottesen et al., 2005a; b; 2007). These features are interpreted to mark the border zone between areas of fast and slower flowing ice and have been used to support evidence of the former existence of ice streams (Stokes and Clark, 1999; Ottesen and Dowdeswell, 2009).

Transverse Ridges. Ridges formed transverse to former northward ice flow in Hinlopen Trough are absent at the resolution of the swath bathymetric images. This observation is consistent with that of Ottesen et al. (2007), who describe how the notable absence of grounding-zone deposits or superimposed moraine ridges suggests rapid deglaciation through floatation and break up of ice took place in this trough (Dowdeswell et al., 2008). The absence of transverse ridges also allows further similarities to be drawn between the elements identified within Hinlopen Trough and the idealised landform assemblage for regions formerly occupied by ice streams (Ottesen and Dowdeswell, 2009).

Meltwater Features. Meltwater features have been identified from a number of former glaciated continental shelves in both hemispheres (e.g. Ó Cofaigh et al., 2002; 2005a; b; Lowe and Anderson, 2003; Hogan, 2008). Where they occur, these features are typically located in inner- to middle-shelf areas and are commonly associated with the presence of a crystalline bedrock substrate. Evidence of channelised meltwater is usually absent from outer-shelf locations associated with deforming sediments because the process of sediment deformation requires the incorporation of meltwater into the substrate (Shipp et al., 1999; Lowe and Anderson, 2003).

No features associated with the presence of subglacial meltwater have been identified from Hinlopen Trough at the resolution provided by the swath bathymetry images. The absence of meltwater channels or cavities, especially from within the inner-shelf bedrock region (Fig. 3.7), suggests that ‘free’ basal meltwater played a minor or insignificant role in the advance and retreat of the ice stream. It is, however, entirely possible that small channel systems exist in the trough below the resolution obtained in this study.

Chapter 4 - Acoustic Stratigraphy

Glacial successions typically contain variable and coarse grain sizes and often possess complex acoustic stratigraphies which exhibit a large amount of horizontal and vertical variability (Davis et al., 1997; Hogan, 2008). Four acoustic facies and two acoustic reflectors were identified from Hinlopen Trough using the criteria discussed in Chapter 2. These acoustic facies and associated reflectors are summarised in Figure 3.11 and each is described below.

4.1 Descriptions of Acoustic Facies

Facies T – Semi-transparent Unit: an acoustically semi-transparent unit crowned by a diffuse and irregular surface reflector composed of many small overlapping hyperbolae. This facies is laterally continuous, persisting for more than 25 km within the trough. Where present, Facies T overlies Reflector B2 and is characterised by depths of between 2 and 12 m.

Facies D - Conformable Drape: an acoustically semi-transparent conformable drape or semi-prolonged sea floor reflector. This unit exhibits a thickness of up to 15 m and occurs over wide regions of the sea floor. Facies D has a strong and continuous surface reflector which reproduces the shape of underlying reflectors.

Facies S - Acoustically Stratified Unit: an acoustically stratified unit with a conformable, flat and continuous upper reflector. This unit exhibits thicknesses of between 5 and 10 m and its internal reflectors are continuous, conformable and parallel.

Facies L: Acoustically-Transparent Unit: an acoustically transparent unit which fills topographical lows and forms thin drapes upon the sides of steep slopes. This facies has a continuous and smooth upper reflector and a maximum thickness of around 20 m. Facies L is the least laterally continuous unit identified within the trough, occurring over less than 5 km of the sea floor in any one place.

4.2 Descriptions of Acoustic Reflectors

Reflector B1: Acoustically Impenetrable Continuous Reflector: an impenetrable and continuous acoustic boundary, below which no internal reflections are imaged and 3.5 kHz profiles appear blank. This reflector is subdivided into Reflectors B1A and B1B based upon its geometry. Reflector B1A is characterised by a hummocky and rugged morphology with frequent multiples, whereas Reflector B1B possesses a smooth and flat shape. Dipping reflectors are commonly identified in association with Reflector B1B.

Reflector B2: Acoustically Impenetrable Discontinuous Reflector: an acoustically impenetrable, weak, and often discontinuous acoustic horizon. This reflector possesses a gently undulating geometry and only occurs in association with Facies T.

Acoustic Facies	3.5 kHz Sample	3.5 kHz Character
T	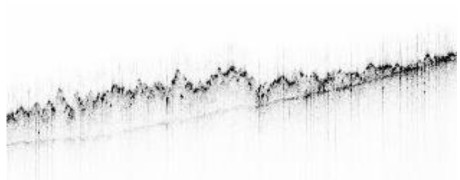	Acoustically semi-transparent facies, overlying Reflector B2
D	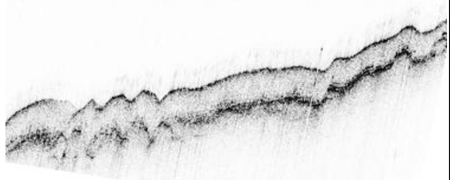	Acoustically semi-transparent facies – a conformable drape to semi-prolonged seafloor reflector
S	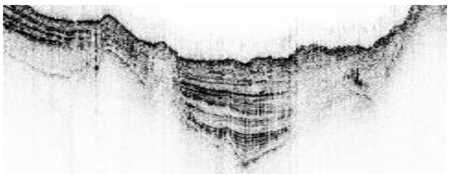	Acoustically stratified facies
L	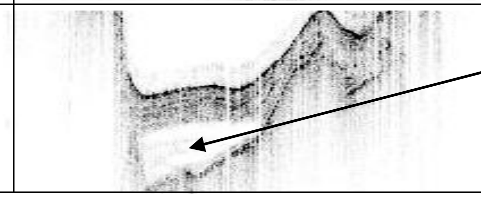	Acoustically transparent facies

Acoustic Reflector	3.5 kHz Sample	3.5 kHz Character
B1A	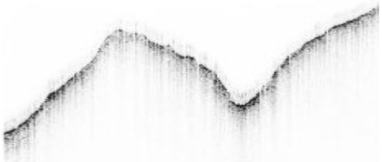	Rugged acoustically impenetrable surface
B1B		Gently undulating acoustically impenetrable surface with dipping reflectors
B2	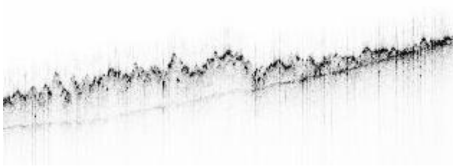	Smooth discontinuous acoustically impenetrable surface below Facies T

Table 4.1 - Table depicting the four acoustic facies and three acoustic reflectors identified from sub-bottom acoustic profiling in Hinlopen Trough

4.3 Acoustic Type Sections

Acoustic type sections can be used to illustrate the different combinations of acoustic facies and reflectors that occur in an area (Damuth, 1975). The stratigraphy of the sea floor in Hinlopen Trough generally consists of either Reflector B1A or B1B overlain by a thin unit of Facies S and capped to varying degrees with a conformable drape of Facies D. Conformable overlying units of Facies S and D are present in all locations where Reflector B1B comprises the base of the acoustic sequence (e.g. Fig. 4.1).

Reflector B1A is commonly overlain by a thin conformable layer of Facies D. However, this overlaying unit is absent in the stratigraphy from regions of the trough with high elevations and steep-sided slopes. Facies L is present in the acoustic stratigraphy at only two locations within the trough. In both instances, this Facies occurs on top of Reflector B1A and is conformably overlain by Facies S and D (Fig. 4.2).

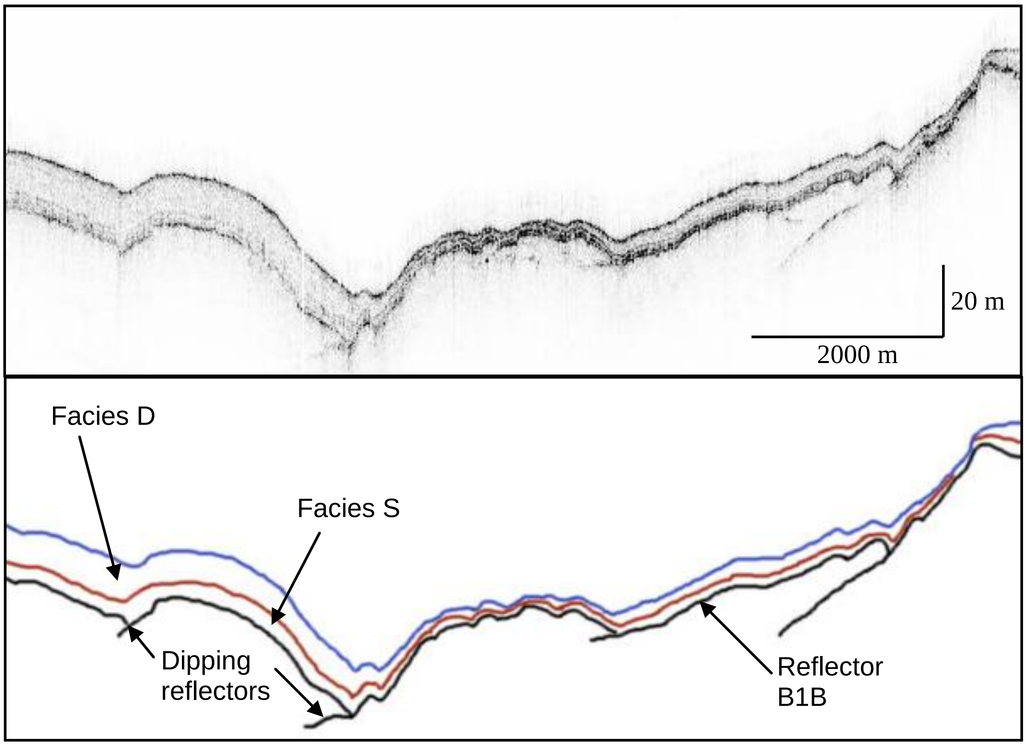

Figure 4.1 - 3.5 kHz profile of the seafloor with corresponding schematic illustration. This image depicts a common type section in Hinlopen Trough, consisting of Reflector B1B, Facies S and Facies D.

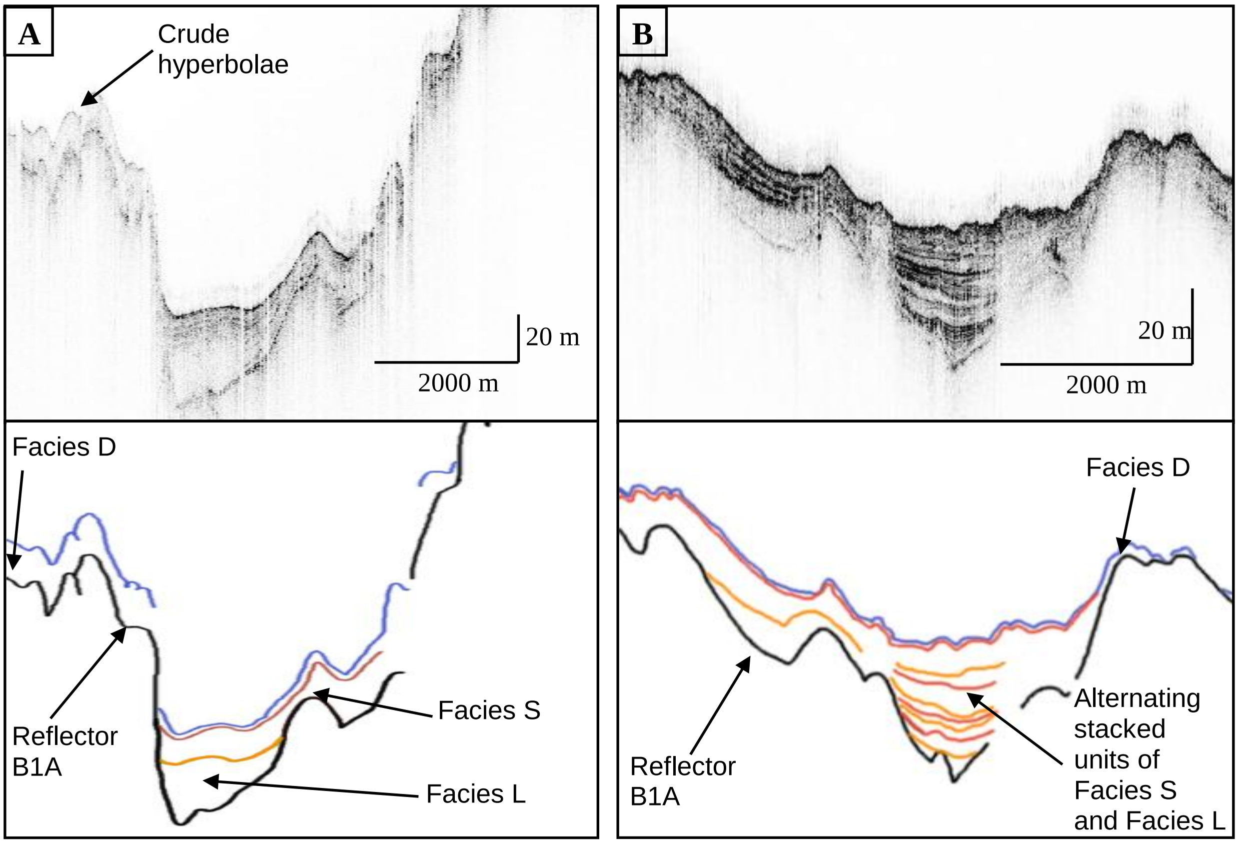

Figure 4.2 A) and B) - 3.5 kHz profiles of the seafloor with corresponding schematic illustrations. These images depict the location of Facies L in the acoustic stratigraphy– Facies L overlies Reflector B1A and is also found in association with Facies S

Large sections of the sea floor are also characterised by Facies T overlying Reflector B2. Reflector B2 becomes faint and discontinuous when beneath thick accumulations of Facies T, indicating a reduction in the intensity of the acoustic signal. The transition from an area characterised by Reflector B1B, Facies S, and Facies D to a region of the trough dominated by Reflector B2 and Facies T in described in Fig. 4.3.

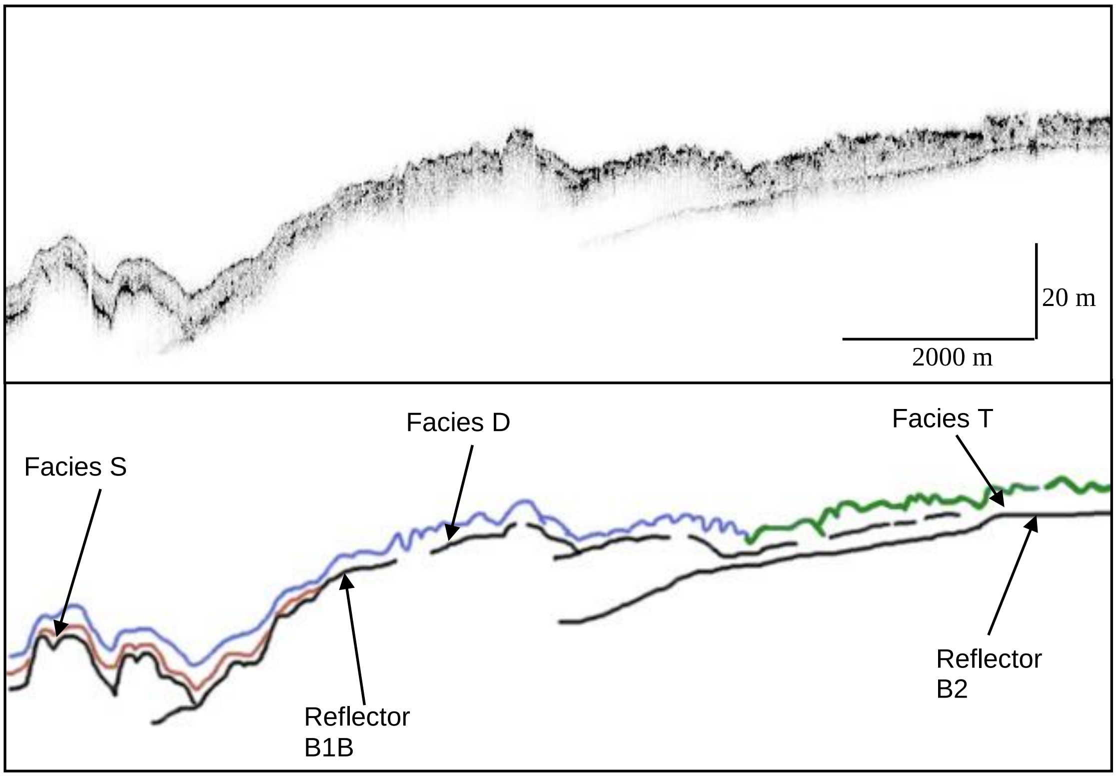

Figure 4.3 - 3.5 kHz profile of the seafloor with corresponding schematic illustration. This image depicts the transition from a type section characterised by Reflector B1B, Facies S and Facies D, to one consisting of Reflector B2 and Facies T

4.4 Distribution of Acoustic Facies in Hinlopen Trough

The distribution of the acoustic type sections identified from Hinlopen Trough in is illustrated in Figure 4.4A. This echo character map was produced by plotting the distribution of different type sections along the ship tracks (Fig. 2.2A). The contoured colour swath bathymetric image presented in 4.4B illustrates how changes in the acoustic nature of the sea floor often correspond with variations in trough depth.

Acoustic sequences composed of Facies T and Reflector B2 are located solely on the heavily-scoured outer-shelf region of Hinlopen Trough. A corresponding decrease in the thickness of Facies T and an increase in the strength of Reflector B2 are observed close to the shelf break.

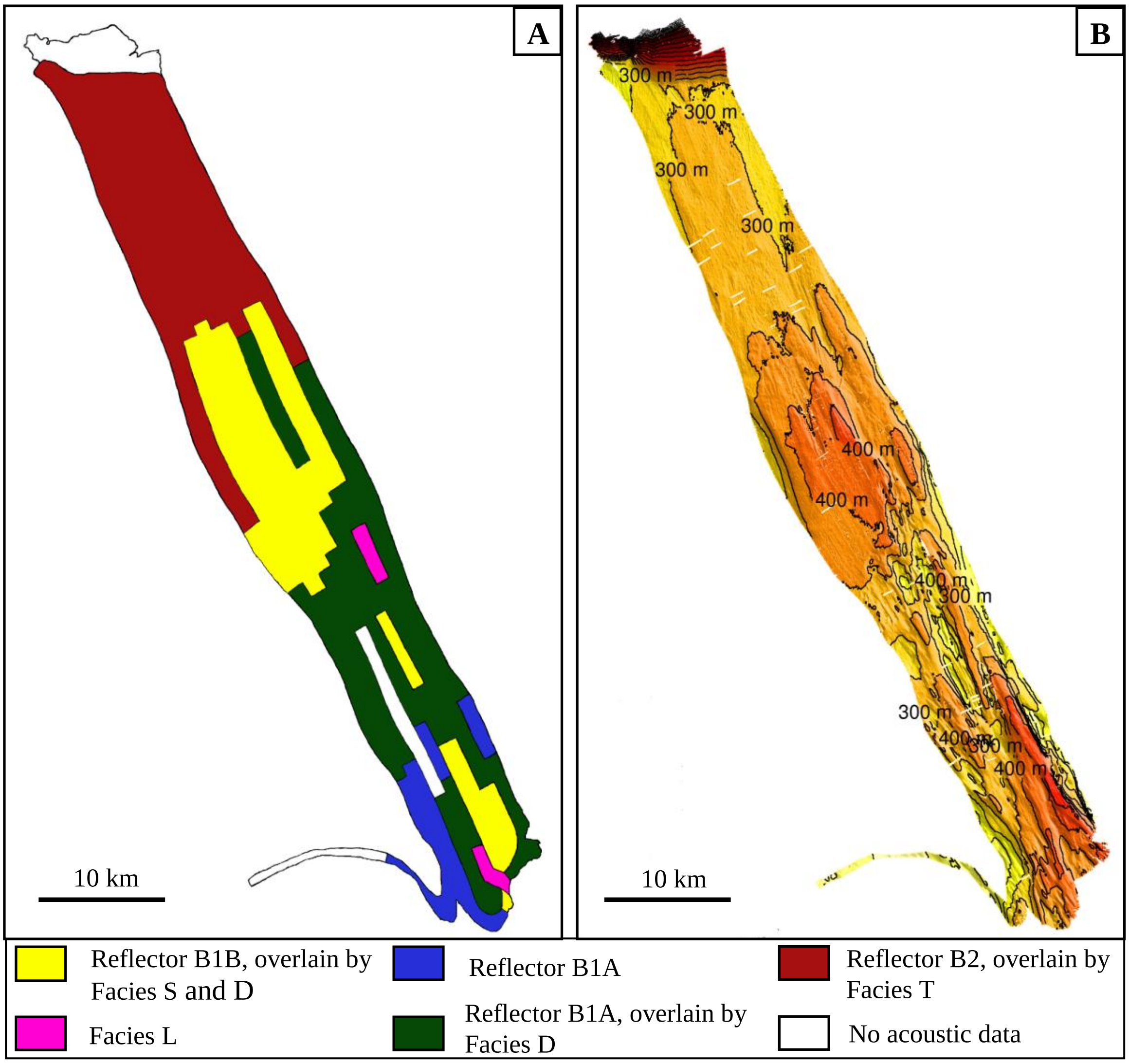

Figure 4.4 A) – Map illustrating the different acoustic type sections identified from Hinlopen Trough B) – Contoured colour swath bathymetric image of Hinlopen Trough

Thick sequences of Facies D and S are found overlying Reflector B2B in the deepest region of the middle-shelf (Fig. 4.4B). Dipping reflectors are common in these locations and there is some evidence of crude hyperbolae formed in the surface of Facies D (Fig. 4.1).

Locations characterised by the presence of Reflector B1A (depicted in blue and green in Fig. 4.4A) are typically situated in the inner-shelf region, associated with a rugged crystalline bedrock topography. Some regions in the inner-shelf are characterised by Reflector B1A, but lack an overlying conformable drape of Facies D (depicted in blue in Fig. 4.4A). These locations are found at the most landward end of Hinlopen Trough and possess the highest sea floor elevations within the surveyed area (100 - 250 m below sea level). The inner-shelf area also contains a few locations in which the acoustic stratigraphy is composed of Reflector B1B, Facies S and Facies D, an identical type section to that of the deepest area of the middle-shelf. Figure 4.4 illustrates how these locations (depicted in yellow) correspond with topographical depressions, which could serve to collect material falling from the sides of adjacent steep slopes.

Facies L is a rare component of the acoustic stratigraphy and is found in two locations within the inner-shelf. This facies is located within deep topographical depressions and is associated with the presence of Reflector B1A and the conformable draping units of Facies S and D (Fig. 4.4A).

4.5 Correlation of Submarine Landforms and Acoustic Facies in Hinlopen Trough

Analysis of the swath bathymetric and sub-bottom profiler data indicates that the nature of the sea floor substrate exerts a fundamental control over the distribution and morphology of the identified submarine landforms. Largely featureless regions of the sea floor are associated with acoustic Reflector B1B, overlain by Facies S and capped with a conformable unit of Facies D (Fig. 4.4). The streamlined sedimentary landforms, identified in the trough in the form of megaflutes and highly attenuated sedimentary drumlins, are also formed within these units. Crude hyperbolae in the acoustic profiles are associated with the submarine landforms (Fig. 3.4), indicating the presence of abrupt interfaces in the subsurface (Davis et al., 1997).

The bedrock landforms identified from the inner-shelf region of the trough are formed within the acoustically impenetrable horizon of Reflector B1A and are often draped by a thin unit of Facies D. The acoustic stratigraphy of the iceberg scoured outer-shelf region of the trough consists of Reflector B2 overlain by Facies T.

4.6 Interpretation of Acoustic Facies

Acoustic stratigraphy can provide a wide range of information about the erosional and depositional processes which have shaped the sea floor. While seismic profiles do not represent geological cross sections of the strata, acoustic parameters such as the arrangement of sub-bottom reflectors, the depth of signal penetration, and the morphology of individual facies, allow insights into the sedimentary processes operating in former environments (Davis et al., 1997). One of the most useful applications of acoustic stratigraphy relates to the correlation which has been identified between certain reflection types and the relative amounts of coarse or bedded sediment within the sea floor (Damuth, 1975, 1978, 1980).

Facies T: The chaotic and crudely hyperbolic nature of the seafloor reflector above Facies T suggests that the surface of this unit is characterised by a hummocky morphology containing many abrupt interfaces. These diffractions are typically caused by features which have dimensions comparable to the wavelength of the acoustic signal (Davis et al., 1997). The rough sea floor topography identified on the 3.5 kHz profiles is also apparent from the swath bathymetric images (e.g. Fig. 3.8 and 3.9), where it is interpreted to have formed from the ploughing action of iceberg keels. Facies T is semi-transparent in nature and is underlain by a diffuse and discontinuous sub-bottom reflector (B2). These acoustic qualities suggest that Facies T contains low to moderate amounts of coarse sediments (Damuth, 1975, 1978, 1980).

The association of this facies with rough sea floor topography and a low to moderate amount of coarse material, combined with its location solely on the heavily iceberg-scoured outer-shelf region of the trough, suggests that Facies T represents iceberg turbate. This term was first introduced by Vorren et al. (1983) to define those areas of strata which have been reworked by the ploughing action of iceberg keels (Barnes and Lien, 1988). Facies T corresponds with Dowdeswell et al.'s (In Press B) acoustic facies T and with Hogan's (2008) chaotic facies 4. This facies does not record a depositional facies, but instead represents the action of a glacimarine reworking process, which served to plough, and sometimes to remobilise and remove, underlying sediment from the outer-shelf.

Facies D: The identification of distinct and continuous reflectors in seismic profiles suggests that the overlying facies lack high concentrations of bedded silt or sand. The presence of these materials would act to reflect or absorb the majority of the acoustic energy and prevent deeper penetration of the signal (Damuth, 1975, 1978, 1980). The distinct and continuous sub-bottom reflector identified below Facies D therefore suggests that this unit contains very little or no coarse material.

The conformable and draping geometry of Facies D suggests that this unit was formed through uniform suspension settling under tranquil sea floor conditions (Davis et al., 1997). Whereas discontinuous reflectors often indicate high energy depositional environments, the continuous nature of the surface and sub-bottom reflectors in Facies D indicates passive deposition within a low energy open-marine environment (Davis et al., 1997).

The location of Facies D at the top of the stratigraphy and its occurrence across large sections of the trough also supports an origin through slow vertical accretion of suspended sediments derived from Holocene meltwater plumes. This unit is only lacking from the iceberg keel turbated region of the trough, and from small sections of the inner-shelf, where it is interpreted to have been unable to settle on steep slopes and instead accumulated in adjacent basins.

Acoustically semi-transparent sediment drapes have been identified from deglaciated regions of continental shelves in both hemispheres (e.g. Dowdeswell et al., 1997; Shipp et al., 1999; Taylor et al., 2000; Kleiber et al., 2000). Facies D corresponds with Damuth's (1978) echo type 1B and Hogan's (2008) Facies 6, both identified as the product of hemipelagic sedimentation by their sharp surface reflectors and continuous sub-bottom reflectors. Facies D does not exhibit any distinct internal stratification – a feature commonly identified from conformable drapes of fine Holocene sediments. Although stratification could be absent from these deposits in

Hinlopen Trough, it is possible that horizons do exist, but are too closely spaced to be recognised at the resolution of the 3.5 kHz profiles.

Facies S: This facies possesses similar acoustic properties to Facies D, but additionally exhibits strong internal stratification of continuous, conformable and parallel reflectors. The distinct and continuous nature of these sub-bottom reflectors suggests that this facies also contains very little or no coarse grain sizes (Damuth, 1975, 1978, 1980). These features also suggest continuous low energy deposition of fine-grained sediments under tranquil open marine conditions.

The presence of lithological boundaries in Facies S indicates that variations in acoustic impedance occur throughout this unit (Davis et al., 1997). This stratification could result from changes in clast content throughout the deposit – layers of coarser material generally create pronounced acoustic layers in 3.5 kHz profiles (Winkelmann et al., 2008a). The fact that Facies S only occurs in the trough directly beneath units of Facies D suggests that this unit represents a more ice-proximal regime of hemipelagic sedimentation than its overlying facies. Stratification may have been produced by fluctuations in the concentration of suspended sediments and IRD which occurred close to the retreating ice front.

Shipp et al. (1999) identified a similar acoustic facies from the formerly-glaciated Antarctic margin, interpreting this acoustically laminated and draping deposit as a record of continuous proglacial and sub-ice shelf deposition. Similar facies have also been identified in the Arctic (e.g. Damuth, 1978; Dowdeswell et al., 1997, In Press B; Taylor et al., 2000; Hjelstuen et al., 2009), where they have been interpreted as glacimarine sediments deposited by retreating ice masses. Kleiber et al. (2000) describe an almost identical unit of laminated glacimarine sediments from the Franz Victoria Trough, northern Barents Sea. This deposit possesses a similar draping character, parallel-layering and thicknesses of between 1 and 5m.

Facies L: Facies lacking acoustic reflections are typical features of both massive marine muds and mass flows (Davis et al., 1997). The lobate geometry of Facies L precludes an origin from hemipelagic sedimentation and allows interpretation of this facies as a debris flow deposit. Whereas units deposited by the vertical accretion of suspended sediments produce a draping geometry which mimics the shape of the underlying sea floor, mass wasting processes produce deposits which become ponded above this reflector, giving the illusion of a flat seabed (Canals et al., 2000). The location of Facies L within basins in the inner-shelf region of the trough supports interpretations of this facies as mass flow deposits. The adjacent steep-sided bedrock highs which exist in this region would have acted as sediment sources for these subaqueous mass movements.

Transparent acoustic units were first interpreted as debris flow deposits by Damuth (1978) and have since been recognised in many locations in the Arctic and on the Antarctic continental shelf (e.g. Dowdeswell et al., 1997; Canals et al., 2000; Taylor et al., 2000; Hjelstuen et al., 2009; Dowdeswell et al., In Press B). Facies L corresponds with Dowdeswell et al.'s (In Press B) L^1 facies and with Hogan's (2008) acoustic facies 5.

The unit of Facies L identified in Fig. 4.2A is located below Facies D and S, suggesting that this mass wasting process occurred prior to deglaciation of Hinlopen Trough. The units of Facies L recognised from Fig. 4.2B are stacked between thin units of Facies S, indicating that multiple mass failures occurred in this area throughout the early phase of deglaciation. The occurrence of these mass flow deposits either just prior to, or during, deglaciation of the trough is a viable interpretation due to the fact that large and unstable amounts of sediment would have been deposited in the inner-shelf area during this period.

4.7 Interpretation of Acoustic Reflectors

Reflector B1A: Combined with its location in the inner-shelf crystalline bedrock region of the trough, the acoustically impenetrable nature of Reflector B1A suggests that this horizon is composed of outcropping bedrock. A bedrock surface, variably draped by a thin unit of glacimarine sediments, would provide the excellent reflector of sound energy which is observed in the 3.5 kHz profiles and would ensure that little or no acoustic signal penetrates below this horizon (Damuth, 1978; Davis et al., 1997;

Canals et al., 2000). Similar acoustic characteristics can also be produced by consolidated subglacial till. It is, however, very unlikely that till deposits would posses such a rugged and topographically variable upper reflector, due to the erosional action of overriding ice.

Reflector B1A frequently exhibits crude hyperbolae (e.g. Fig. 4.2A) and multiple seafloor reflections in the inner-shelf region of the trough. These acoustic features are artefacts but are accentuated by the presence of rugged topography, and by rock and gravel surfaces respectively (Davis et al., 1997). Reflector B1A is therefore interpreted as exposed bedrock, possibly locally overlain by till in some topographical depressions. This reflector corresponds with the acoustically non-structural layer observed by Hjelstuen et al. (2009) on the west coast of Norway and with Hogan's (2008) facies 1 identified from the eastern margin of Svalbard.

Reflector B1B: Reflector B1B also comprises an acoustically impenetrable and continuous reflector, suggesting that this unit is composed from either consolidated subglacial sediments or from bedrock. However, Reflector B1B differs from Reflector B1A in that it is characterised by a smoothly undulating surface, indicative of the action of ice (Dowdeswell et al., In Press A). The location of Reflector B1B in the deepest area of the middle-shelf and its association with the streamlined subglacial landforms in this section, further suggest that this deposit may represent subglacial till. The large amount of acoustic energy reflected from the surface of this unit suggests that any till may be heavily consolidated or even overconsolidated in nature.

Deformation till has been recognised from sub-bottom profiling and identified in association with elongate sedimentary bedforms on a number of formerly glaciated high-latitude margins (e.g. Mangerud and Svendsen, 1996; Shipp et al., 1999; Canals et al., 2000; Ó Cofaigh et al., 2005a). Acoustic profiling has also facilitated the identification of deformation till on Svalbard's eastern margin (Hogan, 2008) and in the nearby Franz Victoria Trough (Kleiber et al., 2000).

Despite its relationship with the streamlined subglacial landforms, Reflector B1B can not be conclusively interpreted as deformation till. Sub-bottom profiling does not allow differentiation between these two substrate types and it is possible that this horizon represents glacially-smoothed regions of bedrock (e.g. Hjelstuen et al., 2009).

Reflector B1B: This reflector is an acoustically impenetrable horizon, characteristic of coarse-grained unsorted material or of exposed bedrock (Damuth, 1978; Davis et al., 1997; Canals et al., 2000). Reflector B2 is only identified on the outer-shelf area of the trough, below Facies T. The diffuse and discontinuous nature of Reflector B2 reflects the acoustic reflection produced by the moderate silt and sand content of the overlying unit of iceberg turbate.

It is not clear whether this reflector represents deformation till or glacially-smoothed bedrock. Although it is possible that this horizon indicates the surface of a unit of deformation till, the action of iceberg keels ploughing the sea floor in this location may have resulted in the incorporation of any till into the overlying Facies T. Some seismic profiles, e.g. Fig. 4.3, appear to show Reflector B2 extending beneath Reflector B1B, suggesting that the former horizon may represent glacially-smoothed bedrock, while latter reflector may represent overlying units of subglacial till.

Chapter 5 - Lithostratigraphy

The glacimarine environment contains a wide range of well-preserved sedimentary sequences, each representing a complex history formed by a variety of processes and patterns of glacimarine sedimentation. The details of the four sediment cores collected from the seafloor of Hinlopen Trough are presented in Table 2.4.

5.1 Sediment Facies: Description

Lithofacies and subfacies were identified within the cored sections using a sediment classification scheme based upon that developed by Eyles et al. (Table 2.5). Two major lithofacies of diamict (D) and fine-grained muds (F) were identified from visual descriptions of the cores and particle size data. Within these major lithofacies, subfacies were defined based on internal structure, the presence or absence of pebble-sized clasts, and the presence of absence of stratification.

5.1.1 Diamict

A very poorly-sorted diamict facies occurs in two of the four sediment cores, constituting the basal facies in GC15, and the uppermost unit of GC16 (Fig. 5.1). These two units of diamict display a number of different sedimentological characteristics.

The diamict in GC15 (Fig. 5.1A) comprises the lowest 23 cm of the core and is matrix-supported (Dm) and dark grey in colour. The matrix has a variable sand content (6-18 %) but is texturally classified as a silty-clay. This diamict unit is characterised by a large number of sub-rounded to sub-angular clasts, which have lengths of 2-30 mm and are composed of a white crystalline lithology. This facies is very stiff and is separated from an overlying unit of fine-grained mud by a wavy sub-horizontal contact.

The diamict identified in GC16 (5.1B) is located in the top 4 cm of the stratigraphic sequence and is clast-supported (Dc). A sharp and strongly sub-horizontal contact separates this thin unit from an underlying facies of fine-grained mud. The sub-angular clasts which constitute this diamict are composed of black and white crystalline lithologies. A sub-horizontal planar structure has been identified within this unit.

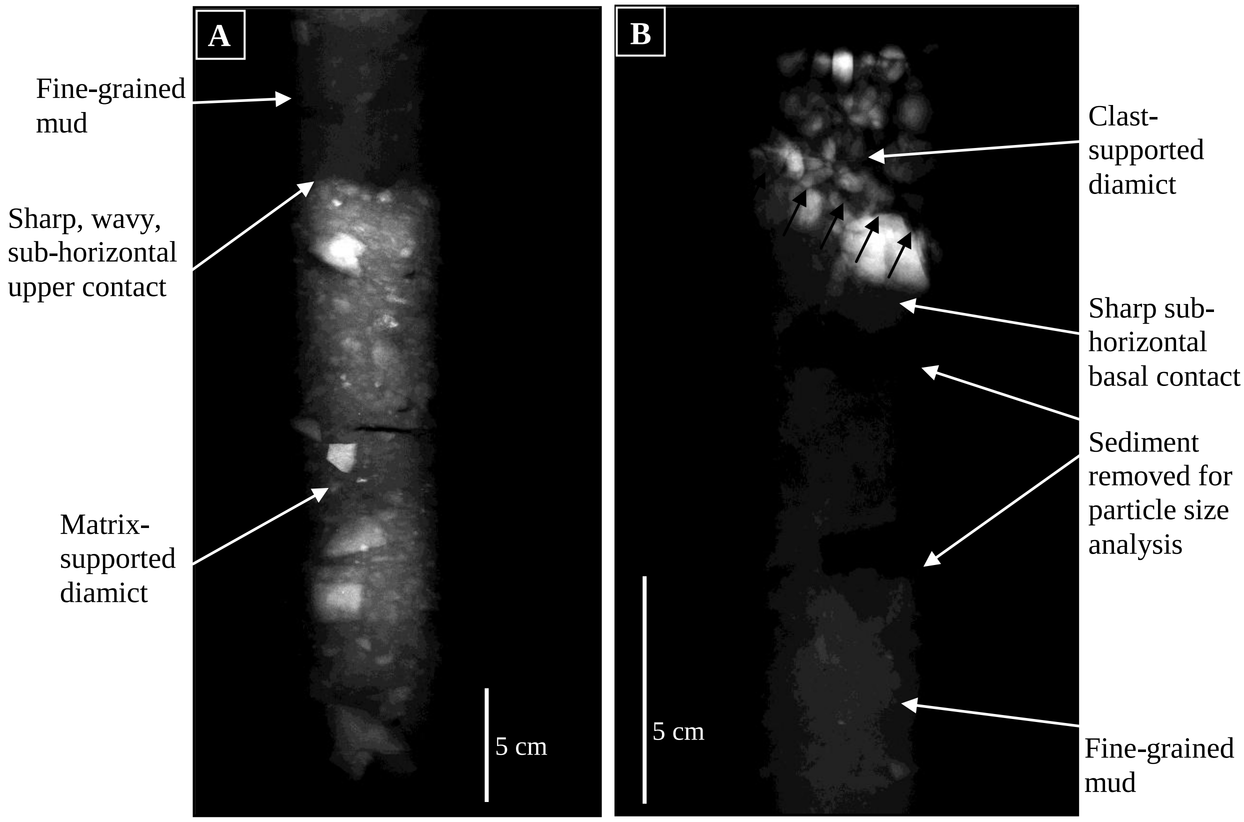

Figure 5.1 A) – X-radiograph of the matrix-supported diamict subfacies identified from the base of GC15. B) – X-radiograph of the clast-supported diamict subfacies identified from the top of GC16. A sub-horizontal planar structure occurs within this unit and is indicated by black arrows

5.1.2 Fine-grained mud

A poorly-sorted fine-grained mud facies (F) occurs in all four cores collected from Hinlopen Trough and is recognised as the only facies present within GC14 and GC17 (Figs 5.3 and 5.9). This facies has a variable sand content (0.3 – 15%) and is texturally classified as a clay or a silty-clay.

This fine-grained mud often contains a minor component of randomly-orientated outsized clasts (Fig. 5.2A), as well as rare thin lenses of sand or coarser material (Fig. 5.2B). Where present, outsized clasts are typically 6-20 mm in length, sub-angular to sub-rounded in shape, and are composed of either a white or black crystalline lithology.

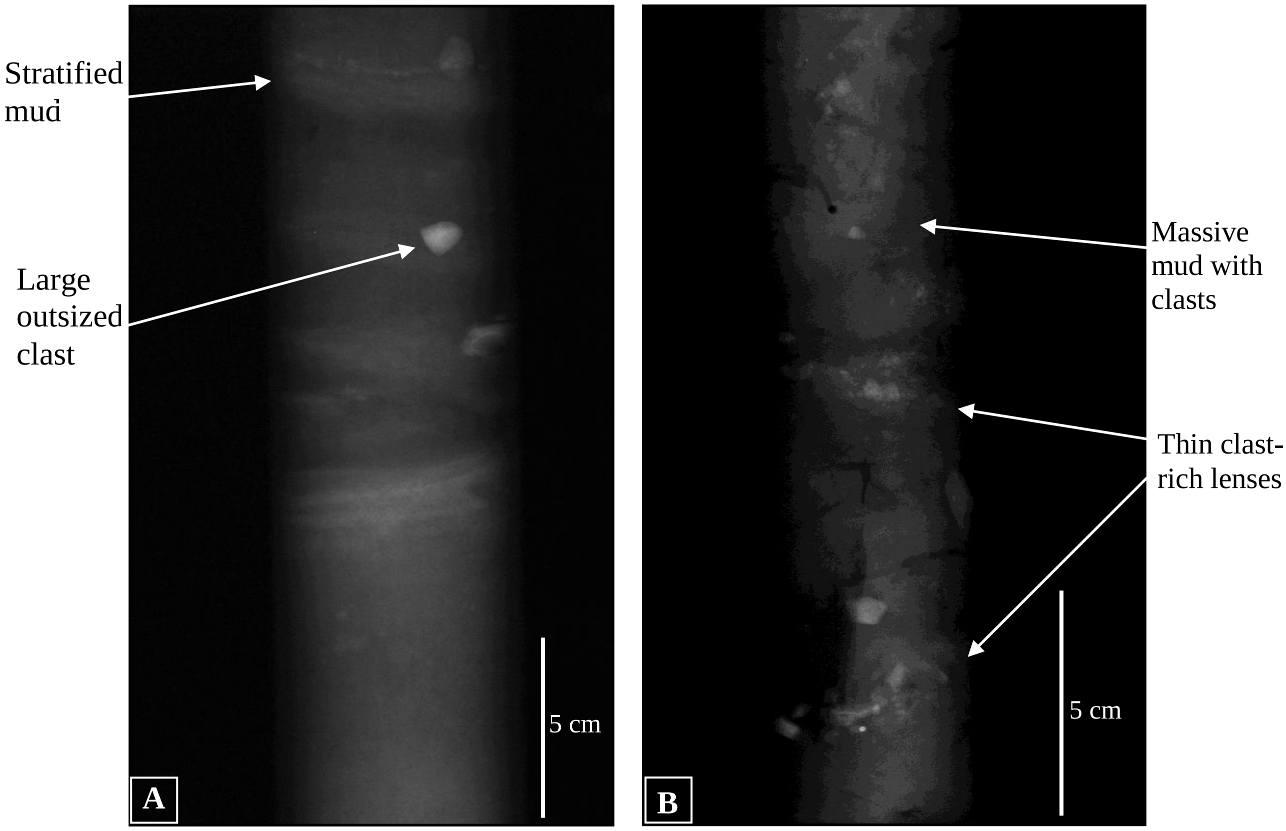

Figure 5.2 A) – X-radiograph of outsized clasts within stratified mud in GC14.
B) – X-radiograph of thin clast-rich lenses within a massive mud with clasts in GC17

Patchy black organic material (e.g. Fig. 5.5A) is commonly associated with the fine-grained mud facies and is present in all of the cores except GC16. Shelly fragments are also variably present and have been identified within all the cores except GC16. The colour of the fine-grained mud facies is typically olive-green to light-brown, although varicoloured stratified mud horizons are observed in GC14 and GC15, with colours ranging from red-brown to dark-grey.

Five subfacies have been identified within the fine-grained mud; massive fine-grained mud (Fm), massive mud with clasts (Fmd), massive mud with rare clasts (Fm(d)), stratified mud (Fs), and weakly stratified mud (F(s)).

5.2 Sediment Facies: Distribution

The distribution of these sediment facies within the four sediment cores will now be described. The order in which this information is presented reflects the location of the cores in the trough, from GC14 on the continental slope, to GC17 near the trough head (Figs 2.4 and 5.12).

5.2.1 GC16

GC16 (Fig. 5.3) is capped by a thin unit of loose pebbles and cobbles with no apparent matrix. Medium/coarse and fine/medium sand horizons occur between 11-15 cm and 21.5-23 cm respectively. These sand horizons are diffuse and wavy in nature and are characterised by relatively sharp upper and lower sub-horizontal contacts. The mud which constitutes the lower half of the core contains abundant outsized clasts and a large dropstone of 40-50 mm in length is observed at 58 cm (Fig. 5.3B).

Particle size analysis reveals a gradual down-core increase in grain size (Fig. 5.4). The magnetic susceptibility values in GC16 display a steady increase until 23 cm, after which values decline. A gradual increase in magnetic susceptibility occurs between 30 and 75 cm, before a further decline towards the end of the core. Variations in lightness and greyscale reflectance values appear to closely resemble the changes in magnetic susceptibility. The dramatic increase in a* values near the start of the core corresponds with a change in sediment colour from the grey (GLEY a 3/5ay) clast-supported diamict to the massive olive-green mud (7.5Yr 4/1) (Fig. 5.4).

5.2.2 GC15

Apart from the massive matrix supported diamict which comprises the bottom 25 cm of the sequence, GC15 is composed entirely from massive and stratified fine-grained mud (Figs. 5.5 and 5.6). This facies, which almost completely lacks outsized clasts, exhibits some variation in colour throughout the core. The top of the sequence is capped by a green-brown mud (5Y 3/2), while the sediment between 150 cm and 179 cm is stratified between a lighter-brown (5YR 6/3) and a darker-brown (10YR 4/1) mud with intervals of between 1.5 cm and 7.5 cm. A thin and discontinuous lense of fine to medium sand occurs between 146 and 146.5 cm. A slight down-core increase in clast abundance is noted and particle size analysis demonstrates that this mirrors a slight down-core increase in mean grain size (Fig. 5.6).

The sediment's magnetic susceptibility increases gradually throughout GC15, before exhibiting a dramatic increase to over 70 SI in association with the start of the diamict facies (Fig. 5.6). Lightness and reflectance values increase slightly throughout the core. The b* values demonstrate a general decrease in the prevalence of yellow hues throughout the core. The diamict facies is shown to posses increased blue hues in relation to the rest of the core, a fact that is supported by its dark grey colour description in the sediment log.

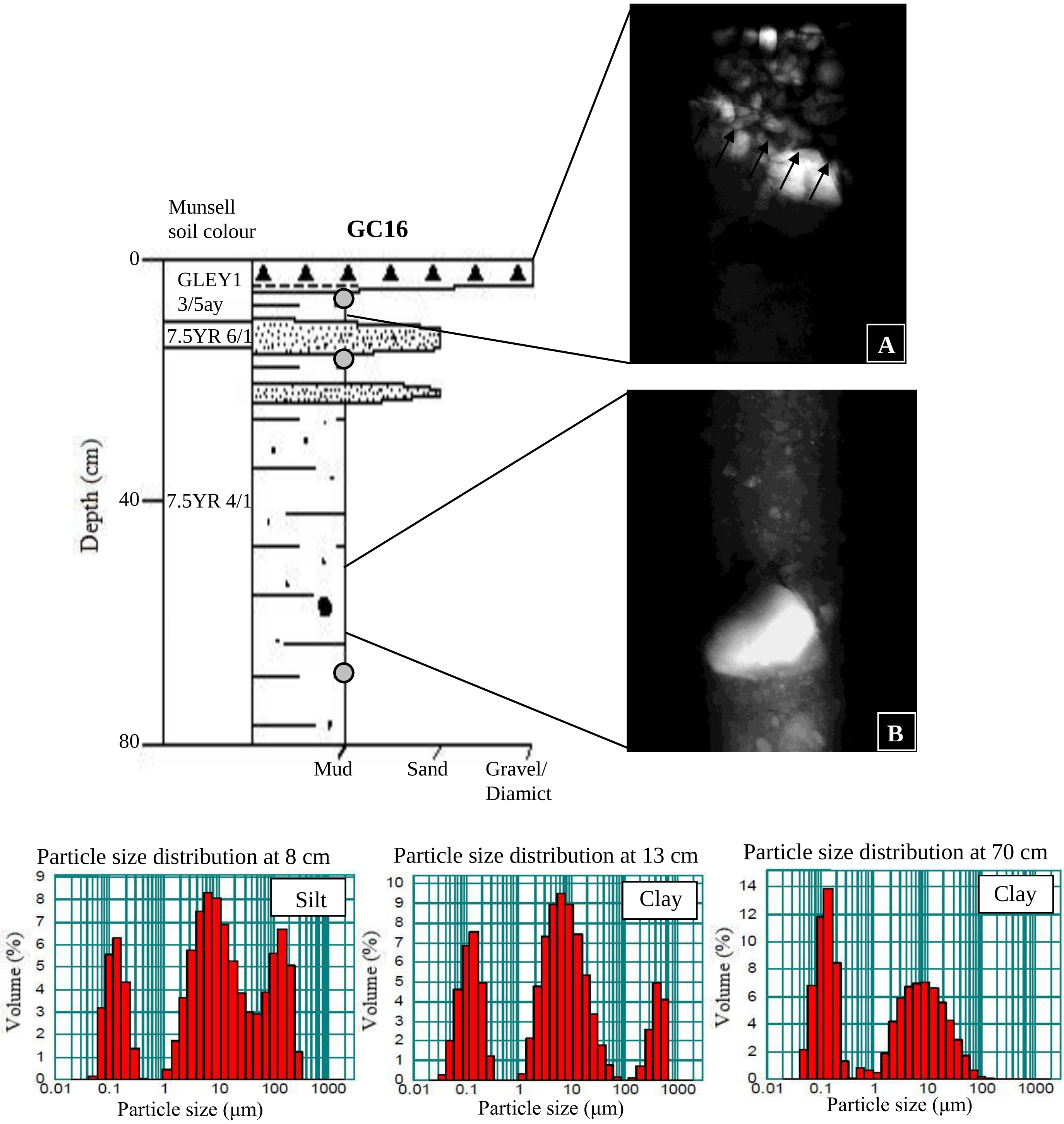

Figure 5.3 – Core log of CG16 with Munsell soil colour and particle size data. A) – X-radiograph of the diamict unit containing a sub-horizontal planar structure. B) – X-radiograph of a large dropstone within massive mud with clasts

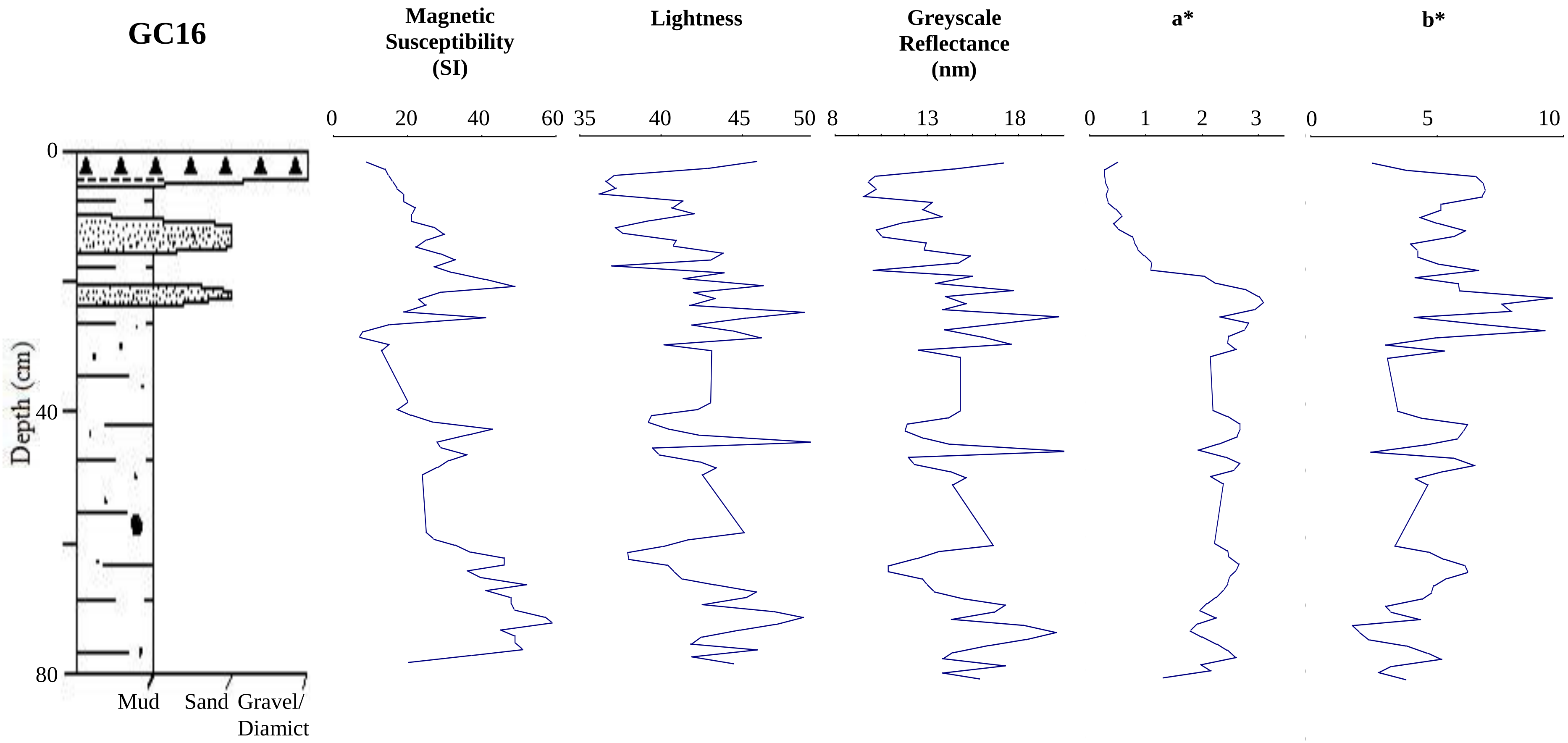

Figure 5.4 – Core log of GC16 presented alongside corresponding magnetic susceptibility, sediment lightness, greyscale reflectance, a* and b* values

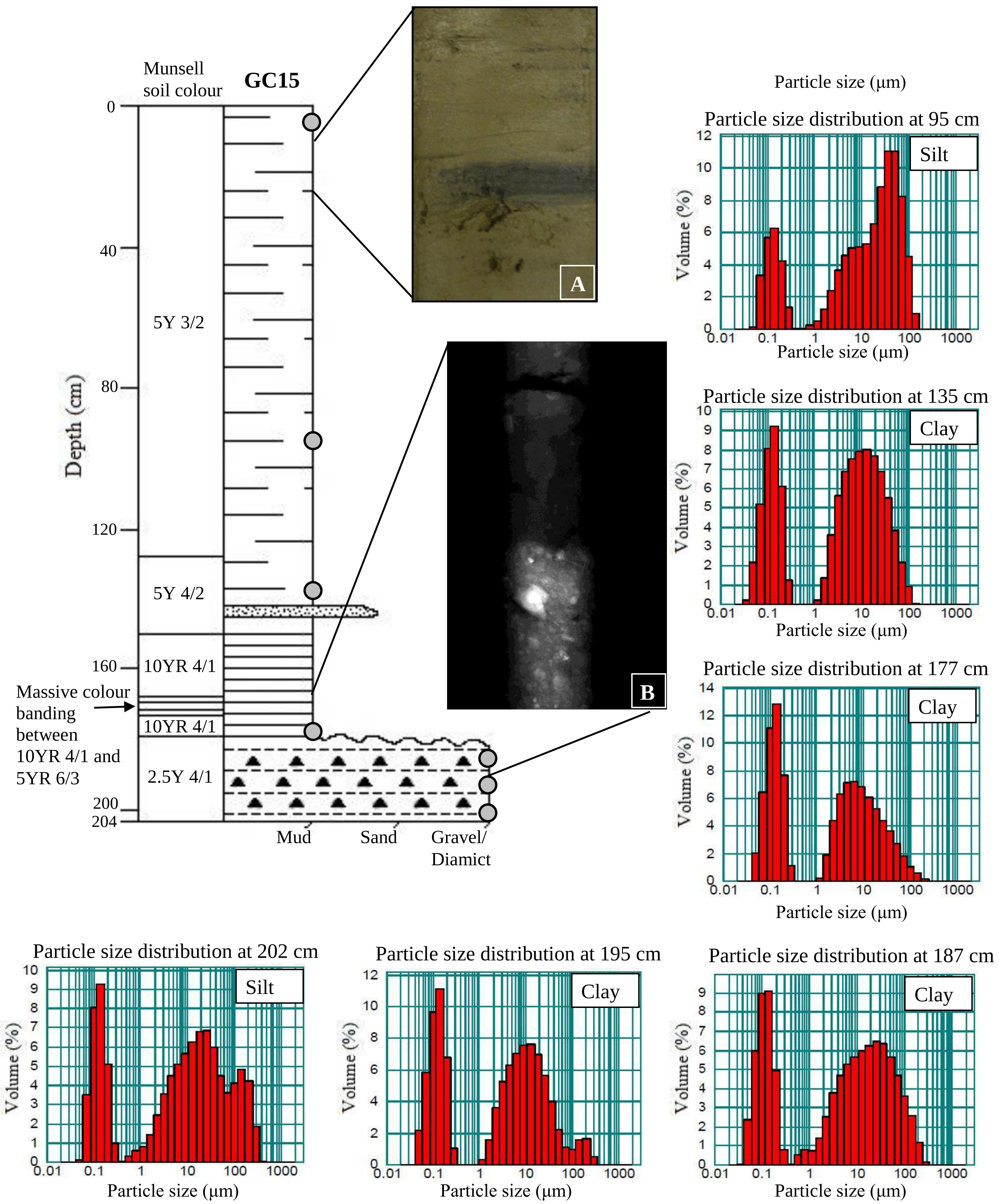

Figure 5.5 – Core log of CG15 with Munsell soil colour and particle size data.
A) – Photograph of a prominent streak of black organic material
B) – X-radiograph of the fine-grained mud underlain by massive diamict

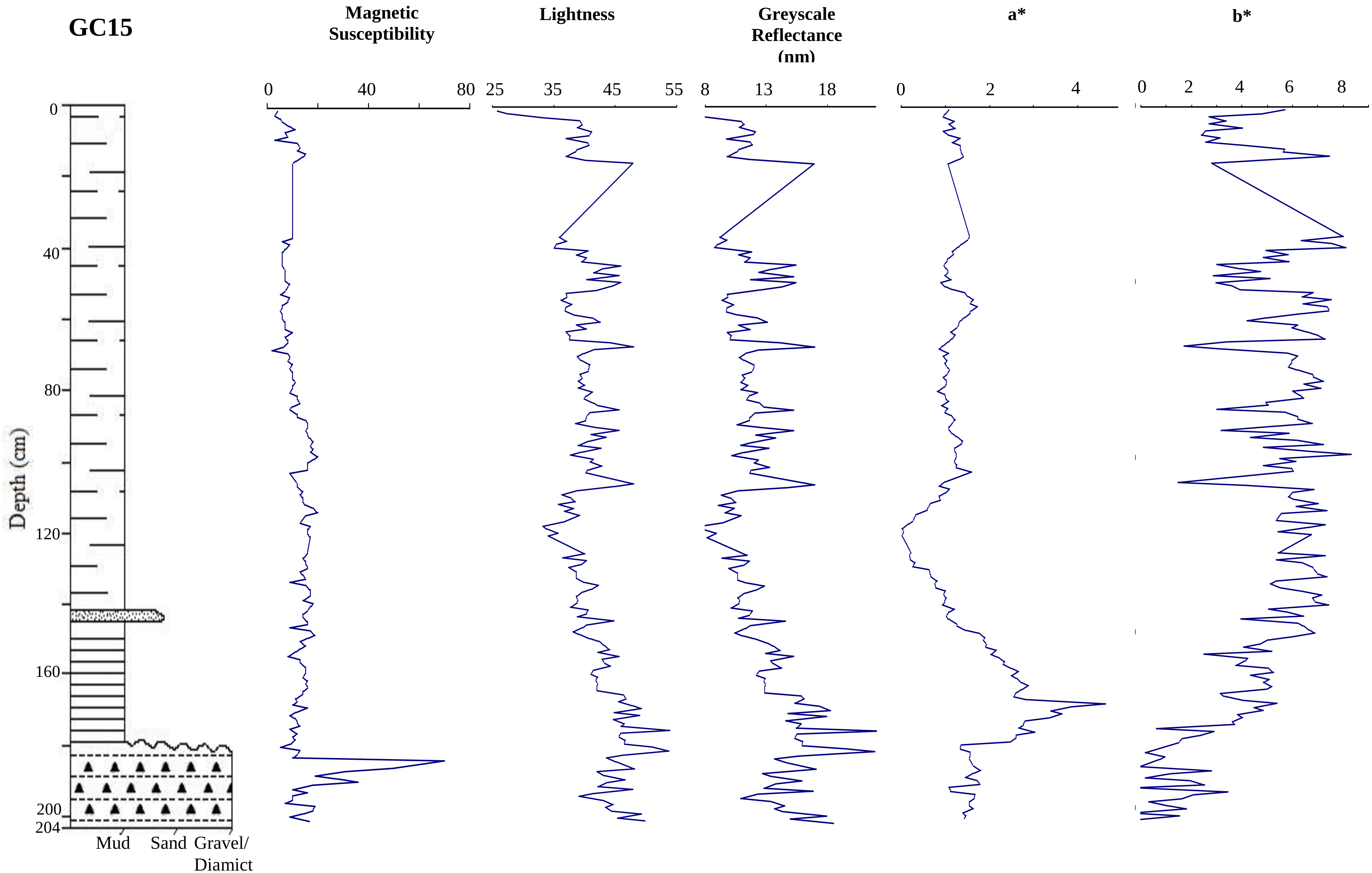

Figure 5.6 – Core log of GC15 presented alongside corresponding magnetic susceptibility, sediment lightness, greyscale reflectance, a* and b* values

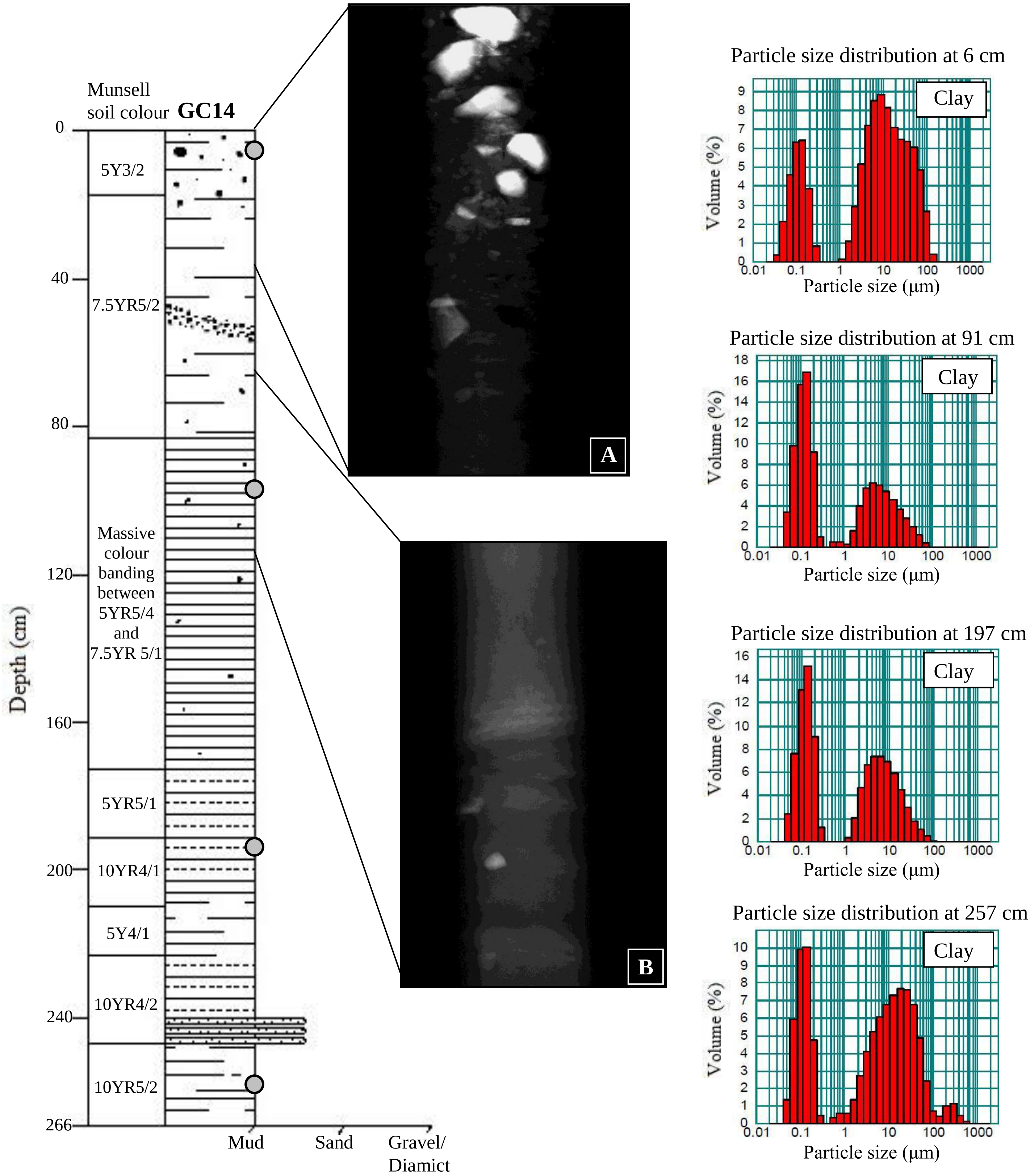

Figure 5.7 – Core log of CG14 with Munsell soil colour and particle size data.
A) – X-radiograph of a section of massive mud with abundant pebble-sized clasts underlain by massive fine-grained mud
B) – X-radiograph of a section of massive fine-grained mud underlain by stratified fine-grained mud

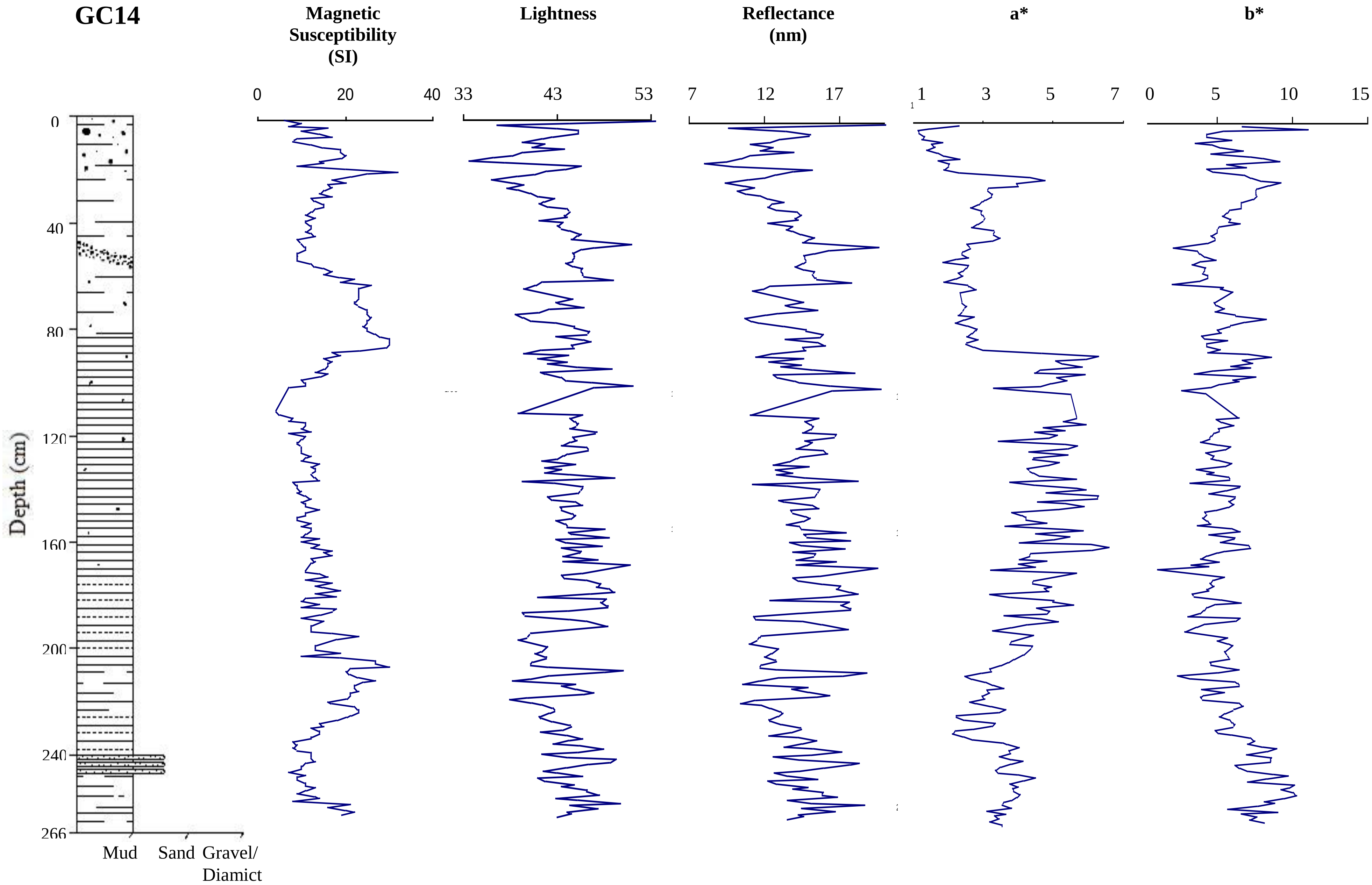

Figure 5.8 – Core log of GC14 presented alongside corresponding magnetic susceptibility, sediment lightness, greyscale reflectance, a* and b* values

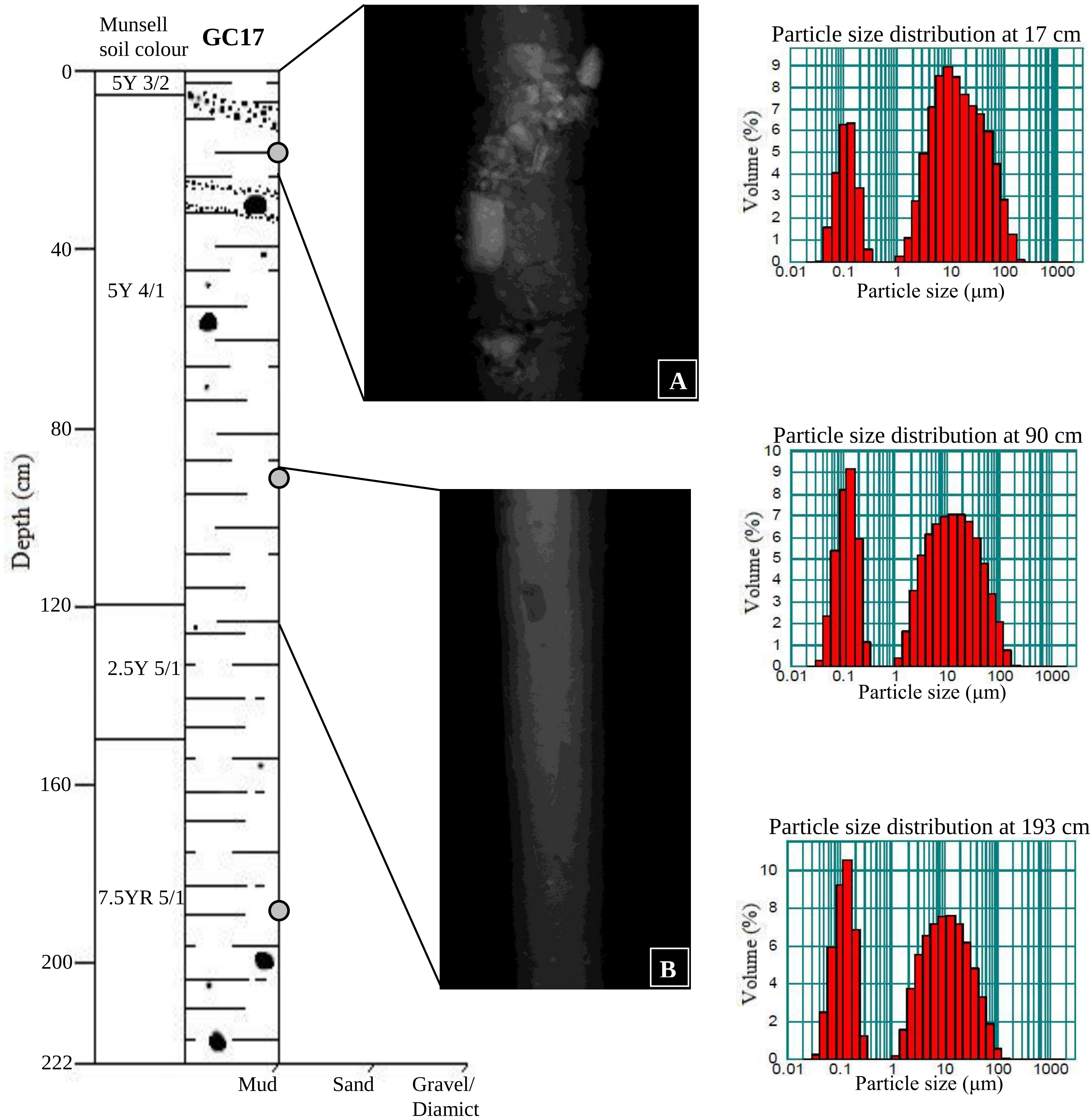

Figure 5.9 – Core log of CG17 with Munsell soil colour and particle size data. A) – X-radiograph of a prominent clast-rich sub-horizontal horizon. B) – X-radiograph of a section of fine-grained mud with rare clasts

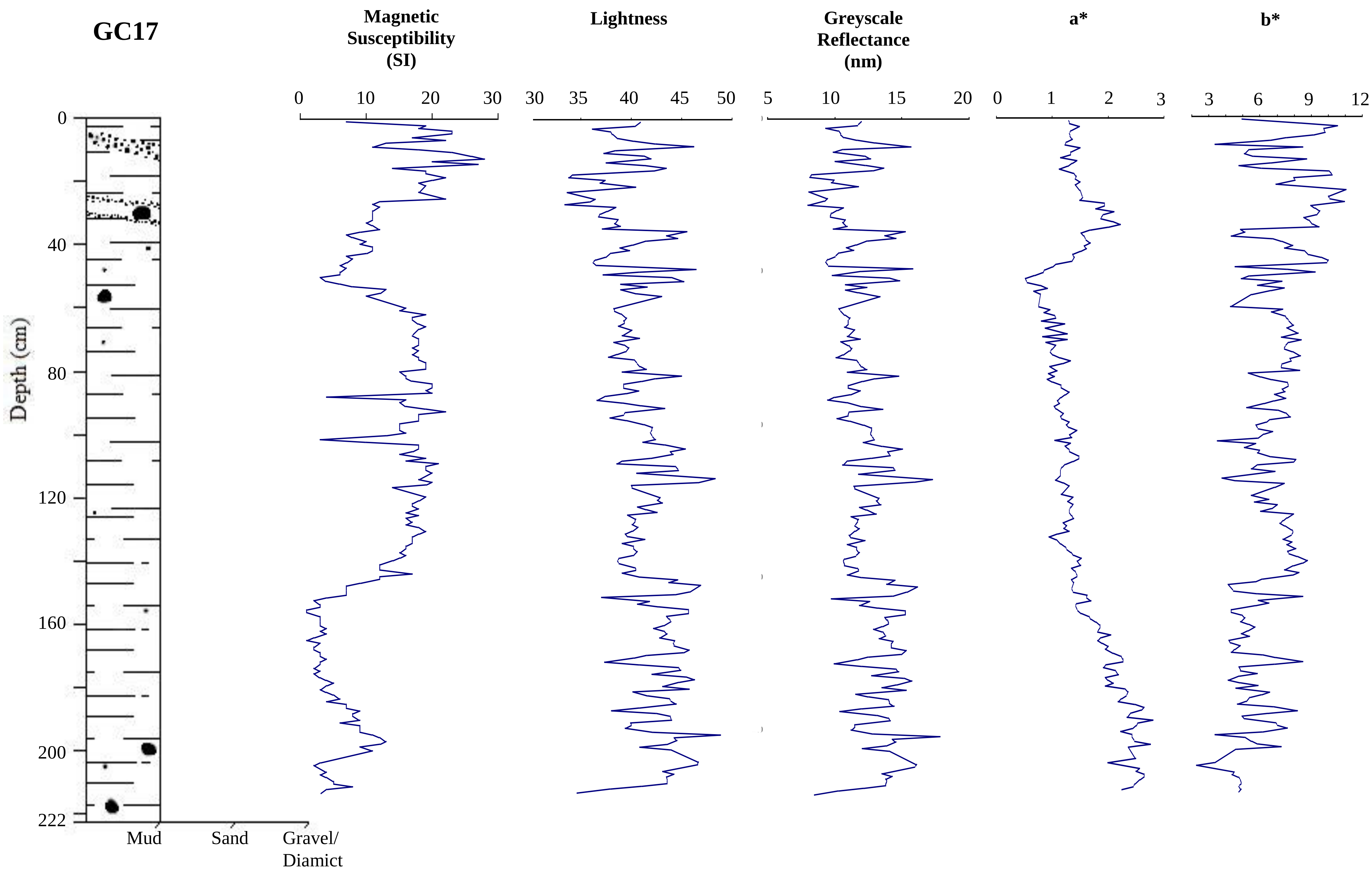

Figure 5.10 – Core log of GC17 presented alongside corresponding magnetic susceptibility, sediment lightness, greyscale reflectance, a* and b* values

5.2.3 GC14

GC14 is composed entirely from massive and stratified fine-grained muds (Figs. 5.7). The top 18 cm of the core is characterised by a massive mud containing abundant pebble-sized clasts (Fig. 5.7A). A distinctive change to a fine-grained mud lacking outsized clasts then dominates the core until a narrow and diffuse sub-horizontal coarse horizon occurs at 53 cm. A small paired bivalve was identified at 33 cm, demonstrating *in situ* deposition. Massive colour banding between red-brown (5YR 5/4) and brown-grey (7.5YR 5/1) mud occurs between 82 and 177 cm with banding at 5 – 20 mm intervals (Fig. 5.7B). Particle size analysis demonstrates that this stratified subfacies does not display any corresponding changes in grain size and that no significant changes in mean particle size are observed along the core (Fig. 5.7). Three thin (<2mm) discontinuous sand lenses occur between 240 and 246 cm.

GC14 exhibits three main peaks in magnetic susceptibility; at 20 cm, between 60 and 80 cm, and at around 200 cm (Fig. 5.8). The low magnetic susceptibility values recognised between 85 and 177 cm correspond with the position of the stratified mud subfacies. No significant patterns or changes are observed within the parameters of sediment lightness or greyscale reflectance throughout the core. The a* and b* values demonstrate a dramatic increase in green colour hues at 82 cm, a change which corresponds with the initiation of stratified colour banding within the core.

5.2.4 GC17

GC17 is composed entirely of a fine-grained mud, which is texturally classified as coarsely-skewed clay (Fig. 5.9). Particle size analysis reveals a slight down-core increase in grain size throughout the length of the core. A distinct clast-rich horizon occurs between 4.5 and 12 cm, characterised by sub-horizontal upper and lower contacts (Fig. 5.10A). The top third of the core is characterised by a massive green-olive mud containing many outsized clasts. Two thin clast-rich horizons occur at around 25 cm and 32 cm and dropstones with lengths of approximately 40 mm occur at 30 cm and 58 cm. Rare sub-angular clasts with black or pink crystalline lithologies are present from 59 cm until the base of the sequence. Organic matter and rare shelly fragments occur throughout the core and dropstones are recognised at 200 cm and 218 cm. High magnetic susceptibility values exist at the start of the core and also between 62 and 150 cm (Fig. 5.10). Lightness and greyscale reflectance values exhibit a slight increase down-core. The a* values increase until 35 cm, where they are dramatically reduced before increasing gradually until the end of the core.

5.3 Correlation of Sediment Cores, Submarine Landforms and Acoustic Facies

5.3.1 GC16

GC16 was obtained from the continental shelf slope of Hinlopen Trough (Figs. 2.4 and 5.12). TOPAS data demonstrates that this core was recovered from a thin layer of acoustic Facies T (Fig. 5.11C). The semi-prolonged nature of the surface reflector suggests that the upper unit of this core is composed of coarse sediment – an observation which is supported by the presence of diamict at the top of the core.

5.3.2 GC15

GC15 was recovered from an area of the sea floor characterised by the presence of elongate subglacial landforms. TOPAS data reveals that the acoustic stratigraphy of this location consists of Facies D and S overlying Reflector B1B (Fig. 5.11B). Facies D and S are shown to exhibit a combined thicknesses of between 1.5 and 4 m in this area. It is therefore likely that GC15 penetrated the acoustically-impenetrable surface of Reflector B1B and that the underlying acoustic unit corresponds to the diamict facies discovered at the base of this core.

5.3.3 GC14

GC14 was recovered from the transitional zone between the middle- and inner-shelf areas of the trough. TOPAS data shows that this core was retrieved from Acoustic Facies D (semi-transparent sediment drape), which is approximately 4 m deep at the core site (Fig. 5.11A). At 2.66 m in length, this core did not sample the underlying unit of acoustic facies S or penetrate the acoustically-impermeable surface of Acoustic Reflector B1B. The identification of stratification within GC14 suggests that Facies D also exhibits some weak stratification below the resolution of the sub-bottom profiler.

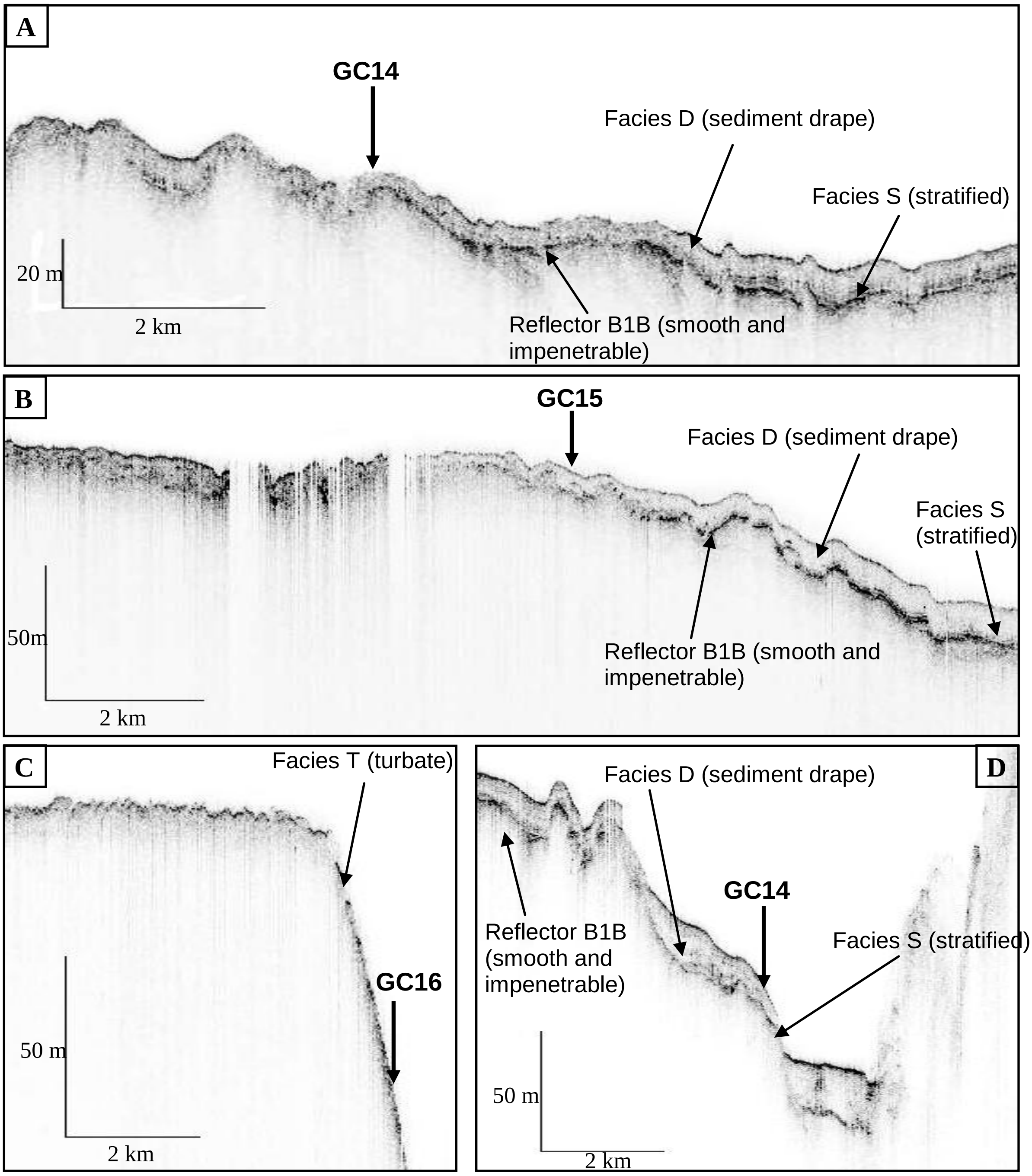

Figure 5.11 – Correlation between sub-bottom profiler data and sediment cores (arrowed)
A) – Location of GC14. B) – Location of GC15 C) – Location of GC16 D) – Location of GC17

5.3.4 GC17

GC17 was recovered from a localised topographic depression within the glacially-sculpted inner-shelf area of the trough. The acoustic stratigraphy of this site consists of a thick unit of Facies D and S, and the acoustically impenetrable surface of Reflector B1B (Fig. 5.11D). TOPAS data demonstrates that the core was recovered from a unit of acoustic Facies D and that it did not penetrate the underlying acoustic units of Facies S or Reflector B1B.

Sedimentological logs for each of the four cores collected from Hinlopen Trough are presented in Fig. 5.12. These core logs allow comparisons of sedimentological properties between cores obtained from different locations within the trough.

5.4 Sediment Facies: Interpretation

5.4.1 Diamict

Diamicts are common sedimentary facies on high latitude continental shelves and can be formed through a variety of different processes, including subglacial deposition, ice rafting of debris, iceberg scouring, and submarine sediment gravity flows. Analyses of sediment lithology, particle size, geometry, position in the stratigraphy, and the nature of facies contacts can allow differentiation between facies deposited by different glacial and glacimarine processes.

Diamict in GC16

The diamict located at the top of the sedimentary sequence in GC16 is characterised by a relatively sharp sub-horizontal basal contact (Figs. 5.3 and 5.12). Although this seems to suggest a subglacial origin (Bennett and Glasser, 1996), its position at the top of the stratigraphy, low magnetic susceptibility values, and very thin vertical duration exclude this mode of formation.

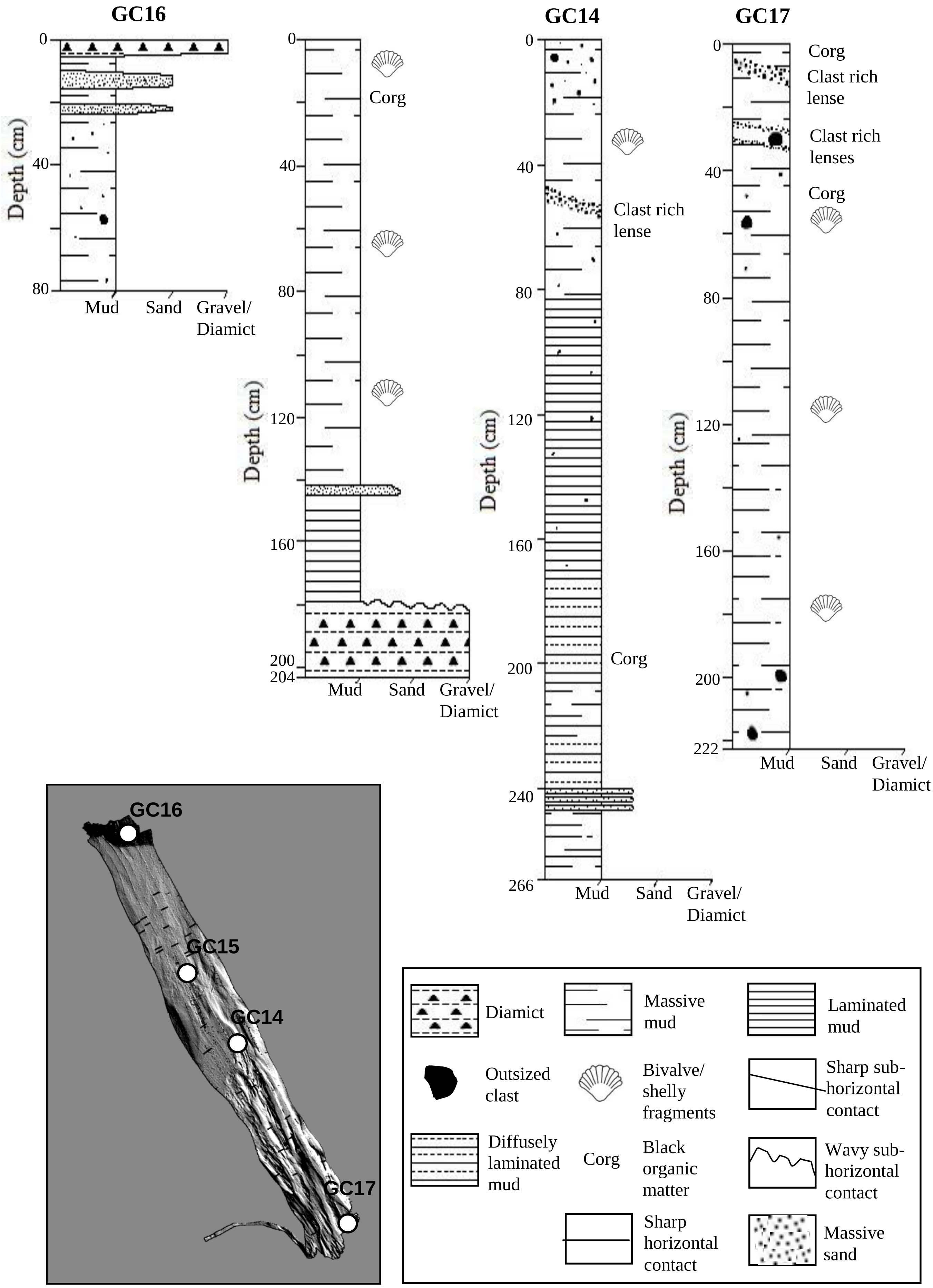

Figure 5.12 – Sedimentological logs of the four cores sampled from Hinlopen Trough (GC14, GC15, GC16 and GC17). The location of the sediment cores is also depicted (inset greyscale image)

This deposit cannot be described as IRD as it does not display the characteristic conforming basal contacts indicative of passive rain-out through the water column (Ó Cofaigh and Dowdeswell, 2001). Although the location of this core on the steep continental slope, combined with the history of subaqueous mass movements in this area (Cherkis et al., 1992, 1999; Vanneste et al., 2006; Winkelmann et al, 2008a), suggests an origin as a debris flow, the absence of acoustically transparent lenses near the cored location prevents such an interpretation.

Iceberg turbate diamicts are typically enriched in sand and usually possess a stratified internal structure (Domack et al., 1998). The clasts in this diamict are generally aligned in a sub-horizontal direction and x-radiograph images display evidence of a sub-horizontal planar structure (Figs. 5.3A). The location of GC16 on the upper continental slope and its recovery from a thin layer of acoustic Facies T (Fig. 5.11, interpreted as iceberg turbate) also support an interpretation as iceberg turbate diamict.

It is likely that the lack of fines identified from within this unit reflects the operation of glacimarine sediment reworking processes. Lag deposits produced by current winnowing can be differentiated by their negatively skewed size distributions and internal stratification (Ó Cofaigh et al, in Dowdeswell and Ó Cofaigh, 2002). The North-Svalbard Branch of the West Spitsbergen Current, which operates in this area, (Harland et al, 1997; Vanneste et al., 2006) provides a likely source for the operation of current winnowing and the creation of pebbly lag deposits.

Diamict in GC15

The location of the diamict deposit in GC15 at the bottom of the sedimentary sequence directly beneath a laminated clast-rich fine-grained mud (Fig. 5.12) suggests a subglacial mode of deposition. The acoustically impenetrable surface reflector of this unit (Reflector B1B), and GC15's location in an area dominated by subglacially-formed sedimentary drumlins, suggests that this diamict represents glacial deformation till.

Similar deposits of subglacial till have been identified from a number of locations on Svalbard’s continental margins (e.g. Elverhoi and Solheim, 1983; Svendsen et al., 1992, 1996; Mangerud and Svendsen, 1996; Kleiber et al., 2000), and are commonly associated with the presence of elongate subglacial bedforms. High magnetic susceptibilities were recorded at the onset of this facies, supporting evidence for a greatly-increased influx of coarse terrigenous material to the cored site.

The stiff nature of this diamict is also suggestive of a subglacial origin. Such evidence of overcompaction is commonly interpreted to have resulted from the weight of an overlying ice sheet acting in combination with a number of deformation processes (Ó Cofaigh et al., 2005a; Heroy et al., 2008). However, subglacially-deformed tills need not be overconsolidated (Kluiving et al., 2009) and microfabric analysis is generally needed to distinguish subglacial and glacimarine diamictons. It is therefore not possible to exclude the possibility that this facies could represent a transitional facies between the subglacial and marine environments, composed of ice-proximal IRD, suspended sediments or ice shelf rain out.

5.4.2 Fine grained muds

Stratified fine-grained muds. This subfacies is located near the bottom of the sedimentary sequence in GC14 and GC15 (Fig. 5.12). Stratification in both cores is parallel, laterally-continuous, and does not exhibit any changes in grain size between bands. Settling of suspended sediment creates unstratified sedimentary structures under uniform conditions (Møller et al, 2001); stratified sequences are only produced due to changes in dynamic conditions, such as those associated with diurnal meltwater fluctuations or annual shifts in meltwater fluxes (Dowdeswell et al, 2000). Deposition from turbid meltwater plumes typically produces either rhythmically laminated couplets of silt and mud, called cyclopels, or of sand and mud, termed cyclopsams (Cowan and Powell,1990). The lack of variation in grain size between colour bands in GC14 and GC15 precludes their interpretation as cyclopels or cyclopsams, and also prevents their interpretation as turbidities, debris flows or current winnowing deposits. The planar, parallel and laterally continuous nature of the stratified muds suggests they were deposited by the settling of suspended material through the water column

(Ó Cofaigh and Dowdeswell, 2001). The colour banding observed in GC14 and GC15 is most likely a result of the changing chemical composition of suspended sediments and possibly describes seasonal variations in organic material.

TOPAS data demonstrates that this subfacies is represented by the acoustically stratified Facies S, which has been interpreted as the produce of hemipelagic sedimentation. The location of this subfacies just above a unit of diamict suggests that these stratifications form part of a deglacial sequence, recording fluctuations in sediment composition as the ice front become progressively more distal.

Glacimarine sedimentation is greatly influenced by the proximity of glaciers; a decrease in mean particle size is typically recorded in a sequence as the core location becomes more distal from the ice front (Dowdeswell et al., 1998; Zeeberg et al., 2003). Magnetic susceptibility values increase down-core within the stratified subfacies in GC14 and GC15, paralleling the observed down-core increase in the frequency and dimensions of outsized clasts. This trend has been noted in a number of sedimentological studies (e.g. Heroy et al., 2008; Nørgaard-Pedersen et al, 2009; Yoon et al., 2000) and represents the decreased supply and deposition of IRD throughout the Holocene (Nam et al., 1995). The sparse occurrence of outsized clasts in the stratified subfacies of GC14 and GC15 do not necessarily represent low levels as IRD, but may record dilution of the IRD signal by large quantities of meltwater-derived sedimentation (Dowdeswell et al., 1998; Evans, in Dowdeswell and Ó Cofaigh, 2002).

The stratified deposits observed in GC14 and GC15 are therefore interpreted to represent ice-proximal sediments recording high rates of sediment delivery from glacial meltwater and IRD during deglaciation. The fining-upwards sequence identified within these two cores represents a gradual shift from an ice-proximal to a more ice-distal environment. Similar deglacial sequences have been identified from a number of locations on Svalbard’s continental shelf (e.g. Svendsen et al., 1992; Svendsen et al., 1996; Dowdeswell et al., 1998; Kleiber et al., 2000; Murdmaa et al., 2006; Hogan et al., 2008), and have been interpreted to represent proximal glacimarine facies produced during and after ice decoupling from the sea bed.

Sand lenses within fine-grained mud. Thin sand lenses occur within three of the four sampled cores; between 11 cm and 15 cm in GC16, between 146 cm and 146.5 cm in GC15, and between 140 cm and 146 cm in GC14 (Fig. 5.12). All of the observed sand lenses display relatively sharp wavy sub-horizontal contacts. These features are not rhythmic, parallel or continuous, and as such were not deposited as cyclopels or cyclopsams from turbid meltwater plumes (Cowan and Powell, 1990). While the small widths of the sand lenses observed in GC14 and GC15 prevents any correlation with data collected from the GEOTEK multi-sensor core logger, the locations of the wider sandy layers within GC16 correlate with small increases in magnetic susceptibility, lightness and reflectance, and yellow hues in the sediment (Fig. 5.4). The increased magnetic susceptibility values illustrate enhanced levels of coarse material within these layers, whilst the lighter colour of these deposits accounts for the observed increases in lightness, reflectance and b* values.

The sand lenses in these cores occur near the bottom of the stratigraphy, within sections of fine-grained mud. Turbidity currents typically represent the major source of sand deposits in deep water environments (Cai et al., 1997). These features allude to relatively ice-proximal settings (Cai et al., 1997; Ó Cofaigh and Dowdeswell, 2001) and can be distinguished in the sedimentological record by their sharp basal contacts and characteristic upwards-fining sequences. The lack of upwards-fining within the sand lenses identified from Hinlopen Trough does not necessarily exclude a turbidity current origin for these deposits; the small widths of these sand lenses may have prevented identification of fining.

The sandy lenses identified from Hinlopen Trough may have alternatively been created, or at least partially reworked, by the operation of along-slope currents. The sandy layers in GC14, GC15 and GC16 are morphologically similar to horizons described by Hogan (2008) from Svalbard's continental shelf and interpreted to have formed through variations in the intensity of along-slope currents. There is typically a large degree of interplay between turbidity currents and contourites and the morphological similarities of the resulting facies ensures it is not generally possible to differentiate sandy contourites from other re-worked deposits such as outer-shelf sands or thin turbidites (Faugeres and Stow, 1993).

Clast-rich horizons within fine-grained mud. Clast-rich horizons occur within two of the four sampled cores; between 4.5 cm and 12 cm and at 25 cm and 32 cm in GC17, and at 73.5 cm in GC14 (Fig. 5.12). The widest clast-rich horizon in GC17 displays relatively sharp sub-horizontal upper and lower contacts and contains a large number of randomly orientated clasts of a few mm in length. This deposit cannot be interpreted as IRD due the sharp nature of its contacts, and its position near the top of the sedimentary sequence (Ó Cofaigh et al., in Dowdeswell and Ó Cofaigh, 2002).

This core is obtained from a topographic depression within the inner-shelf region of glacially-sculpted bedrock (Fig. 5.11). The presence of acoustically transparent units has revealed that this area has experienced a number of debris slides and that material from these slides frequently collects within topographical depressions (Dowdeswell et al., 1997; Canals et al., 2000; Taylor et al., 2000; Møller et al, 2001; Hjelstuen et al., 2009). It is therefore likely that this clast-rich horizon represents a minor debris slide deposit.

The smaller clast-rich horizons identified in GC14 and GC17 are interpreted to either represent minor debris flow events, high-energy turbidity currents, or variations in cross-shelf currents. Clast-rich horizons are identified near the top of the stratigraphy and are found in association with facies of fine-grained mud. It is therefore likely that these deposits represent debris slides resulting from the gradual overloading of inner-shelf steep slopes during a period of Holocene hemipelagic sedimentation.

Massive fine-grained mud. Fine-grained mud occurs in all four of the cores collected from Hinlopen Trough (Fig. 5.12). This facies is interpreted to have been deposited by the continuous vertical accretion of suspended sediment through the water column, combined with the occasional deposition of IRD. This conclusion is supported by the conformable nature of the deposits, their position at the top of the stratigraphy, and the abundant Holocene shelly fragments and organic material associated with this facies. The general down-core increase in magnetic susceptibility and clast content illustrates a decrease in the supply of coarse material and suspension setline in response to retreat of the ice front.

The a* values display down-core increases within all four cores, whilst the b* values display corresponding down-core decreases. These trends describe the changing colour of the sediments from red and yellow hues at the start of the sequence, to green and blue hues at the base of the cores. These changes may reflect the darker and greyer nature of the sediments as they become enriched in clay particles down-core. Lightness and reflectance measurements can be used as proxies for climatic changes due to their ability to indicate variations in the calcium carbonate and clay contents of sediment (Dowdeswell and Ó Cofaigh, 2002). Glacial periods are typically characterised by increased amounts of dark detrital clay particles combined with decreased levels of lighter-coloured biogenic carbonate derived from foraminifera (Cartijo et al., 1995; Balsam et al., 1999; Grutzner et al, 2002; Nederbragt et al., 2006; Rogerson et al., 2006). However, whereas lightness and reflectance values would therefore be expected to decrease down-core these parameters exhibit a slight down-core increase in all of the four cores. This apparent discrepancy can be explained through examination of the organic content of the cores; organic material is recorded as black pellets and streaks, serving to darken the sediment and reduce lightness and reflectance values. The decreasing lightness and reflectance values identified within the cores therefore illustrate a scenario in which the amount of organic material decreases throughout the deglaciation of Hinlopen Trough in response to warmer waters and a more ice-distal environment.

Chapter 6 - Synthesis

6.1 Synthesis and Identification of Glacial Landsystems

Detailed geophysical and geological analysis has permitted the identification and interpretation of a number of glacigenic features from the sea floor of Hinlopen Trough, north of Svalbard. A synthesis of these data is now required in order to illustrate the spatial and temporal landform patterns in this area and to provide insights into the dynamics of past ice stream behaviour.

The distribution of the submarine landforms identified from Hinlopen Trough is summarised in Fig. 6.1.

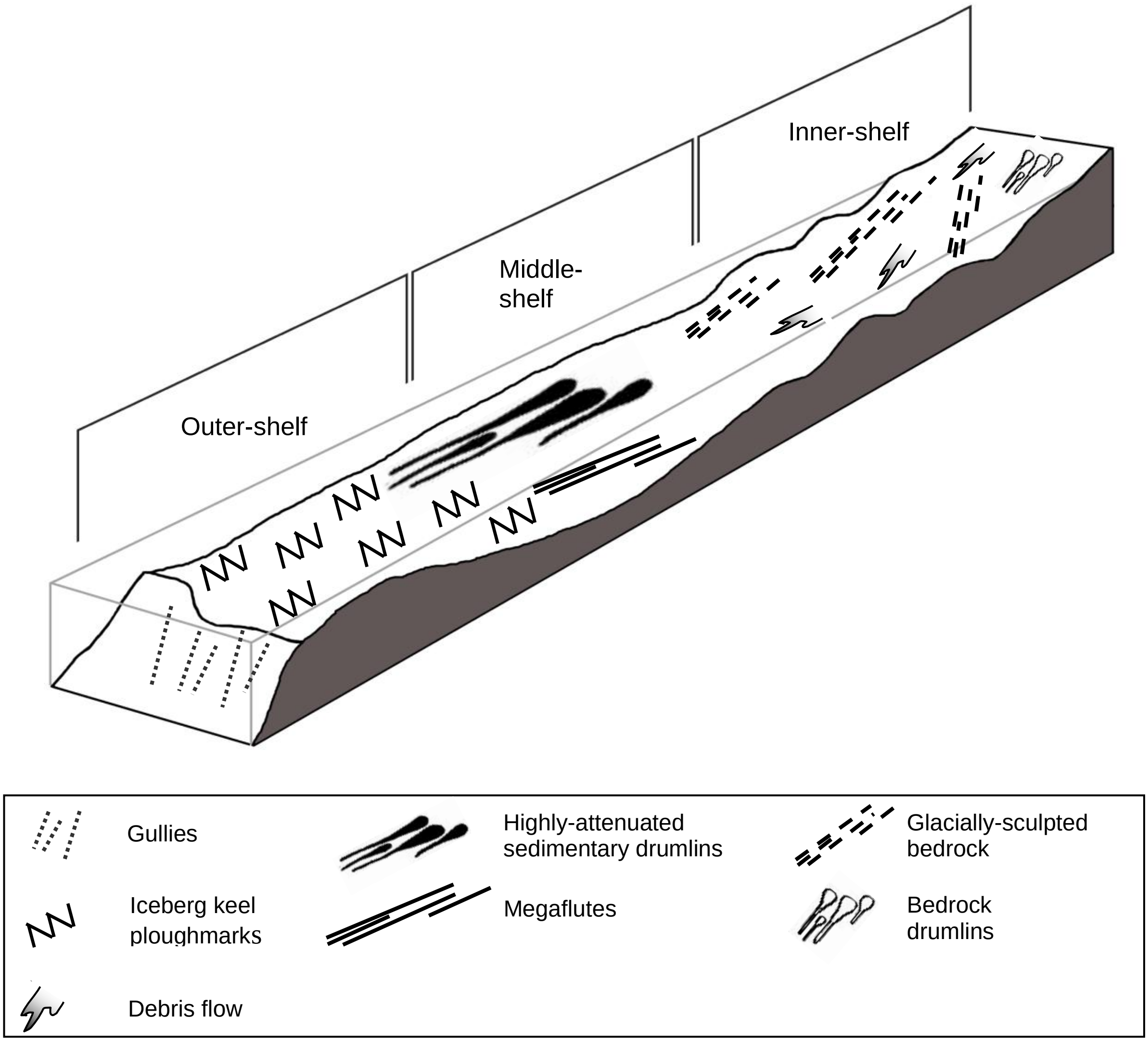

Figure 6.1 – Schematic model of the distribution of submarine landforms within Hinlopen Trough

This schematic model illustrates how the inner-shelf region of the trough contains glacially-sculpted bedrock and drumlins. The crystalline bedrock substrate is variably overlain by a thin post-glacial sediment drape, which has accumulated in local basins and is absent from topographical highs (Fig. 4.4). Sediment accumulation on steep slopes has led to the development of debris flows within this region, the evidence for which has been identified from acoustic profiles (Fig. 4.2).

The transition to the middle-shelf is signified by a change from bedrock to a sedimentary substrate and by the presence of elongate subglacial landforms. These features are formed within subglacial till, overlain by stratified ice-proximal meltwater sediments and a post-glacial sediment drape (Fig. 4.4). The outer-shelf is dominated by a large number of linear to curvilinear iceberg keel ploughmarks formed within a chaotic sedimentary unit, interpreted as iceberg turbate. Gullies are present on the uppermost continental slope.

A simple glacial inversion model (Table 2.2) will now be employed in order to reduce the complexities associated with landform analysis and to facilitate interpretations of the glacimarine record in Hinlopen Trough. The morphological elements identified within Hinlopen Trough were classified into five landform assemblages according to their inferred origins and relative ages. Genetically-linked landform assemblages were then compiled in order to define two glacial landsystems; the subglacial and the ice-distal landsystems (Table 6.1).

Landform Assemblage	Landform System	Relative Age
Iceberg keel ploughmarks	Ice-distal	Younger
Highly attenuated sedimentary drumlins	Subglacial	Older
Megaflutes	Subglacial	Older
Bedrock drumlins	Subglacial	Older
Glacially-sculpted bedrock	Subglacial	Older

Table 6.1 – The five landform assemblages and two landform systems identified within Hinlopen Trough

The superimposition of iceberg keel ploughmarks upon the subglacial features in the trough allowed their relative age to be inferred. The absence of additional cross-cutting relationships within the surveyed area prohibited any inferences about the relative ages of the subglacially-produced landforms.

The four landform assemblages which comprise the subglacial landsystem were interpreted to have formed at the base of a grounded ice sheet during the same ice flow event. Evidence for the contemporaneous formation of these features includes their similar 'fresh' appearances on swath bathymetry images and the comparable depths of their overlying post-glacial sediment drapes identified from acoustic profiles. Some minor variation in the timing of landform genesis is, however, expected between features within this landsystem; it is likely that the distinct basal conditions suitable for the formation of certain landforms shifted along the trough over time. In addition to these four landform assemblages, the subglacial landsystem can also be seen to include the unit of subglacial till identified from a sediment core (Figs. 5.6 and 5.11) and from acoustic profiles. Given that Hinlopen Trough was almost certainly occupied by ice during earlier Quaternary glaciations, particularly the Saalian (Svendsen et al., 2004), the bedrock landforms may contain some imprint of earlier full-glacial episodes.

No ice-proximal landform assemblages, such as transverse terminal or recessional moraine ridges, were identified from the morphological record. Sediment cores and acoustic profiling have, however, revealed the presence of a stratified sedimentary unit directly above the facies of subglacial till. This feature has been interpreted to record an ice-proximal environment during deglaciation and represents fluctuations in sediment composition as the ice front became progressively more distal.

Iceberg keel ploughmarks represent the only landform assemblage recorded from the ice-distal landsystem. These features are superimposed upon the tails of highly attenuated sedimentary drumlins and are formed on the outer-shelf within a sedimentary unit of iceberg turbate. The thin drape of hemipelagic sediments, which variably overlies landforms in all regions of the trough, can also be considered to have formed within an ice-distal environment, and probably continued to form during the Holocene.

6.2 Interpretation of Past Ice Stream Behaviour

6.2.1 The Hinlopen Trough Ice Stream

This investigation has facilitated the recognition of a wide range of geomorphological features indicative of the former presence of fast ice flow within Hinlopen Trough (Fig. 6.1). Although the notion of a Hinlopen Trough ice stream is not novel (Ottesen et al., 2007), the wide range of geophysical and geological data analysed in this project allows detailed new insights into the dynamics of former ice flow in this region.

The identification of streamlined bedforms with high elongation ratios (up to 20:1) provides strong evidence of former fast-flowing ice in Hinlopen Trough (Stokes and Clark, 1999, 2002; Ottesen et al., 2005a, 2007). Whilst it is recognised that streaming ice flow will not always produce highly attenuated bedforms, such features have been observed forming at the bases of modern ice streams (King et al., 2009) and are firmly established morphological indicators of the locations of former ice streams (e.g. Shipp et al., 1999; Canals et al., 2000; Ó Cofaigh et al., 2002, 2005a; Ottesen et al., 2005a, b, 2007; Dowdeswell et al., 2010a).

The formation of these elongate bedforms within an inferred unit of subglacial till provides additional evidence for former fast ice flow. Pervasive and spatially-extensive units of deformed sediment indicate areas of former ice-streaming through the deformation of soft sediments at the base of an ice sheet (Clark, 1993; Stokes and Clark, 1999, 2002). This investigation could not constrain the lateral or vertical extent of this unit within Hinlopen Trough, and therefore can only hypothesise that widespread deformable sediments may exist within this region.

Analysis of the orientation of subglacial landforms can allow interpretations of past ice flow directions (e.g. Dowdeswell et al., 2006, 2010a). The elongate sedimentary landforms identified on the middle-shelf in Hinlopen Trough are consistently orientated in an NNW off-shore direction. In contrast, the drumlinised landforms on the inner-shelf exhibit a wider range of orientations and appear to follow the structural grain of the bedrock. The orientation of landforms identified from Hinlopen Trough confirms that ice flowed in a northerly direction through the trough towards the shelf break. The slightly more easterly orientation of the megaflute assemblage (Fig. 3.5) may represent the convergence of ice from the adjacent Wijdefjorden Trough in the west.

The landform elements identified within Hinlopen Trough (Fig. 6.1) compare closely with those described by an ice-stream landform model for major Svalbard fjord and trough systems (Fig. 6.2).

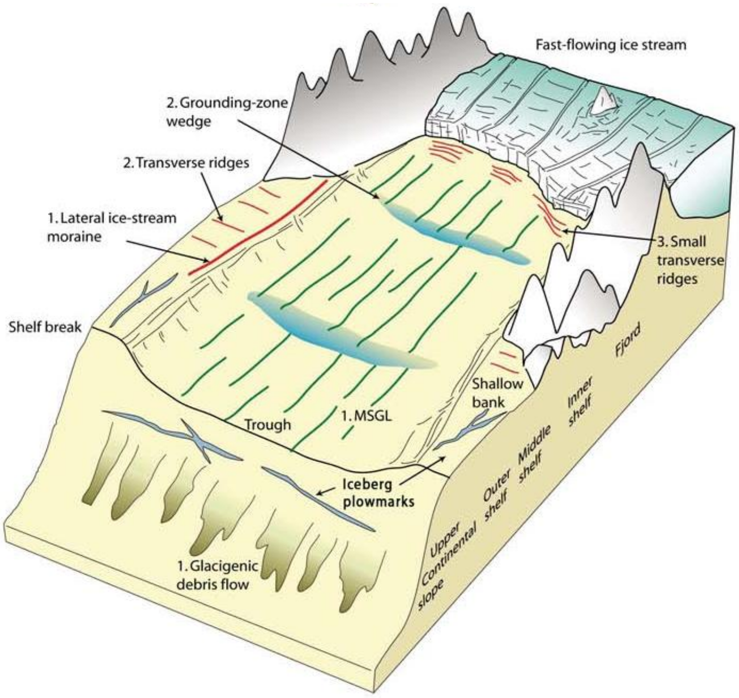

Figure 6.2 – An ice stream glacial landform assemblage produced from swath bathymetric data of major Svalbard fjord and trough systems (from Ottesen and Dowdeswell, 2009)

This model describes how ice streams are typically located within cross-shelf troughs and are dominated by the presence of elongate landforms orientated parallel to the inferred ice flow direction. This assemblage contrasts to the inter-ice stream model, which is dominated by landforms orientated transverse to ice flow and produced through slow retreat of the ice margin (Ottesen and Dowdeswell, 2009). The landform model constructed for Hinlopen Trough (Fig. 6.1) possess a number of similarities with the idealised schematic model; elongate glacial lineations comprise the main morphological element within the trough, with iceberg ploughmarks also present near the shelf break. In contrast to this model, grounding-zone wedges and lateral ice stream moraines were not identified from the morphological record in Hinlopen Trough, suggesting rapid retreat of the ice margin during deglaciation (Dowdeswell et al., 2008).

6.2.2 Landform Progression within Hinlopen Trough

Swath bathymetry data has revealed a down-flow landform progression within Hinlopen Trough; inner-shelf drumlins and glacially-sculpted bedrock are replaced by more elongate sedimentary landforms on the middle and outer-shelf (Fig. 6.1).

A similar pattern of progressive bedform elongation has been observed on the Norwegian-Svalbard margin (Ottesen et al., 2005a, b) and from several locations on the Antarctic continental margin (e.g. Shipp et al., 1999; Ó Cofaigh et al., 2002, 2005a, b; Lowe and Anderson, 2003; Mosola and Anderson, 2006; Wellner et al., 2006). This bedform continuum (Ó Cofaigh et al., 2002) is suggested to represent a change from net erosion to net deposition within the trough (Shipp et al., 1999; Lowe and Anderson, 2003). The most landward region of the shelf is typically characterised by meltwater features and glacially-sculpted bedrock. These landforms become more uniformly-orientated down-trough and streaming ice flow is generally initiated down-flow of a boundary between crystalline bedrock and a sedimentary substrate. Cross-shelf troughs generally become wider and shallower at this point and are characterised by the presence of glacial lineations and iceberg keel ploughmarks (Ottesen et al., 2005a, b). Lineations typically occur in the deepest parts of a trough as these areas possess the highest ice velocities (Ó Cofaigh et al, 2005a).

The landform progression identified in Hinlopen Trough possesses a number of similarities to this general model. The presence of sedimentary lineations in the deepest section of the middle-trough, beyond the transition from bedrock to a sedimentary substrate, provides strong evidence of former fast ice flow in this location. Ice flow velocities in Hinlopen Trough are inferred to have increased towards the north. Although fast ice flow may have occurred across both substrates, the lower elongation ratios exhibited by the streamlined bedforms on the inner-shelf suggests that the highest flow velocities occurred within the sedimentary substrate in the middle-trough. This transitional region probably represents a zone of ice acceleration and it is likely that fast ice flow was initiated in this area as a result of the availability of deformable sediment (Ó Cofaigh et al., 2002).

6.2.3 Evolution of the Hinlopen Trough Ice Stream

The geophysical and geological data collected from Hinlopen Trough can be compiled to provide a simple description of ice evolution in this area. This narrative represents a lateral shift in depositional environment and is responsible for creating the characteristic deglacial sequence identified within the sediment cores and acoustic profiles.

1) Ice Flow Phase. A period of grounded ice advance over the continental shelf is recorded by the presence of elongate landforms and subglacial till within the trough. The long and highly attenuated nature of these subglacial landforms suggests that fast ice flow occurred in at least some regions of the trough and was possibly initiated close to the middle-shelf transition from bedrock to a sedimentary substrate. This ice flow phase is interpreted to represent the last major ice advance on Svalbard – the Late Weichselian glaciation. This inference is supported by the 'fresh' appearance of these features on swath bathymetry images and by the relatively thin (<15 m) overlying drapes of hemipelagic sediment identified from acoustic profiles. Radiocarbon dates have confirmed that Late Weichselian ice reached Svalbard's continental shelf edge in a number of comparable cross-shelf trough locations, resulting in the formation of similar assemblages of subglacial landforms (Svendsen et al., 1992; 1996; Elverhøi et al., 1995; Landvik et al., 1998; 2005; Dowdeswell and Elverhøi, 2002). Some instances of streaming ice flow have been suggested to occur as glacidynamic responses to regional deglaciation (Ó Cofaigh et al., 2005a). However, it is not possible to infer the stage during the Late Weichselian at which fast flow became initiated in Hinlopen Trough.

2) Deglaciation. The retreat of ice through Hinlopen Trough is not recorded in the morphological record. The absence of transverse landforms suggests that deglaciation of the trough was rapid and did not involve any significant still-stands of the ice margin (Dowdeswell et al., 2008). The stratified sediments identified near the base of the stratigraphy (Fig. 5.11) have been interpreted to signify meltwater fluctuations during relatively ice-proximal deglacial conditions. The timing of regional deglaciation could not be constrained due to an absence of dateable material recovered from the sediment cores collected from Hinlopen Trough. The retreat of Late Weichselian ice from Svalbard's continental margins has been inferred to have been largely step-wise in nature and is generally accepted to have commenced between 13 and 15 kyr, based on dated cores elsewhere around the archipelago (Svendsen et al., 1992, 1996; Elverhøi et al., 1995; Dowdeswell and Elverhoi, 2002).

3) Ice-free conditions. The fine-grained organic-rich sediments observed within the sediment cores (Fig. 5.12) represent a largely ice-free open water environment. This unit is located at the top of the sedimentary and acoustic sequence and is interpreted to have formed through the vertical accretion of suspended sediments through the water column. The association of this facies with open water conditions is illustrated by the high levels of organic material and shelly fragments identified within this unit (Fig. 5.12). It is likely that the majority of this facies was deposited during the Holocene. Radiocarbon dating of material within a long (713 cm) sediment core obtained from Hinlopen Trough has previously revealed that ice began to retreat from the shelf margin between 13.7 and 13.9 kyr, facilitating the opening of surface waters in this region around 10.8 kyr (Koç et al., 2002). This sediment core was collected from 80°21.346'N, 16°17.970'E (400 m water depth) and was therefore obtained from a similar location to the 266 cm long core GC14 which was analysed in this project (80°23.460'N, 16°26.450'E, 352 m water depth).

6.2.4 Basal Conditions

The geophysical and geological data collected from Hinlopen Trough permit some limited inferences about the basal conditions of ice in this area. Although their mechanism of formation remains relatively enigmatic, elongate subglacial landforms are associated with the operation of certain basal conditions. Ice-bed coupling involves the penetration of subglacial water into underlying soft sediments and can facilitate fast ice flow through deformation of the substrate (Dowdeswell et al., 2004; Ó Cofaigh et al., 2005a; Hogan, 2008). This mechanism requires the presence of liquid water at the base of an ice mass. It is therefore likely that wide regions of middle- and outer-shelf basal ice reached its pressure-melting point, allowing warm-based ice to exist in some regions of the ice mass in Hinlopen Trough.

If fast ice flow were to have occurred in this region, as indicated by the presence of streamlined bedrock landforms, it may have been facilitated by ice sliding at the ice-bed interface. Any meltwater produced at the base of the ice mass would have been unable to permeate into the substrate. The lack of meltwater features observed from the inner-shelf (Fig. 3.7) suggests that subglacial meltwater played a minor or insignificant role in the advance and retreat of the ice stream.

6.2.5 Rates of Sediment Delivery

The Hinlopen Slide, beyond the mouth of Hinlopen Trough, took place at a minimum of 30 kyr ago (Winkelmann et al., 2008a). A post-slide trough-mouth fan has been identified from the continental slope north of Hinlopen Trough (Vanneste et al., 2006; Winkelmann et al., 2008a). Post-slide sediment infill occurred in the form of a sediment wedge and a debris lobe; these features drape the headwall scarp, producing a relatively gentle shelf slope (<10°) in this location (Fig. 6.3). These depocentres have been interpreted as glacigenic debris infill produced by the ice stream which drained Hinlopen Trough during the last glacial period (Vanneste et al., 2006; Winkelmann et al., 2008a). The accumulation of this sediment began directly after the mega-slide event and consequently provides a useful opportunity to examine the rate of sediment delivery to the continental margin during the post-slide period.

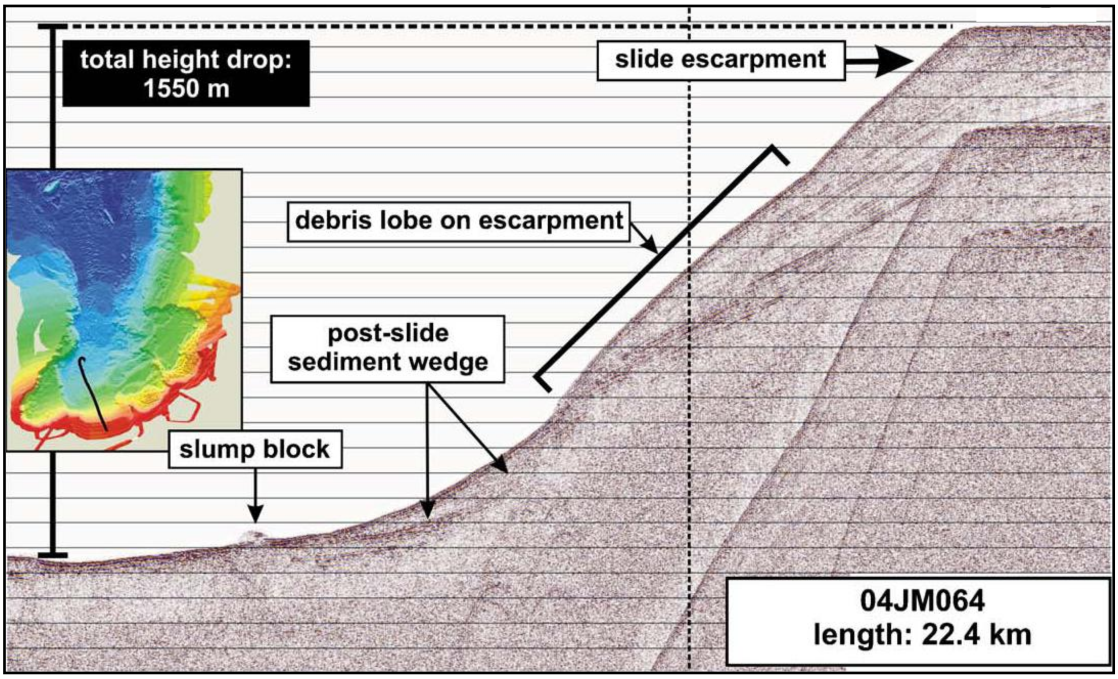

Figure 6.3 – A down-slope seismic profile across the Hinlopen headwall, depicting evidence of post-slide sediment infill in the form of a sediment edge and debris lobe (from Vanneste et al., 2006)

The average sediment delivery rate during this period was calculated through an analysis of the post-side infill data obtained by Vanneste et al. (2006), who proposed that the sediment wedge feature had a maximum thickness of 150 m and extended for 12 km into the slide zone. Seismic profiles illustrate that the debris lobe feature has a maximum thickness of 150 m and a lateral extent of roughly 6 km (Fig. 6.3). The total post-slide sediment depocentre was therefore interpreted to have a width of 10 km, a lateral extent of 18 km and an average thickness of 75 m; providing a trough-mouth fan area of around 180 km ^{2} and a volume of approximately 13.5 km^3.

The data used to calculate an average rate of sediment delivery to the Hinlopen margin between 30 and 15 kya, and between 25 and 15 kya, are displayed in Table 6.2. An average sediment delivery rate of 5 m/kyr was calculated by dividing the depocentre volume by the depocentre area and the defined time interval. This rate of sediment delivery can be considered as a conservative estimate as it does not include the small proportion of debris which may have bypassed the depocentre within icebergs or as suspended sediment in the water column (Dowdeswell et al., 2010b). Comparable rates of sediment delivery of between 1 and 6 m/kyr were calculated for the Bear Island and Storfjorden fans by Dowdeswell and Siegert (1999).

Age (kyr)	Time interval (kyr)	Depocentre volume (km³)	Average sediment delivery rate (m/kyr)
30-15	15	13.5	5
25-15	10	13.5	7.5

Table 6.2 – Sediment volume and rates of sediment delivery on the continental slope beyond Hinlopen Trough. Upper and lower time intervals were estimated at 30-15kyr and 25-15kyr respectively. These figures assume a depocentre area of 180 km². The sediment delivery rate was calculated by dividing the depocentre volume by its area and the time interval.

6.3 Implications for Late Quaternary Ice Sheet Dynamics

The identification, description and interpretation of submarine landforms can provide detailed regional information about the maximum extent and flow patterns of former ice masses. When compiled over wide areas of the sea floor, this information can greatly contribute to our understanding of the dimensions and dynamics of former ice sheets (e.g. Shipp et al., 1999; Wellner et al., 2001; Ottesen et al., 2005a, 2007; Dowdeswell et al., 2010b). The geophysical and geological investigation of Hinlopen Trough has provided high-resolution data concerning the nature of ice flow in this area. This information can be seen to have wider implications, both in terms of the regional dynamics of the last ice sheet over Svalbard, and in terms of the relationship between fast ice flow and submarine landforms more generally.

6.3.1 Submarine Landforms and Ice Sheet Dynamics

This investigation has confirmed that the bathymetric depression of Hinlopen Trough was occupied by a fast flowing ice stream during the Late Weichselian glacial period. The high rates of sediment delivery to the continental slope demonstrate that this ice stream represented a major pathway for the drainage of ice along the northern margin of the last ice sheet present over Svalbard. Rates of Late Weichselian sediment delivery are of similar magnitude to those on the huge Bear Island and Storfjorden fans, which derived from ice drainage from much of the Barents Sea (Dowdeswell and Siegert, 1999).

Evidence for streaming ice flow includes the presence of elongate submarine landforms formed within a unit of subglacial till. This information contributes to a wealth of data which stresses the strong and widespread relationship between elongate bedforms, subglacial till, and regions of formerly fast-flowing ice (e.g. Wellner et al., 2001; Ottesen et al., 2005a, b; Ó Cofaigh et al., 2005a, b; Hogan, 2008). The geomorphological imprint of the ice stream in Hinlopen Trough (Fig. 6.1) clearly conforms to the idealised landform model for ice streams in Svalbard (Fig. 6.2; Ottesen and Dowdeswell, 2009). The landform assemblages in Hinlopen Trough also exhibit a characteristic down-trough progression in morphology and elongation; an observation which is consistent with descriptions from the beds of many other former ice streams in both hemispheres (e.g. Shipp et al., 1999; Ó Cofaigh et al., 2002, 2005a, b; Ottesen et al., 2005a, b; Lowe and Anderson, 2003; Mosola and Anderson, 2006; Hogan, 2008).

6.3.2 Style of Deglaciation

Diagnostic assemblages of submarine landforms can allow the relative speed and style of ice sheet deglaciation to be inferred. The preservation of unmodified megaflutes and highly attenuated drumlins in Hinlopen Trough indicates that ice retreated rapidly through the surveyed area. It is likely that this ice thinned and became ungrounded during deglaciation, retreating rapidly through the mechanism of iceberg calving (Ottesen et al., 2007; Dowdeswell et al., 2008). This conclusion is in general agreement with data collected from other high-latitude continental shelves, in which ice has been found to generally retreat more rapidly from ice streams compared with inter-ice stream areas (Ottesen et al., 2007).

In contrast to the beds of other former ice streams in Svalbard, the geomorphology of Hinlopen Trough appears to lack any evidence of grounding-zone wedges. These features have been observed within Isfjorden and Kongsfjorden on Svalbard's western continental shelf and are indicative of episodic ice retreat (Ottesen et al., 2007). The

Hinlopen Trough ice stream may have been more sensitive to climatic changes than these locations; it is likely that the geometry of this trough, which lacks any significant ice-pining points, enabled continuous and rapid ice retreat.

Chapter 7 - Conclusions

7.1 Project Aims

This project aimed to utilise extensive data sets from EM120 swath bathymetry, TOPAS sub-bottom acoustic profiling and sediment cores to outline the distribution of the submarine landforms in Hinlopen Trough, Northern Svalbard margin. Geomorphological analysis of the sea floor aimed to facilitate interpretations of Late Quaternary ice flow dynamics in this region and to add to the growing amount of information on the geomorphological imprint of palaeo-ice streams more generally.

7.2 Summary of Results

Geophysical and geological evidence demonstrates that Hinlopen Trough was occupied by a palaeo-ice stream during the Late Weichselian glaciation (Fig. 6.1). Landform orientations demonstrate that ice flowed through this depression in a NNW direction towards the shelf break. Order of magnitude calculations of the volume of glacigenic infill on the continental shelf indicate that this ice stream provided high rates of sediment delivery to the margin (5-7.5m/kyr; Table 6.2). This suggests that the Hinlopen ice stream represented a major route for the transfer of ice and debris to the northern continental margin of Svalbard during the last, Late Weichselian, glacial period.

Topographic images produced from swath bathymetry data have revealed five assemblages of submarine landforms within Hinlopen Trough (Table 6.1). The inner-shelf region of this trough is characterised by bedrock drumlins and ice-sculpted bedrock (Fig. 6.1). The middle-shelf area illustrates the transition from bedrock to a sedimentary substrate and contains two assemblages of elongate subglacial landforms (highly-attenuated drumlins and megaflutes). These elongate features are formed within a unit capped by an acoustically impenetrable reflector (B1B in Fig. 4.1). Core data confirmed that this reflector represents the upper-contact of a dark-grey matrix-supported diamict, interpreted as subglacial till (Fig. 5.11). The association of glacial lineations and subglacial till suggests that bed deformation occurred beneath the ice stream in this area.

The geomorphology of the outer-shelf is dominated by a series of furrows formed by the ploughing action of iceberg keels as they grounded on the sea floor (Figs. 3.8 and 3.9). These ancient ploughmarks derived from icebergs with keels of up to 300 m and were likely to have been produced during regional deglaciation of the Late Weichselian Svalbard-Barents Sea Ice Sheet.

The lack of grounding-zone features imaged from swath bathymetry data suggests that deglaciation was rapid within the trough. This interpretation complements observations from other palaeo-ice streams, in which retreat occurred more rapidly than from intervening shallow banks. It is likely that rapid retreat of the ice in Hinlopen Trough occurred through flotation and breakup of the ice margin, and was possibly facilitated by the geometry of the trough, which lacks obvious ice pining points. The deglacial sequence, identified from acoustic profiles and sediment cores, is generally capped by a thin (<15 m) draping unit of fine-grained sediments (e.g. Fig. 4.1 and 4.3), inferred to represent the product of hemipelagic sedimentation during ice-free marine conditions in the Holocene.

The geomorphological imprint described from Hinlopen Trough largely represents that of a ‘classical’ ice stream; the morphology and distribution of the identified landforms conforms closely to the landform assemblage patterns described by idealised models of ice streams in Svalbard (Fig. 6.2). The geomorphology of the trough is dominated by the presence of elongate landforms orientated parallel to the inferred flow direction and is completely lacking in those transverse features indicative of inter-ice stream locations (Fig. 6.1). The geomorphological signature of this trough also exhibits a characteristic down-flow progression in landform elongation. This is likely to represent an increase in ice velocity through the trough, which probably culminated with the initiation of ice streaming in the soft sediments on the middle-shelf.

7.3 Recommendations for Further Investigation

This thesis provides a high-resolution and comprehensive analysis of submarine landforms and past ice dynamics in Hinlopen Trough. Further investigations could build upon these results through the analysis of a greater number of sediment cores. A larger quantity of geological data would allow more ground truthing of the sediments and could facilitate greater correlation between data sets. The radiocarbon dating of bivalves or other material collected from sediment cores could also allow the derivation of an absolute chronology of ice evolution in the area. This procedure could serve to constrain directly the timing of deglaciation within Hinlopen Trough and to allow comparisons with ice retreat from other locations on Svalbard's continental margins (Svendsen et al., 2004). Geophysical and geological investigations could also be employed to describe further the patterns of Late Quaternary ice flow on Svalbard's northern margin. Analyses of submarine landforms could also be utilised to constrain the precise location of any palaeo- ice divide to the south of Hinlopen Strait.

8. Bibliography

BALSAM, W. L., DEATON, B.C., and DAMUTH, J.E., 1999. Evaluating optical lightness as a proxy for carbonate content in marine sediment cores. *Marine Geology*, v. 161, p.141-153.

BARNES, P. W., and LIEN, R., 1988. Icebergs rework shelf sediments to 500 m off Antarctic. *Geology*, v.16, p. 1130-1133.

BENN, D. I. and EVANS, D.J.A., 1998. Glaciers and Glaciation.

BENNETT, M. R., and GLASSER, N. F., 1996. Glacial Geology: Ice Sheets and Landforms.

BOND, G., HEINRICH, H., BROECKER, W., LABEYRIE, L., MCMANUS, J., ANDREWS, J., HUON, S., JANTSCHIL, R., CLASEN, S., SIMET, C., TEDESCO, K., KLAS, M., BONANNI, G., and IVY, S., 1999. Evidence for massive discharges of icebergs into the North Atlantic ocean during the last glacial period. *Nature*, v.360, p.245-249.

BOULTON, G.S.,1979. Glacial history of the Spitsbergen archipelago and the problem of a Barents Shelf ice sheet. *Boreas*, v.8, p.31-57.

CAI, J., POWELL, R.D., COWAN, E. A., CARLSON, P.R., 1997. Lithofacies and seismic-reflection interpretation of temperate glacimarine sedimentation in Tarr Inlet, Glacier Bay, Alaska. *Marine Geology*, v.143, p.5-37.

CANALS, M., URGELES, R., and CALAFAT, A. M, 2000. Deep sea-floor evidence of past ice streams off the Antarctic Peninsula. *Geology*, v.28, p.31-34.

CHERKIS, N.Z., MAX, M. D., MIDTHASSEL, A., CRANE, K., SUNDVOR, E., VOFT, P.R., 1992. Deep ice scour and mass-wasting features on the northern Svalbard insular shelf and slope. *ICAM Proceedings*, p.333.

CHERKIS, N. Z., MAX, M. D., VOGT, K. C., MIDTHASSEL, A., SUNDVOR, E., 1999. Large-scale mass wasting on the north Spitsbergen continental margin, Arctic Ocean. *Geo-Marine Letters*, v.19, p.131-142.

CLARK, C.D., 1993. Mega-scale glacial lineations and cross-cutting ice-flow landforms. *Earth Surface Processes and Landforms*, v. 18, p.1–29.

CLARK, P.U., DYKE, A.S., SHAKUN, J.D., CARLSON, A.E., CLARK, J., WOHLFARTH, B., MITROVICA, J.X., HOSTETLER, S.W., McCABE, A.M., 2009. The last glacial maximum. *Science*, v.325, no.5941, p.710-714.

CORTIJO, E., PASCAL, Y., LABEYRIE, L., and CREMER, M., 1995. Sedimentary record of rapid climatic variability in the North Atlantic Ocean during the last glacial cycle. *Paleoceanography*, v.10, n.5, p.911-926.

COWAN, E. A., SERAMUR, K. C., CAI, J., and POWELL, R. D., 1999. Cyclic sedimentation produced by fluctuations in meltwater discharge, tides, and marine productivity in an Alaskan fjord. Sedimentology, v.46, p.1109-1126.

COWAM, E.A., and POWELL, R.D., 1990. Suspended sediment transport and deposition of interlaminated sediments in a temperate glacial fjord, Alaska, USA. In Dowdeswell and Scourse, Glacimarine environments: processes and sediments, *Geological Society of London, Special Publications*, v.53, p.75-89.

DAMUTH, J.E., 1975. Echo character of the western equatorial Atlantic floor and its relationship to the dispersal and distribution of terrigenous sediments. *Marine Geology*, v.18, p.17-45.

DAMUTH, J.E., 1978. Echo character of the Norwegian-Greenland sea: relationship to Quaternary sedimentation. *Marine Geology*, v.281, p.36.

DAMUTH, J.E., 1980. Use of high-frequency (3.5-12 kHz) echograms in the study of near-bottom sedimentation processes in the deep-sea: a review. *Marine Geology*, v.38, p.51-75.

DAVIS, T.A., BELL, T., COOPER, A.K., JOSENHANS, H., POLYAK, L., SOLHEIM, A., STOKER, M.S., STRAVERS, J.A., 1997. Glaciated continental margins: an atlas of acoustic images.

DIMAKIS, P., BRAATHEN, B.I., FALEIDE, J.I., ELVERHØI, A., GUDLAUGSSON, S.T., 1998. Cenozoic erosion and the pre-glacial uplift of the Svalbard–Barents Sea region. *Tectonophysics*, v.300, p.311-327.

DOMACK, E. W., JACOBSON, E. A., SHIPP, S., ANDERSON, J.B., 1999a. Late Pleistocene–Holocene retreat of the West Antarctic Ice-Sheet system in the Ross Sea: Part 2—Sedimentological and stratigraphic signature. *GSA Bulletin*, v.111, n.10, p.1517-1536.

DOWDESWELL, J. A., and ELVEHØI, A., 2002. The timing of initiation of fast-following ice streams during a glacial cycle inferred from glacimarine sedimentation. *Marine Geology*, v.188, p.3-14.

DOWDESWELL, J.A., and FORSBERG, C.F., 1992. The size and frequency of icebergs and bergy bits derived from tidewater glaciers in Kongsfjorden, northwest Spitsbergen. *Polar Research*, v. 11, p.81–91.

DOWDESWELL, J.A., and Ó COFAIGH, C., 2002. Glacier-influenced sedimentation on high-latitude continental margins: introduction and overview. *Geological Society, London, Special Publications*, v.203, p.1-9.

DOWDESWELL, J. A. and SCOURSE, J. D., 1990. Introduction, in Glacimarine Environments: Processes and Sediments. *Geological Society, London, Special Publication* No. 53

DOWDESWELL, J. A. and SIEGERT, M. J, 1999. Ice-sheet numerical modelling and marine geophysical measurements of glacier-derived sedimentation on the Eurasian Arctic continental margins. *Geological Society of America Bulletin,* v. 111, no.7, p.1080-1097.

DOWDESWELL, J.A., JAKOBSSON, M., HOGAN, K.A., O´REGAN, M., BACKMAN, J., EVANS, J., Hell, B., LÖWEMARK, L., MARCUSSEN, C., NOORMETS, R., Ó COFAIGH, C., SELLEN, E. and SÖLYSTEN, M., In Press A. High-resolution geophysical observations of the Yermak Plateau and northern Svalbard margin: implications for ice-sheet grounding and deep-keeled icebergs. *Quaternary Science Reviews.*

DOWDESWELL, J.A., EVANS, J. and Ó COFAIGH, C., In Press B. Submarine landforms and shallow acoustic stratigraphy of a 400 km-long fjord-shelf-slope-transect, Kangerdlussuaq margin, East Greenland. *Quaternary Science Reviews.*

DOWDESWELL, J.A., HOGAN, K.A., EVANS, J., NOORMETS, R., Ó COFAIGH, C. and OTTESEN, D., 2010a. Past ice-sheet flow east of Svalbard inferred from streamlined subglacial landforms. *Geology,* v. 38, p. 163-166.

DOWDESWELL, J.A., OTTESEN, D. and RISE, L., 2010b. Rates of sediment delivery from the Fennoscandian Ice Sheet through an Ice Age. *Geology*, v. 38, p. 3-6.

DOWDESWELL, J.A., OTTESEN, D., EVANS, J., Ó COFAIGH, C. and ANDERSEN, J.B., 2008. Submarine glacial landforms and rates of ice-stream collapse. *Geology*, v. 36, p. 819-822.

DOWDESWELL, J.A., OTTESEN, D. and RISE, L., 2006. Flow-switching and large-scale deposition by ice streams draining former ice sheets. *Geology*, v. 34, p. 313-316.

DOWDESWELL, J.A., WHITTINGTON, R.J., JENNINGS, A.E., ANDREWS, J.T., MACKENSEN, A., and MARIENFELD, P., 2000. An origin for laminated glacimarine sediments through sea-ice build-up and suppressed iceberg rafting. Sedimentology, v.47, p.557-576.

DOWDESWELL, J.A., Ó COFAIGH, C. and PUDSEY, C.J., 2004. Thickness and extent of the subglacial till layer beneath an Antarctic paleo-ice stream. *Geological Society of America*, v. 32, p. 13-16.

DOWDESWELL, J.A., and ELVERHØI, A., 2002. The timing of initiation of fast-flowing ice streams during a glacial cycle inferred from glacimarine sedimentation. *Marine Geology*, v.188, p.3-14.

DOWDESWELL, J.A., KENYON, N.H. and LABERG, J.S., 1997. The glacier-influenced Scoresby Sund Fan, East Greenland continental margin: evidence from GLORIA and 3.5 kHz records. *Marine Geology* v. 143, p. 207-221.

DOWDESWELL, J.A., VILLINGER, H., WHITTINGTON, R.J. and MARIENFIELD, P., 1993. Iceberg scouring in Scoresby Sund and on the East Greenland continental shelf. *Marine Geology*, v. 111, p. 37-53.

DUPLESSY, J.C., IVANOVA, E., MURDMAA, I., PATERNE, M., LABEYRIE, L., 2001. Holocene paleoceanography of the northern Barents Sea and variations of the northward heat transport by the Atlantic Ocean. *Boreas*, v. 30, p.2–16.

ELVERHØI, A., HOOKE, R. LeB., SOLHEIM, A., 1998. Late Cenozoic erosion and sediment yield from the Svalbard-Barents Sea region: implications for understanding erosion of glacierized basins. *Quaternary Science Reviews*, v. 17, p.209-241.

ELVERHØI, A., and SOLHEIM, A., 1983. Physical environments in the Western Barents Sea: 1:500 000 surface sediment distribution. *Norsk Polarinstitutt Skrifter*, v.179A, p.1-23.

ELVERHØI, A., ANDERSEN, E.S., DOKKEN, T., HEBBELN, D., SPIELHAGEN, R., SVENDSEN, J.I., SØRFLATEN, M., RØRNES, A., HALD, M. and FORSBERG, C.F., 1995. The growth and decay of the Late Weichselian Ice Sheet in western Svalbard and adjacent areas based on provenance studies of marine sediments. *Quaternary Research*, v. 44, p. 303-316.

EVANS, J., DOWDESWELL, J.A., Ó COFAIGH, C., BENHAM, T. J., ANDERSON, J.B, 2006. Extent and dynamics of the West Antarctic Ice Sheet on the outer continental shelf of Pine Island Bay during the last glaciation. *Marine Geology*, v. 230, p53–72.

EVANS, J., DOWDESWELL, J.A., GROBE, H., NIESSEN, F., STEIN, R., HUBBERTEN, H.W., and WHITTINGTON, R.J., 2002. Late Quaternary sedimentation in Kejser Franz Joseph Fjord and on the continental margin of East Greenland. In: DOWDESWELL, J.A., and Ó COFAIGH, C. Glacier-influenced sedimentation on high-latitude continental margins. *Geological Society of London, Special Publication*, v.203, p.149-179.

EYLES, C.N., EYLES, N., MIALL, A.D., 1983. Models of glaciomarine sedimentation and their application to the interpretation of ancient glacial sequences. *Palaeogeography, Palaeoclimatology, Palaeoecology*, v.51, p.15—84.

FAUGERS, J.C., and STOW, D.A.V., 1993. Bottom-current-controlled sedimentation: a synthesis of the contourite problem. *Sedimentary Geology*, v.82, p.287-297.

FORMAN, S.L., LUBINSKI, D., MILLER, G.H., SNYDER, J., MATISHOV, G., MYSLIVETS, V., 1995. Postglacial emergence and distribution of late Weichselian ice-sheet loads in the northern Barents and Kara seas, Russia. *Geology*, v.23, no. 2, p.113-116.

FORMAN, S.L., LUBINSKI, D.J., IFSSON, O., ZEE BERG, J.J., SNYDER, J.A., SIEGERT, M.J., MATISHOV, G.G., 2004. A review of postglacial emergence on

Svalbard, Franz Josef Land and Novaya Zemlya, northern Eurasia. *Quaternary Science Reviews*, v. 23, p.1391–1434.

GRUTZNER, J., GIOSAN, L., FRANZ, S.O., TIEDEMANN, R., CORTIJO, E., CHAISSON, W.P., FLOOD, R.D., HAGEN, S., KEIGWIN, L.D., POLI, S., RIO, D., WILLIAMS, T., 2002. Astronomical age models for Pleistocene drift sediments from the western North Atlantic (ODP Sites 1055^1063). *Marine Geology*, v.189, p.5-23.

HARLAND, W.B., ANDERSON, L.M., MANASRAH, D., BUTTERFIELD, N.J., 1997. The Geology of Svalbard.

HEROY, D.C., SJUNNESKOG, C., ANDERSON, J.B., 2008. Holocene climate change in the Bransfield Basin, Antarctic Peninsula: evidence from sediment and diatom analysis. *Arctic Science*, v.20 (1), p.69-87.

HEBBELN, D., DOKKEN, T.M., ANDERSON, E.S., HALD, M., ELVERHOI, A., 1994. Moisture supply for northern ice sheet growth during the last glacial maximum. *Nature*, v.370, p.357-359.

HJELLE, A., 1993. The Geology of Svalbard. Oslo, Norsk Polarinstitutt, 163 pp.

HOGAN, K.A.,2008. The geomorphic and sedimentary record of glaciation on high-latitude continental margins with specific reference to the North-eastern Svalbard margin. Ph.D. Thesis, University of Cambridge. 225 pp.

INGOLFSSON, Ó., RÖGNVALDSSON, F., BERGSETN, H., HEDENAS, L., LEMDAHL, G., LIRIO, J.M., and SEJRUP, H.P., 1995. Late Quaternary glacial and environmental history of Kongsøya, Svalbard. *Polar Research*, v.14, p.123–139.

JAKOBSSON, M., GARDNER, J.V., VOGT, P.R., MAYER, L.A., ARMSTRONG, A., BACKMAN, J., BRENNAN, R., CALDER, B., HALL, J.K., KRAFT, B., 2005. Multibeam bathymetric and sediment profiler evidence for ice grounding on the Chukchi Borderland, Arctic Ocean. *Quaternary Research*, v.63, p.150-160.

JOKAT, W., 2005. The sedimentary structure of the Lomonosov Ridge between 88◦N and 80◦N. *Geophysical Journal International*, v. 163, p.698-726.

KING, E.C., HINDMARSH, R.C.A., STOKES, C.R., 2009. Formation of mega-scale glacial lineations observed beneath a West Antarctic ice stream. *Nature Geoscience*, v.2, p.585-588.

KLEIBER, H.P., KNIES, J., NIESSEN, F., 2000. The Late Weichselian glaciation of the Franz Victoria Trough, northern Barents Sea: ice sheet extent and timing. Marine *Geology*, v.168, p.25-44.

KLUIVING, S.J., BARTEK, L.R., VAN DER WATEREN, F.M., 1999. Multi-scale analyses of subglacial and glacimarine deposits from the Ross Sea continental shelf, Antarctica. *Annals of Glaciology*, v.28, p.90-96.

KNIES, J., KLEIBER, H.P., MATTHIESSEN, J., MÜLLER, C., NOWACZYK, N., 2001. Marine ice-rafted debris records constrain maximum extent of Saalian and Weichselian ice-sheets along the northern Eurasian margin. *Global and Planetary Change*, v.31, p.45-64.

KOÇ, N., KLITGAARD-KRISTENSEN, D., HASLE, K., FORSBERG, K.F., SOLHEIM, A., 2002. Late glacial palaeoceanography of Hinlopen Strait, northern Svalbard. *Polar Research*, v. 21(2), p.307-314.

KUIJPERS, A., DALHOFF, F., BRANDT, M.P., HÜMBS, P., SCHOTT, T., ZOTOVA, A., 2007. Giant iceberg plough marks at more than 1 km water depth offshore West Greenland. *Marine Geology*, v.246, p.60-64.

LAMBECK, K., 1995. Constraints on the Late Weichselian ice sheet over the Barents Sea from observations of raised shorelines. *Quaternary Science Reviews*, v. 14, p.1–16.

LAMBECK, K., 1996, Limits on the areal extent of the Barents Sea ice sheet in Late Weichselian time. *Global and Planetary Change*, v. 12, p.41–51.

LANDVIK, J.Y., BONDEVIK, S., ELVERHØI, A., FJELDSKAAR, W., MANGERUD, J., SALVIGSEN, O., SIEGERT, M.J., SVENDSEN, J.I., VORREN, T.O., 1998. The last glacial maximum of Svalbard and the Barents Sea area: ice sheet area and configuration. *Quaternary Science Reviews*, v. 17, p. 43-75.

LANDVIK, J.Y., INGÓLFSSON, O., MIENERT, J., LEHMAN, S.J., SOLHEIM, A., ELVERHØI, A. and OTTESEN, D., 2005. Rethinking Late Weichselian Ice Sheet dynamics in coastal NW Svalbard. *Boreas*, v. 34, p. 7-24.

LOWE, A.L., and ANDERSON, J.B., 2003. Evidence for abundant subglacial meltwater beneath the paleo-ice sheet in Pine Island Bay, Antarctica. Journal of Glaciology, v.49, p.125-138.

MANGERUD, J. and LANDVIK, J.Y., 2007. Younger Dryas cirque glaciers in western Spitsbergen: smaller than during the Little Ice Age. *Boreas*, v. 36(3), p. 278-285.

MANGERUD, J. and SVENDSEN, J.I., 1992. The last glacial-interglacial period on Spitsbergen, Svalbard. *Quaternary Science Reviews*, v. 11, p. 633-664.

MANGERUD, J. and SVENDSEN, J.I., 1996. The retreat of the Barents Sea Ice Sheet on the western Svalbard margin. *Boreas*, v.25, p.244-256.

MØLLER, H.S., CHRISTIANSEN, C., NIELSEN, N., and RASCH, M., 2001. Investigation of a modern glacimarine sedimentary environment in the fjord Kuannersuit Sulluat, Disko, West Greenland. *Geografisk Tidsskrift, Danish Journal of Geography*, v.101, p.1-10.

MOSOLA, A. B. and ANDERSON, J. B., 2006. Expansion and rapid retreat of the West Antarctic Ice Sheet in eastern Ross Sea: possible consequence of over-extended ice streams? *Quaternary Science Reviews*, v. 25, p. 2177-2196.

MURDMAA, I., IVANOVA, E., DUPLESSY, J.C., LEVITAN, M., KHUSID, T., BOURTMAN, M., ALEKHINA, G., ALEKSEEVA, T., BELOUSOV, M., SEROVA, V., 2006. Facies system of the Eastern Barents Sea since the last glaciation to present. *Marine Geology*, v.230, p.275-303.

NAM, S., STEIN, R., GROBE, H. and HUBBERTEN, H., 1995. Late Quaternary glacial-interglacial changes in sediment composition at the East Greenland continental margin and their paleoceanographic implications. *Marine Geology*, v.122, p.243-262.

NEDERBRAGT, A.J., DUNBAR, R.B., OSBORN, A.T., PALMER, A., THUROW, J.W., WAGNER, T., 2006. Sediment colour analysis from digital images and correlation with sediment composition. *Geological Society of London, Special Publications*, v. 267, p.113-128.

NØRGAARD-PEDERSEN, N., MIKKELSEN, N., POULSEN, M.D., and SIMONSEN, A.S., 2009. Holocene climate variability in southern Greenland: results from the Galathea 3 expedition. *Geological Survey of Denmark and Greenland Bulletin*, v.17, p.77–80.

Ó COFAIGH, C., TAYLOR, J., DOWDESWELL, J.A., ROSELLE MELE, A., KENYON, N.H., EVANS, J., and MIENERT, J., 2002. In: DOWDESWELL, J.A., and Ó COFAIGH, C. Glacier-influenced sedimentation on high-latitude continental margins. *Geological Society of London, Special Publication*, v.203, p.325-349.

Ó COFAIGH, C., DOWDESWELL, J. A., ALLEN, C. S., HIEMSTRA, J. F., PUDSEY, C. J., EVANS, J. and EVANS, D. J. A., 2005a. Flow dynamics and till genesis associated with a marine-based Antarctic palaeo-ice stream. *Quaternary Science Reviews*, v. 24, p. 709-740.

Ó COFAIGH, C., LARTER, R.D., DOWDESWELL, J.A., HILLENBRAND, C.D., PUDSEY, C.J., EVANS, J. and MORRIS, P., 2005b. Flow of the West Antarctic Ice Sheet on the continental margin of the Bellingshausen Sea at the Last Glacial Maximum. *Journal of Geophysical Research*, v. 110, B11103.

Ó COFAIGH, C., PUDSEY, C.J., DOWDESWELL, J.A., MORRIS, P., 2002. Evolution of subglacial bedforms along a paleo-ice stream, Antarctic Peninsula continental shelf. *Geophysical Research Letters*, v.29, no.8, p.1199.

Ó COFAIGH, C., and DOWDESWELL, J.A., 2001. Laminated sediments in glacimarine environments: diagnostic criteria for their interpretation. *Quaternary Science Reviews*, v.20, p.1411-1436.

OTTESEN, D. and DOWDESWELL, J. A., 2009. An inter-ice stream glaciated margin: submarine landforms and a geomorphic model based on marine-geophysical data from Svalbard. *Geological Society of America, Bulletin*, v. 121, p. 1647-1665.

OTTESEN, D. and DOWDESWELL, J. A., 2006. Assemblages of submarine landforms produced by tidewater glaciers in Svalbard. *Journal of Geophysical Research*, v. 111, F01016.

OTTESEN, D., DOWDESWELL, J. A. and RISE, L., 2005a. Submarine landforms and the reconstruction of fast-flowing ice streams within a large Quaternary ice sheet: the 2,500 km-long Norwegian-Svalbard margin (57° to 80°N). *Geological Society of America, Bulletin*, v. 117, p. 1033-1050.

OTTESEN, D., RISE, L., KNIES, J., OLSEN, L., HENRIKSEN, S., 2005b. The Vestfjorden-Traenadjupet palaeo-ice stream drainage system, mid-Norwegian continental shelf. *Marine Geology*, v.218., p.175-189.

OTTESEN, D., DOWDESWELL, J.A., LANDVIK, J.Y. and MIENERT, J., 2007. Dynamics of the Late Weichselian ice sheet on Svalbard inferred from high-resolution sea-floor morphology. *Boreas*, v. 36, p. 286-306.

OTTESEN, D., DOWDESWELL, J. A., BENN, D. I., KRISTENSEN, L., CHRISTIANSEN, H. H., HANSEN, L., LEBESBYE, E., FORWICK, M. and VORREN, T. O., 2008. Submarine landforms characteristic of glacier surges in two Spitsbergen fjords. *Quaternary Science Reviews*, v. 27, p. 1583-1599.

POLYAK, L., FORMAN, S.L., HERIHY, F.A., IVANOV, G., KNINITSKY, P., 1997. Late Weichselian deglacial history of the Svyataya (Saint) Anna Trough, northern Kara Sea, Arctic Russia. *Marine Geology*, v.143, p.169–188.

POLYAK, L., EDWARDS, M.H., COAKLEY, B.J., JAKOBSSON, M., 2001. Ice shelves in the Pleistocene Arctic Ocean inferred from glaciogenic deep-sea bedforms. *Nature*, v.410, p.453-457.

ROGERSON, M., WEAVER, P.P.E., ROHLING, E.E.J., LOURENS, L.J., MURRAY, J.W., HAYES, A., 2006. Colour logging as a tool in high-resolution palaeoceanography. *New Techniques in Sediment Core Analysis, Geological Society, London, Special Publications*, v.267, p.99-112.

SALVGISEN, O., ADRIELSSON, L., HJORT, C., KELLY, M., LANDVIK, J.Y. and RONNERT, L., 1995. Dynamics of the last glaciation in eastern Svalbard as inferred from glacier-movement indicators. *Polar Research*, v. 14(2), p. 141-152.

SCHOOF, C.G., and CLARK, G.K.C, 2008. A model for spiral flows in basal ice and the formation of subglacial flutes based on a Reiner-Rivlin rheology for glacial ice. *Journal of Geophysical Research*, v.113, B05204, doi:10.1029/2007JB004957.

SHIPP, S., ANDERSON, J., DOMACK, E., 1999. Late Pleistocene–Holocene retreat of the West Antarctic Ice-Sheet system in the Ross Sea: Part 1—Geophysical results. *Geological Society of America, Bulletin*, v.111, no.10, p.1486-1516.

SIEGERT, M.J., DOWDESWELL, J.A., HALD, M. and SVENDSEN, J.I., 2001. Modelling the Eurasian Ice Sheet through a full (Weichselian) glacial cycle. *Global and Planetary Change*, v. 31, p. 367-385.

SPIELHAGEN, R.F., BAUMANN, K., ERLENKEUSER, H., NOWACZYK, N. R., NØRGAARD-PEDERSEN, N., VOGT, C. and WEIEL, D., 2004. Arctic Ocean deep-sea record of northern Eurasian ice sheet history. *Quaternary Science Reviews*, v. 23, p. 1455-1483.
.

STOKES, C. R. and CLARK, C. D., 2002. Are long subglacial bedforms indicative of fast ice flow? *Boreas*, v. 31, p. 239-249.

STOKES, C. R. and CLARK, C. D., 1999. Geomorphological criteria for identifying Pleistocene ice streams. *Annals of Glaciology*, v.28, p.67-74

SUNDVOR, E. and ELDHOLM, O., 1979. The western and northern margin off Svalbard. *Tectonophysics*, v.59, p.239–250.

SVENDSEN, J.I., ALEXANDERSON, H., ASTAKHOV, V.I., DEMIDOV, I., DOWDESWELL, J.I., FUNDER, S., GATAULLIN, V., HENRIKSEN, M., HJORT, C., HOUMARK-NIELSEN, M., HUBBERTEN, H.W., INGÓLFSSON, O., JOKOBSSON, M., KJÆR, K. H., LARSEN, E., LOKRANTZ, H., LUNKKA, J.P., LYS, A., MANGERUD, J., MATIOUCHKOV, A., SAARNISTO, M., SIEGERT, C., SIEGERT, M.J., SPEILHAGEN, R.F. and STEIN, R., 2004. Late Quaternary ice sheet history of northern Eurasia. *Quaternary Science Reviews*, v. 23, p. 1229-1271.

SVENDSEN, J.I., MANGERUD, J., ELVERHØI, J., SOLHIEM, A., and SCHUTTENHELM, R.T.E., 1992. The Late Weichselian glacial maximum on western Spitsbergen inferred from offshore sediment cores. *Marine Geology*, v.104, p.1-17.

SVENDSEN, J.I., ELVERHØI, J., MANGERUD, J., 1996. The retreat of the Barents Sea Ice Sheet on the western Svalbard margin. *Boreas*, v.25, p.244-256.

SVENDSEN, J.I., ASTAKHOV, V.I., BOLSHNANOV, D.Y., DEMIDOV, I., DOWDESWELL, J.A., GATAFLIN, V., HJORT, C., HUBBERTEN, H.W., LARSEN, E., MANGERUD, J., MELLES, M., MOLLER, P., SAARNISTO, M., SIEGERT, M.J., 2002. Maximum extent of the Eurasian ice sheets in the Barents and Kara Sea region during the Weichselian. *Boreas*, v.28, p.234-242.

SYVITSKI, J.P.M., STEIN, A.B., ANDREWS, J.T., 2001. Icebergs and the Sea Floor of the East Greenland (Kangerlussuaq) Continental Margin. *Arctic, Antarctic, and Alpine Research*, v. 33, no. 1, p.52-61.

TAYLOR, J., DOWDESWELL, J.A., KENYON, N.H., WHITTINGTON, R.J., van WEERING, Tj.C.E., MIENERT, J., 2000. Morphology and Late Quaternary sedimentation on the North Faeroes slope and abyssal plain, North Atlantic. *Marine Geology*, v.168, p.1-24.

VANNESTE, M., MIENERT, J., BÜNZ, S., 2006. The Hinlopen Slide: A giant, submarine slope failure on the northern Svalbard margin, Arctic Ocean. *Earth and Planetary Science Letters*, v. 245, p.373–388

VELICHKO, A.A., KONONOV, Y.M. and FAUSTOVA, M.A., 1997. The last glaciation of Earth: size and volume of ice sheets. *Quaternary International*, vs. 41/42, p.43-51.

VORREN, T.O., and LABERG, J.S., 1997. Trough-mouth fans – palaeoclimate and ice sheet monitors. *Quaternary Science Reviews*, v.16, p.865-881.

VORREN T.O., HALD, M., EDVARDSEN, M., LINDHANSEN, O.W., 1983. Glacigenic sediments and sedimentary environments on continental shelves: general principles with a case study from the Norwegian shelf. In Ehlers, J (eds), Glacial deposits in north-west Europe, p.61-73.

VORREN, T.O., LABERG, J.S., BLAUME, F., DOWDESWELL, J.A., KENYON, N.H., MIENERT, J., RUMOHR, J., WERNER, F., 1998. The Norwegian-Greenland Sea Continental margins: morphology and Late Quaternary sedimentary processes and environment. *Quaternary Science Reviews*, v.17, p.273-302.

WELLNER, J.S., LOWE, A.L., SHIPP, S.S., ANDERSON, J.B., 2001. Distribution of glacial geomorphic features on the Antarctic continental shelf and correlation with substrate: implications for ice behaviour. *Journal of Glaciology*, v.47, no.158, p.397-411.

WELLNER, J.S., HEROY, D.C., ANDERSON, J.B., 2006. The death mask of the Antarctic ice sheet: Comparison of glacial geomorphic features across the continental shelf. *Geomorphology*, v.75, p.157-171.

WINKELMANN, D., GEISSLES, W., SCHNEIDER, J., STEIN, R., 2008a. Dynamics and timing of the Hinlopen/Yermak Mega-slide north of Spitsbergen, Arctic Ocean. *Marine Geology*, v.250, p.34-50.

WINKELMANN, D., SCHAFER, C., STEIN, R., MACKENSEN, A., 2008b. Terrigenous events and climate history of the Sophia Basin, Arctic Ocean. Geochemistry, Geophysics, Geosystems, v.9, no.7, Q07023, doi:10.1029/2008GC002038

YOON, H.I., PARK, B-K., KIM, Y., KIM, D., 2000. Glaciomarine sedimentation and its paleoceanographic implications along the fjord margins in the South Shetland Islands, Antarctica during the last 6000 years. *Palaeogeography, Palaeoclimatology, Palaeoecology*, v.157, p.189–211.

ZEEBERG, J.J., FORMAN, S.L., and POLYAK, L., 2003. Glacier extent in a Novaya Zemlya fjord during the little ice age inferred from glaciomarine sedimentary records. *Polar Research*, v.22 (2), p.385-394.

www.intute.ac.uk/worldguide/countrymap.com

MB-System cookbook (www.Ideo.columbia.edu/res/pi/MB-System/mb-cookbook)